Division of Biomedical Engineering

Department of Human Biology

Faculty of Health Sciences

University of Cape Town

Role of Extracellular Environment in Mechanical Properties of Cardiac Fibroblasts and Myofibroblasts

Dissertation

submitted to

The University of Cape Town

in partial fulfilment of the requirements for the degree:

Master of Science in Biomedical Engineering

by

Pieter Daniël Haasbroek

Supervisor: Professor Thomas Franz

Co-supervisor: Associate Professor Neil Davies

October 2020

Declaration

I, Pieter Daniël Haasbroek, hereby declare that the work on which this dissertation/thesis is based is my original work (except where acknowledgements indicate otherwise). Neither the entire work nor any part of it has been, is being, or will be submitted for another degree in this or any other university.

This dissertation has been submitted to the Turnitin module, and I confirm that my supervisor has seen my report and any concerns revealed by such have been resolved with my supervisor.

I authorise the university to reproduce the work as a whole or any portion of its contents for the purpose of research.

Signature: Signed by candidate

Date: 23 September 2020

Abstract

Acute MI results in adverse remodelling of the myocardium, eventually leading to contractile dysfunction and chronic heart failure. Collectively, the formation of fibrotic scar tissue in the left ventricle inhibits its contractile function and leads to a cardiac output loss. Cardiac fibroblast and myofibroblast cells are integral in the remodelling of injured tissue and are the most anticipated therapeutic target for cardiac fibrosis. To date, there is no anti-fibrotic therapy, which we argue, is due to the lack of knowledge on the functionality of the cardiac fibroblast.

It was hypothesised that a change in stiffness of the remodelling extracellular environment associated with fibrosis leads to a change of the mechanical properties and contractile forces of cardiac fibroblasts and myofibroblasts. Hence, this dissertation aimed to investigate the effects of extracellular stiffness on mechanical properties of cardiac fibroblasts and myofibroblasts using engineered *in vitro* microenvironments with tuneable physical properties.

Polyethylene Glycol (PEG) hydrogels offer ideal properties to serve as an extracellular matrix (ECM) mimicking biomaterial. Different techniques of mechanical characterisation used in this study established that the elastic modulus of 20 kDa 8-arm PEG-VS hydrogel crosslinked with dithiothreitol (DTT) reagent, is directly proportional to the concentration of PEG precursor used to form the material. Rheological measurements indicated an elastic shear modulus of 500 ± 13 Pa and 2721 ± 39 Pa for PEG gels of 4% (m/v) and 10% (m/v), respectively. Specialised micro-indentation and uniaxial tensile testing found PEG gels of 7%, 10%, 14% and 18% concentration to have elastic moduli of 42.0 ± 2.8 kPa, 65.3 ±8.0 kPa, 78.2 ± 8.4 kPa, and 121.5 ± 11.9 kPa, respectively. The volumetric swelling ratio was shown to be inversely proportional to the precursor concentration. The addition of cell adhesion proteins, such as RGD peptides, resulted in a decrease in the shear modulus (G') of the hydrogel, as the peptides take up PEG arms which are potential crosslinks. This slight compromise to the structural integrity is relevant when tuning *in vitro* 3D extracellular environments to desired conditions.

Cardiac fibroblasts (CFs) and cardiac myofibroblasts (MFs), the latter obtained through stimulation with transforming growth factor-beta 1 (TGF-β1) of CF, were cultured and embedded in 3D PEG hydrogel matrices. PEG was supplemented with RGD peptides to provide cellular adhesion points, imitating the native myocardial environment. The intracellular stiffness of the embedded cells was quantified through passive mitochondrial particle tracking.

We investigated the isolated effect of soft (4% m/v) and stiff (10% m/v) matrices on the stiffness of CFs and differentiated MFs. An increase in cell stiffness with was observed with an increase in matrix stiffness from soft to stiff PEG gel, with α = 0.19-0.36 through all delay times for cells in soft matrices and α = 0.09-0.18 throughout all delay times for cells in stiff matrices ($p \leq 0.05$) for both standard CFs as well as for maladaptive MFs. This direct proportionality confirms that CFs behave according to the principles of mechanotransduction, using cytoskeleton-based rigidity-sensing mechanisms between themselves and their environment, and as a consequence, their inherent stiffness is regulated by the rigidity of their environment. No considerable difference of cell fluidity was found between cell phenotypes (CF & MF) in soft matrices. In stiff matrices, MFs seemed to become somewhat stiffer across the delay times, although with no significant effect.

The knowledge of the extent to which the mechanics of cardiac fibroblasts and myofibroblasts and their ECM are interrelated is essential for the understanding of pro-fibrotic mechanotransduction and ECM production to prevent, attenuate and reverse cardiac fibrosis.

Acknowledgements

This research was funded from the South African Medical Research Council (Grant SIR 328148, PI: T Franz) and the National Research Foundation of South Africa (grant UID 93542, PI: T Franz). Views and opinions expressed are those of the author and not of the funding organizations. The Max and Lillie Sonnenberg scholarship for international travel of the University of Cape Town provided funding for an international research visit.

From the Cardiovascular Research Unit (CVRU) at the University of Cape Town, I would like to humbly thank Mrs Helen Ilsley (Senior Histologist) for giving me training in cell culture and teaching me the sanitary conventions of the tissue culture laboratory. Mrs Ilsley was ever willing and present to give me advice and assistance with my lab-work; be it cell growth and proliferation, antibody treatments, or preparing for my differentiation assays. From the CVRU I would also like to acknowledge Ms Sibu Maseko, a PhD candidate in Biomaterials, for demonstrating to me how to use the rheometer and how to prepare PEG hydrogel samples of the appropriate size and shape for this mechanical testing.

From the Confocal and Light Imaging Facility at the University of Cape Town, I would like to thank Mrs Susan Cooper for training and briefing me in confocal and fluorescent microscopy, overseeing my sessions, and for facilitating a well-organised, uninterrupted and reliable microscope booking system. I would also like to thank Dr Dirk Lang for explaining to me the practical theory behind MPT microrheology and how to select the optimal imaging settings to record my experiment.

From the Experimental Continuum Mechanics group at the ETH Zurich (Swiss Federal Institute of Technology), I would like to thank Professor Eduardo Mazza for allowing my visit to them. To Dr Raoul Hopf, thank you for inviting me and setting up what was an enriching studying experience for me. Your enthusiastic, inquisitive and pragmatic approach to the work inspired me, and your teachings helped me to gain new and valuable practical insights into the intricate mechanics of soft materials. I thank Dr Aldo Ferrari and Dr Costanza Giampietro for welcoming me into their laboratory and guiding me in performing TFM on endothelial cells, work that is not being presented in this dissertation, but that formed part of my research visit.

A sincere thank you to Professor Thomas Franz, from the Mechanobiology group of the University of Cape Town, for being an excellent and committed supervisor from the onset and throughout. Your subtle guidance and strong vision gave me the direction I needed. You often gave me just enough insight and advice for me to proceed independently with new clarity and focus. It has been an honour to learn under you.

To my co-supervisor, Associate Professor Neil Davies, from the CVRU at the University of Cape Town, I express gratitude for introducing me to the cellular biology field and for giving me the support to undauntedly bridge into cell-based work with my mechanical engineering background. When I needed advice about cellular biology and polymer science, in terms of cardiac fibroblast cells and polyethylene-glycol hydrogels respectively, you had the answers. I am happy to have gained this knowledge through your input.

In addition, from the Mechanobiology group at the University of Cape Town, I thank Ms Ghodeejah Higgins (PhD candidate in Mechanobiology) for offering me preliminary council regarding MPT microrheology, which helped me plan my experiments. Furthermore, her assistance with the software analysis, post-processing, and analysis of my results was invaluable to me. I also thank the entire Mechanobiology-lab group for their input towards my work during presentations. Thank you to Ms Lee Kruse and Ms Juliet Nagawa for your informative lessons about statistics, null hypotheses, and

Two-way ANOVA tests. The group's habitual tea and cupcake meetings would also provide me with the calmness and the sanity to carry on with the work, and for that, I am thankful.

Thank you to my splendid parents, Paul and Reinette Haasbroek, and my sister Anelza Haasbroek, for your love, support and genuine care throughout this time. You offered me the means and the upbringing that got me to where I am today. To the lovely Ms Inge Roeloffze, thank you for bearing with me from the start of this degree, and for putting my best interests first, when I (occasionally) placed the interests of this project first.

This dissertation has been an enhancing and transformative journey for me. While there were gruelling times, it was a period where I explored many new fields and tapped into vast spheres of knowledge. I have truly learned what it means to do research, and it has led me to fully comprehend the excitingly endless possibilities that exist in discovering our natural world through scientific interest and genuine curiosity. The people mentioned above provided me with the necessary advice, guidance and mentorship that I needed at the various stages of this study, and to them, I am eternally grateful. Lastly and importantly, I would like to thank God, who gave me everything I have and who enabled me every day to pursue this degree.

Table of Contents

List of Figures

List of Tables

Abbreviations

α-SMA	Alpha Smooth Muscle Actin
2D	Two-Dimensional
3D	Three-Dimensional
ANOVA	Analysis of Variance
CF	Cardiac Fibroblast
CVD	Cardiovascular Disease
Cy-3	Cyanine 3
DAPI	4′,6-diamidine-2′-phenylindole
DMEM	Dulbecco's Modified Eagle Medium
DTT	Dithiothreitol
EC	Endothelial Cell
ECM	Extracellular Matrix
EDTA	Ethylenediaminetetraacetic Acid
FBS	Foetal Bovine Serum
FEA	Finite Element Analysis
HFpEF	Preserved Ejection Fraction
HFrEF	Reduced Ejection Fraction
LAP	Linear Assignment Problem
LoG	Laplacian OF Gaussian
MF	Myofibroblast
MI	Myocardial Infarction
MMP	Matrix Metalloproteinase
MPT	Mitochondrial Particle Tracking
MSD	Mean-square Displacement
MTGr	Photomultiplier Tube – Green
PBS	Phosphate Buffered Saline
PEG	Polyethylene Glycol
Pen-strep	Penicillin-streptomycin
PTFE	Polytetrafluoroethylene
RGD	Arginylglycylaspartic Acid
SI	Semi-infinite
TGF-β1	Transforming Growth Factor Beta 1
TIFF	Tagged Image File Format
TMPT	Transmission Photomultiplier Tube
UA	Uni-axial
VS	Vinyl Sulphone
XML	Extensible Markup Language

1. Introduction and Background

Myocardial infarction (MI) is defined as cell death due to sustained myocardial ischaemia, as a consequence of a perfusion imbalance between oxygen supply and demand to the heart (Bax *et al.* 2012). MI is an event that stems from a chronic cardiac disease known as coronary atherosclerosis, or coronary artery disease (CAD). MI is most commonly caused by the ischaemia that results from the rupture of an atherosclerotic plaque in the coronary arteries that supply heart tissue with oxygenated blood (Thygesen *et al.* 2018). The occluded vessel, if not rapidly treated, will result in death or loss of heart function that can lead to heart failure (Deleon-Pennell *et al.* 2017).

MI is the primary cause of morbidity and mortality worldwide, with an estimated 7 million people suffering from all forms of acute MI each year (Statistics South Africa 2018). Recently, a shift has occurred in the incidence of MI from being more predominant in developed countries to become increasingly more common in developing countries (White and Chew 2008). Developing countries are subject to rapidly increasing urbanisation and growing economies, causing lifestyle changes which are directly correlated to progressive rates of illnesses such as obesity, diabetes and coronary heart disease.

A plethora of impairments develop after myocardial infarction, and contemporary medical interventions only partially address these. Acute myocardial infarction results in adverse remodelling of the myocardium, eventually leading to contractile dysfunction and chronic heart failure. Collectively, the formation of fibrotic scar tissue in the left ventricle inhibits its contractile function to eject blood, and the lowered ejection in effect causes a loss in cardiac output. This cardiac output loss could lead to what is known as systolic heart failure with reduced ejection fraction (HFrEF). Heart failure may also occur through a preserved ejection fraction (HFpEF), when the cardiac fibrosis increases the myocardial stiffness impairing its distensible function reducing the filling capacity of the ventricle (Tschope and Lam 2012).

Cells respond mechanically, as well as biochemically, to their environment; however, comparatively less is known about cellular mechanical processes than about biochemical processes. How these different processes converge, interact and influence each other is even less well understood. Mechanical stimuli have emerged as ubiquitous regulators of normal physiological processes, contributing to the orchestration of embryogenesis, cell differentiation, wound healing and extravasation of immune cells, for example (Janmey and Miller 2011). Abnormal tissue and cell mechanics can be implicated in a variety of pathologies. Mechanical phenomena have roles to play in cancer progression, cardiovascular disease, malaria and fibrotic disease (Suresh *et al.* 2005, Wells 2013)

A deeper understanding of the mechanics of cardiac fibroblast and endothelial cells is required to develop robust and accurate models of single-cell mechanics in the context of myocardial infarction. Specifically, the role of mechanical phenomena in the transition from a physiologically healthy phenotype to a maladaptive, reactive phenotype needs to be clarified. Distinguishing protective mechanobiological processes from reactive/maladaptive ones will guide the development of targeted therapeutics. Characterising the physical properties of cells is essential for understanding and modelling cellular and tissue response to mechanical cues. In the context of injectable biomaterial and cell therapeutics, it is crucial to understand the effects of the microenvironment on cellular mechanobiology. Such knowledge will instruct the design of materials which can provide a mechanical niche that promotes beneficial rather than adverse remodelling, to reverse or attenuate the danger presented by MI.

1.1. Mechanical Interactions of Cells with their Environment in 2D and 3D

Cells respond to mechanical signals by generating “cell-matrix”, and “cell-cell” contact forces exerted back to their external environment. Many cell functions such as motility, proliferation, and differentiation that are conventionally thought to be controlled by chemical signals alone are also affected by mechanical inputs. These mechanical inputs are typically fluctuations in the stiffness of the extracellular environment. However, the primary mechanism(s) that cells use to detect the stiffness of their surrounding matrix remains mostly unclear and has only recently become a subject of investigation (Janmey and Miller 2011).

Cells do not behave mechanically according to any single, descriptive mechanical model. A major theoretical challenge in the field of cellular mechanobiology is to adapt or develop a model that describes, with an acceptable degree of accuracy and predictive capability, the mechanical behaviour and resulting physiological response of cells. Such a model should account for stress-dependent stiffening and weak power-law rheology, two observed phenomena which have not been successfully described by a single model (Hoffman *et al.* 2006).

Adhering cells actively probe the stiffness of their environments as they anchor and pull at mechanotransduction sites. During biological processes, cells exert traction (surface) forces at these areas of focal adhesions. The stress sensed at adhesion sites are directly proportional to the substrate “rigidity”. This proportionality is because of a more rapid accumulation of traction forces for larger substrate stiffnesses. It has furthermore been proven that the mechanical rigidity-sensing is facilitated by a non-local, large-scale mechanism originating in the cytoskeleton (Trichet *et al.* 2012). Traction forces originate from actomyosin interactions within the cell, are balanced primarily by the actin cytoskeleton, and are exerted by the single cell to its substrate (Califano and Reinhart-King 2010).

This cytoskeleton-based rigidity-sensing mechanism is visualised in Figure 1.1. Normal cells that adhere to a soft substrate display a smaller magnitude in traction/actuating force than cells adhering to a stiff substrate. This trend is effectively illustrated due to an increase in focal adhesion size and number (red dots), as well as the increased number cytoplasmic actin fibres (green arrows) present in the activated cell. The presence of actin is a major determinant of a cell’s mechanical properties, and therefore the cumulation of actin fibres in cells subjected to stiffer environments indicate that the cells themselves are stiffer (Byfield *et al.* 2009).

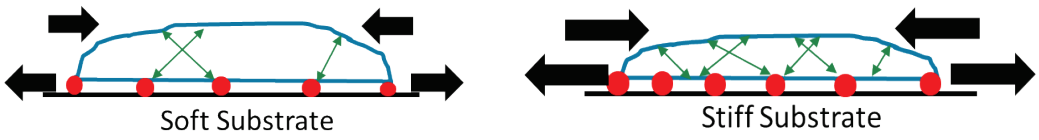

Figure 1.1. An illustration showing the responses of cells to soft and stiff matrices due to cellular cytoskeletal-based rigidity-sensing mechanisms. Cells adhered to a soft substrate (LEFT) exhibit smaller actuation forces (black arrows), and less intracellular stress fibres (green arrows) than those adhered to a stiff substrate (RIGHT).

The trend observed in changes in stiffness in the two-dimensional (2D) environment is similarly observed in the three-dimensional (3D) environment, since a 2D geometry is generally a simplification of the 3D environment experienced by cells *in vivo*. For example, Byfield *et al.* (2009) reported that endothelial cell stiffness is regulated by both the *in vitro* extracellular environments of a 3D surrounding collagen gel, as well as a 2D underlying surface of collagen-coated polyacrylamide gels.

1.2. Cardiac Fibroblasts, Myofibroblast and Endothelial Cells in Myocardial Infarction

Atherosclerosis with the threat of subsequent myocardial infarction is the most prevalent cardiovascular disease and compromises the core functionality of the cardiovascular system (Frostegård 2013). At the cellular level, apart from the loss of cardiomyocytes, two other kinds of cells play significant roles in MI, from the onset and throughout the progression of the disease.

Firstly, cardiac fibroblasts are the effector cells in the myocardium that regulate the physical structure and their phenotype, myofibroblasts, that control the progression of MI.

Secondly, endothelial cells regulate the vascular flow of blood throughout the body, including the regions affected during MI. Mechanotransduction within the cardiovascular system has been extensively investigated but is still not fully comprehended (Chen 2008, Hoffman *et al.* 2006, Trichet *et al.* 2012). It is well recognised that haemodynamic shear stress regulates atherosclerosis progression and the arterial endothelial cell phenotype (Zaragoza *et al.* 2012).

1.2.1. Cardiac fibroblasts and myofibroblasts

Cardiac fibroblasts (CFs) account for up to 70% of cells in the adult heart, thus being the most abundant cell type in the myocardium. They are linked mechanically, biochemically and electrically to cardiomyocytes and mainly responsible for the maintenance of the cardiac extracellular matrix (ECM) architecture, i.e. deposition of ECM (Mackenna *et al.* 2000). This crosstalk between the cardiomyocytes and cardiac fibroblasts exists to maintain homeostasis and for the heart to adapt to physiological changes that occur due to cardiac load, e.g. during exercise (Rohr 2012). The matrix protects adherent cardiac myocytes from sarcomere overstretching and sequesters and releases cytokines by mechanically regulated processes.

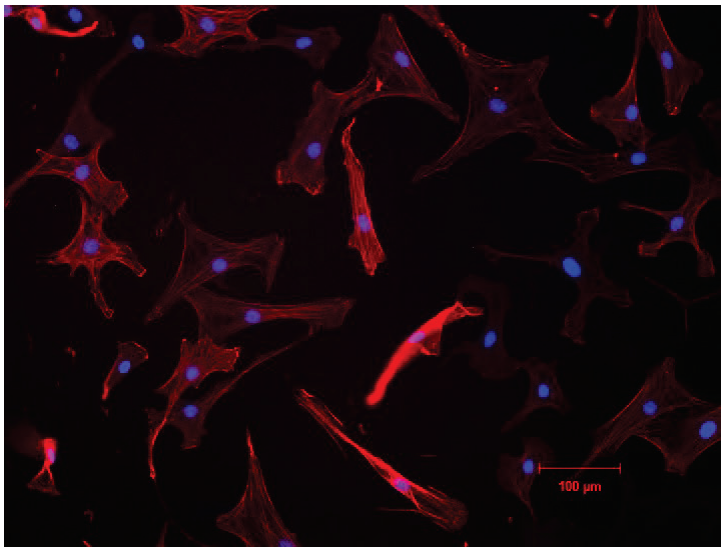

Figure 1.2. Fluorescent microscope image of Adult Rat Cardiac Fibroblast Cells isolated in vitro, with immunolabelled nuclei (blue) and cytoplastic smooth muscle actin fibres (red), portraying their general elongated structures and spindle-like shapes.

As a population, cardiac fibroblasts are heterogeneous and will alter their phenotype and number depending on the developmental stage as well as in response to injury. After an ischaemic insult, resident CFs and a few other cell types such as endothelial cells, pericytes and bone marrow-derived

cells can be induced to take on an activated phenotype and are then referred to as myofibroblasts (Weber *et al.* 2013). They are highly responsive to inflammatory and proliferative signals and play a vital role in strengthening the myocardium after the massive loss of cells following MI and preserving the structural integrity of the tissue. However, pathological remodelling occurs when these activated cells persist beyond the initial, beneficial stage of reparative/adaptive fibrosis (Lajiness and Conway 2014). Their continued presence, both within the infarcted tissue and in the surrounding tissue, results in the excessive formation of a maladaptive fibrotic scar (reactive fibrosis). Excess deposition of cardiac ECM has been closely linked to pathophysiological mechanical overloading and eventual heart failure (Mackenna *et al.* 2000).

The multi-step process of cardiac myofibroblast (MF) activation is initiated by stress fibres that form from cytoplasmic actin and myosin in response to mechanical stress. Such stress fibres terminate in transmembrane integrin-containing adhesions sites on activated proto-myofibroblasts (see image Figure 1.3) that are also extracellularly trussed to the surrounding extracellular matrix to transmit and perceive stress (Chen *et al.* 2016). Further stiffening and straining of the ECM develop larger, 'super mature' focal adhesions together with more robust substrate adhesions that mediate high mechanical stress and the release of transforming growth factor-beta 1 (TGF-β1), which promotes the integration of α-smooth muscle actin (α-SMA) into fibres (Figure 1.3) (Dugina *et al.* 2001, Goffin *et al.* 2006). Consequently, the high concentration of α-SMA in stress fibres is widely used to identify and diagnose the functional and fully developed myofibroblasts. This high concentration can be clearly distinguished with the light blue stained α-SMA in the two images in Figure 1.4.

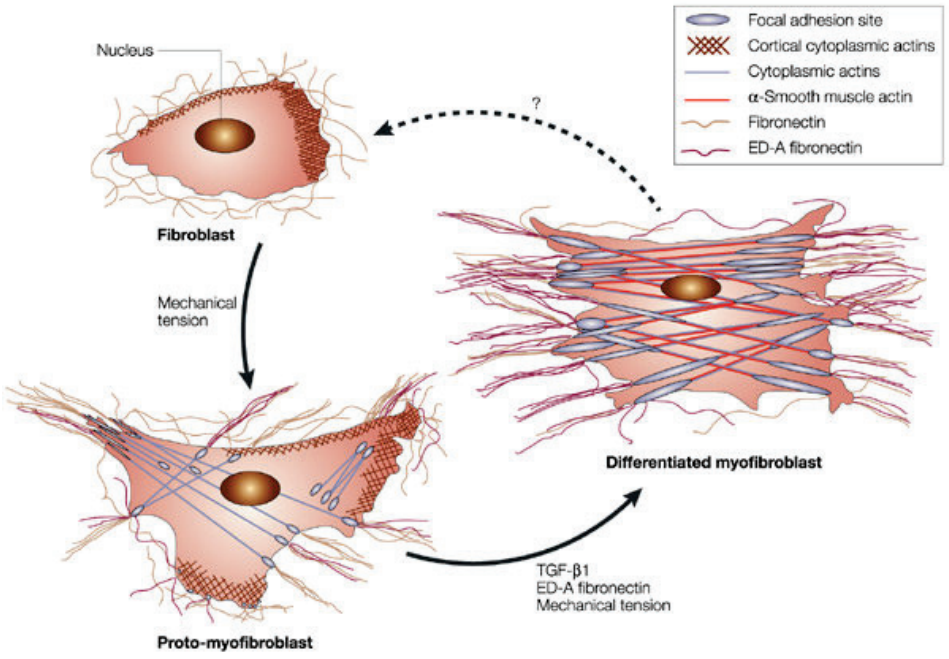

Figure 1.3. The two-stage model of myofibroblast cell differentiation. In healthy tissues in vivo, fibroblasts contain cortical cytoplasmic actin fibres, without stress fibres or large focal adhesion complexes. Under mechanical tension such as stress from injury, fibroblasts differentiate in proto-myofibroblasts, forming cytoplasmic actin-containing stress fibres. These express cellular fibronectins, including an ED-A splice fibronectin variant from their surfaces to generate contractile force. Further mechanical force, together with the release of transforming growth factor-beta 1 (TGF-β1), stimulate transformation into fully differentiated myofibroblasts, characterised by the internal expression of smooth muscle actin in more widespread stress fibres, and extensive, super mature focal adhesions. With permission from Tomasek et al. (2002).

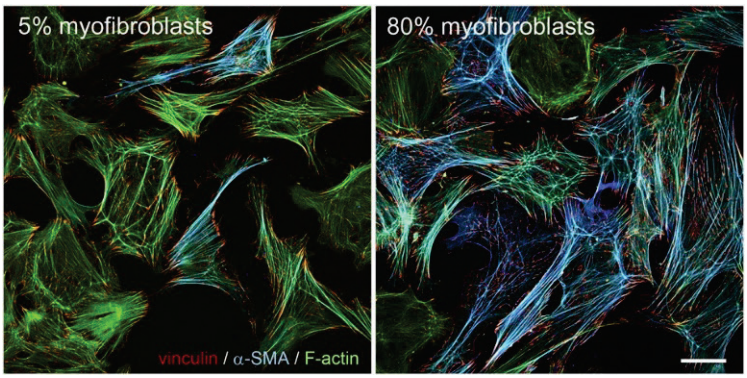

Figure 1.4. Fibroblasts in a healthy (left) and fibrotic (right) rat myocardium showing the transcendence of myofibroblasts identified by the presence of immunostained α-SMA. With permission from Van Putten et al. (2016).

In the interest of understanding how normal healthy CFs and MFs might function *in vivo*, it is vitally important to recognise how they might react/behave in a passive environment, as a result of the stiffness of the extracellular matrix or substrate alone.

1.3. The Role of the Extracellular Environment in Cardiovascular Tissue Degeneration

The mechanical environment of a cell is shown to be a key regulator of its functions. This is demonstrated when cellular functions like motility, proliferation, and differentiation can be altered by changes in the substrate stiffness that cells adhere to while the chemical environment remains unchanged. Clinical and animal studies have shown that such mechanical environmental changes have the potential to address specific disease characteristics and that for example, restoring normal tissue mechanics may avert cell dysfunction (Janmey and Miller 2011).

Furthermore, the mechanical properties of the extracellular environment determine not only cellular mechanical properties like stiffness and contractibility but also its phenotype. As such, the degeneration of tissue-level structures within the heart and endothelium layers of blood vessels is closely linked to the state of the extracellular environment.

1.3.1. Cardiac fibrosis

The cardiac ECM has the principal function of providing structural support to cells and is represented by a three-dimensional assortment of active molecules such as proteins, proteoglycans and polysaccharides. It also binds soluble ligands and transmembrane receptors to provide mechanosensitive cellular adhesion and the spatial coordination of signalling processes which govern cellular functions (Byron *et al.* 2013, Chang *et al.* 2016)

Following an ischaemic insult, necrotic cardiomyocyte death occurs, eliciting an inflammatory response which initiates the first phase of post-infarction ventricular remodelling. The inflammatory phase is followed by proliferative and maturation phases, resulting in the formation of a fibrotic scar with markedly different mechanical and biochemical properties to normal myocardium. Throughout each phase, cardiac fibroblasts and activated myofibroblasts play a central role in orchestrating and actively remodelling the damaged tissue while being exposed to a multitude of mechanical and biochemical signals (Janmey and Miller 2011, Wells 2013). Cardiac fibrosis is characterised by the

excessive accumulation of collagenous ECM. More specifically, the unregulated production post-translational alteration, enzymatic processing and turnover of collagens (mainly types I and III) (Gyongyosi *et al.* 2017, Rienks *et al.* 2014).

To date, there is no effective anti-fibrotic therapy due to the lack of knowledge on the functionality of the cardiac fibroblast. This issue renders the myofibroblast the most anticipated therapeutic target for cardiac fibrosis. Thus, understanding pro-fibrotic mechanotransduction signalling pathways in cardiac fibroblasts and processes leading to ECM production and accumulation is essential in preventing, attenuating and reversing cardiac fibrosis (Gyongyosi *et al.* 2017). The extent to which the mechanics of cardiac fibroblasts, myofibroblasts and the ECM are interrelated is therefore fundamentally important information.

Due to the dynamic functional properties of cardiac muscle, cells are continuously subjected to different types of mechanical forces, and the consequent stresses and strains are three-dimensional and non-uniform. The elastic modulus, or stiffness, is the extent to which a material resists deformation in response to an applied force. ECM stiffness is largely determined by the crosslinking of collagen fibres, whereas cell stiffness is determined by prestressing (López *et al.* 2012, Wang *et al.* 2002). The prestress within a cell is the balance between the tension in cytoskeletal fibres and the compression by cytoplasmic pressure. The stiffness for a normal and healthy myocardium is 10-15 kPa, while that of fibrotic myocardium is in the range of 20-100 kPa (Engler *et al.* 2008).

1.4. Biomaterials for Engineered 3D Extracellular Environments

Hydrogels are three-dimensional networks of hydrophilic polymers that can retain large quantities of water relative to their mass and are used especially in biomedical applications. They can be designed to augment or replace tissues, organs or functions in the body (Drury and Mooney 2003, Peppas and Hoffman 2013). Recent research has focussed on applying specific functionality to hydrogels with properties beneficial to their application (Yesildag *et al.* 2019).

Natural ECMs are extensively hydrated, a property that can be mimicked by synthetic hydrogels (Lutolf MP and Hubbell 2005). Mechanically, this hydrated network allows the ECM or hydrogel to resist compressive stresses. Crosslinked hydrogel networks can also be designed to mimic tissue-like properties such as viscoelasticity and interstitial fluid flow. Engineered polyethylene glycol (PEG) hydrogels have been successfully used as ECM-mimetic substrates for *in vitro* and *in vivo* experimentation (Dobner *et al.* 2009, Kadner *et al.* 2012, Raeber *et al.* 2005) in MI studies. Integrin-binding sequences are incorporated into the gels, allowing cells to bind to and exert forces on the hydrogel matrix.

Extracellular mimetic hydrogels permit cell-controlled invasion. Essentially, synthetically engineered matrixes with distinct protease-specific degradation create an *in vitro* environment that favours the invasion of one cell type over another (Bracher *et al.* 2013). Studies have shown, for example, that fibroblasts embedded in hydrogels crosslinked with matrix metalloproteinase (MMP) sensitive peptides could migrate within the biomaterial whereas the cells could not migrate in hydrogels polymerised with plasmin sensitive peptides (Raeber *et al.* 2005). Hydrogels can thus be designed to allow certain cell-type ingrowth with the use of MMP specific peptides and by altering the protease specificity of the crosslinking peptide sequences.

1.4.1 Mechanical properties of PEG-based biomaterials

PEG-based hydrogels are especially desirable due to their non-toxicity, non-immunogenicity, and bio-inert characteristics (Zalipsky and Harris 1997). The mechanical properties of PEG hydrogels can be varied by modulating the molecular weight and concentration of the PEG precursor/macromer, the crosslinking density and the synthetic procedure. Armed or branched PEG variants, such as 8-PEG-VS (Figure 1.5), with the appropriate end groups, could be tuned to possess multiple functions. Certain end groups crosslink (via covalent chains) with other PEG molecules, whereas others are left for additional functionalities, for example, cell adhesions sites.

Material	**8-arm PEG Vinyl Sulfone (8PEG-VS)**
Structure	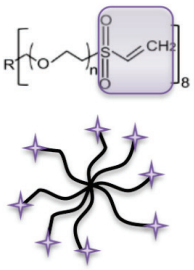
M_W [Da]	20k
Chain length	n ~ 40
State at r.t.	Solid
Gel formation	UV or Michael type addition (non-degradable)

Figure 1.5. Properties of PEG-VS macromer used as an element for preparing PEG-based hydrogel (Yesildag et al. 2019)

The properties of a hydrogel are governed by its polymer structure, and its mechanical behaviour can theoretically be understood using the theory of rubber elasticity (and viscoelasticity). This tendency is because in their swollen state (full water-retention to the point of equilibrium), hydrogels, however weak, generally satisfy the criteria of rubber in that they respond to stresses nearly instantaneously and with fully reversible deformation. Like rubbers, hydrogels are lightly crosslinked networks with relatively large free volumes which allows for such response to external stresses with rapid rearrangement of their polymer segments. Internal entropic changes govern the extensibility and recovery of the polymeric structure of the hydrogel (Anseth *et al.* 1996).

The mechanical properties of PEG hydrogels are typically modulated by the molecular weight and the concentration of the PEG precursor. The concentration is defined by the weight of solid PEG macromer (w_{PEG}) over the volume of buffer solution (v). At constant concentration (m/v), lower molecular weights result in tensile failure at lower strain, i.e. more brittle behaviour. In addition, an increase in molecular weight also drastically decreases the elastic (tensile) modulus (Figure 1.6 a). A higher concentration of PEG will also cause higher elastic (tensile) modulus, as shown in Figure 1.6 b as E_{ten}, where molecular weight was kept constant. The same pattern is found when measuring the compressive modulus (Nguyen *et al.* 2012).

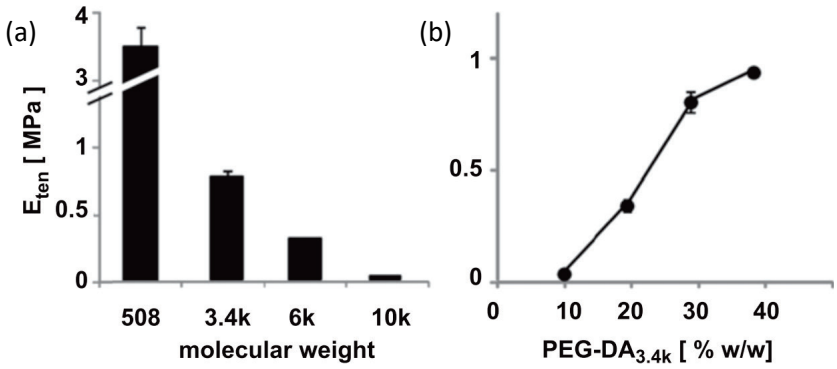

Figure 1.6. Variation of equilibrium tensile modulus, E, with (a) molecular weight (constant concentration) and (b) concentration (constant molecular weight). With permission from Nguyen et al. (2012).

The stiffness of ECMs and substrates are usually quantified as elastic modulus (describes a material's resistance to deformation) defined as the ratio of stress to strain. More specifically, the elastic modulus (E) is often used to quantify elastic resistance to deformation due to tension or compression. The shear modulus (G) is used to describe the resistance of a material to deformation in shear. When considering the dynamic mechanical properties, shear testing is typically applied to hydrogels, and the storage (elastic) (G') and loss (G'') moduli are measured.

Both the PEG molecular weight and the crosslinker concentration can be used to alter the shear modulus since the hydrogel shear modulus is directly related to the molecular weight between crosslinks, based on thermodynamic principles. These principles predict that an increase in the density of the crosslinks will decrease the shear moduli of the corresponding hydrogel. Indeed, tensile testing has confirmed that changes in the PEG concentration will have a directly proportional effect on the elastic modulus. However, this effect diminishes as the molecular weight between crosslinks is increased, i.e. the crosslinker-to-PEG ratio (Parlato *et al.* 2014).

1.4.2. 2D and 3D extracellular environments *in vitro*

There is a growing acknowledgement of the profound effect that the mechanical stiffness of the local environment has on cellular function. Many experiments have been performed two-dimensionally (2D), where cells were grown on top of substrates of varying stiffness, which generally serves as a simplification of a three-dimensional (3D) environment that cells experience in vivo (Byfield *et al.* 2009). However, it is often unclear how a given response to changes in cellular stiffness in 2D correlates to changes in 3D.

We have looked to create extracellular environments with dimensionalities that are near representative of the cells' native environment where possible. Cardiac fibroblasts (CF), for example, exist within a 3D extracellular network, whereas endothelial cell (EC) monolayers that line the intimal layer of blood vessels exist in 2D networks.

Endothelial cells can spontaneously assemble into 2D stress fibre networks, like their native monolayers, using extracellular matrix cues. Like with CFs, it is well accepted that both matrix mechanics and chemistry affect EC spreading and monolayer formation. More particularly, the ECM includes collagen and fibronectin that provide chemical and mechanical cues that drive invasion and migration for vessel formation. Fibronectin is typically added to gel substrates for ECs to adhere to

when seeded, which will allow cell-substrate connection and mechanosensing. Substrate mechanics have a direct effect on ECs' in vitro organisation, and the rigidity of the substrate promotes cytoskeletal and focal adhesion organisation (Califano and Reinhart-King 2008, Engler *et al.* 2004). ECs also have an increased spread area with more apparent actin stress fibres with increasing substrate stiffness (Yeung *et al.* 2005).

In cell culture, creating a 2D environment involves manufacturing a continuous layer hydrogel matrix. This is achieved by preparing hydrogel substrates before seeding cells. Gel mixtures of desired concentrations are pipetted onto the glass surface of an experimental container and immediately covered by a glass coverslip. Once the hydrogel is synthesized, and gelation had occurred, the coverslip is removed, and cells are seeded and left to adhere to a single plane (Figure 1.7). Previous studies that typically measure the effects of substrate stiffness on ECs will create polyacrylamide (PA) gels of 2.5 to 10 kPa in stiffness, that mimics the range of mechanical properties of subendothelial matrices from young to aged blood vessels (Califano and Reinhart-King 2010, Huynh *et al.* 2011, Kohn *et al.* 2015, Krishnan *et al.* 2011).

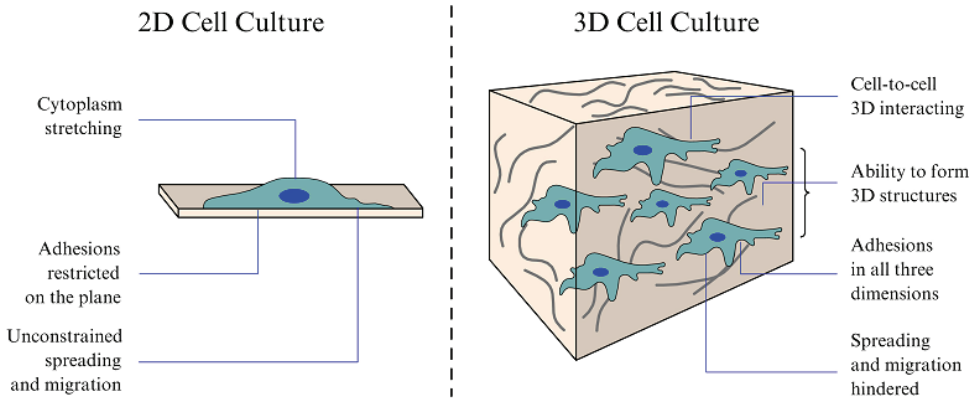

Figure 1.7. An illustration comparison the main differences between 2D and 3D cell culture, presenting the behaviour and constraints of cells plated on a slide (2D) compared to cells cultivated in a matrix (3D) (Ustyugov et al. 2018).

When considering cardiac fibroblasts, it is appropriate to consider physiologically more relevant 3D matrices. When grown in 2D, fibroblasts adopt a flat morphology, and due to unconstrained spreading and migration, they display prominent actomyosin stress fibres for contraction. In contrast, fibroblasts embedded in 3D matrices adopt their native spindle-like morphology, commonly lack stress fibres and distinct focal contacts, and move through integrin-dependent processes linked to matrix re-assembly (Walpita and Hay 2002). The crosslinked insoluble hydrophilic network that a hydrogel provides, is widely used to mimic ECMs in 3D due to their biophysical (e.g. porosity, branched vasculature) and mechanical (e.g. stiffness, viscoelasticity) properties that can be precisely designed. The fact that CFs are constrained in three directions means that they will be able to take up an innate configuration. Some challenges exist with 3D hydrogel matrices, such as replicating the inhomogeneous and anisotropic properties of native ECMs (Gillette *et al.* 2008).

When creating a 3D cell culture, a hydrogel monomer is prepared at the desired concentration, and all constituents are added for crosslinking to take place. An adhesion peptide such as arginylglycylaspartic acid (RGD), is then added to be covalently bonded to the matrix, due to its effectiveness in promoting cell attachment in biomaterials, followed by the addition of the desired number of cells to be embedded in the hydrogel (Bellis 2011). Finally, the gel-cell mixture is pipetted into test sample configuration and incubated, during which gelation occurs.

1.5. Quantification of Cell Mechanics in 2D and 3D Extracellular Environments

The importance of understanding cell mechanics and cell responses to mechanical stimuli has emerged. However, how to best measure, interpret and model the mechanical properties of cells remains unclear (Hoffman *et al.* 2006). Characterising and quantifying the physical properties of cells is essential to model the cellular and tissue response to mechanical stimuli properly. There are different methods to study cell mechanics. Some utilise force application such as optical techniques, cantilever manipulation (e.g. Atomic Force Microscopy – AFM), acoustic and flow techniques, and micropipette aspiration (Rodriguez *et al.* 2013). A different group of techniques make use of microrheology, such as passive Particle Tracking Microrheology (PTM), whereas others measure cell mechanics through force sensing, such as Traction Force Microscopy (TFM). (Moeendarbary and Harris 2014, Rodriguez *et al.* 2013). This section focusses on the latter two examples of methods mentioned, as they are the most suitable to be used in this research.

1.5.1 Passive mitochondrial particle tracking microrheology

Many methods to assess the mechanical properties of cells are based on rheological characterisation with external probes. These include AFM, magnetic twisting, micromanipulation, or optical stretching (Shen *et al.* 2013). These methods are suitable for 2D adherent cells, but they cannot measure the mechanical response of cells embedded in a 3D matrix as they require direct contact to the cell surface. Thus, one major shortfall of most of these cell rheological techniques is that they require external intrusion to measure cell mechanics.

Microrheology is a category of techniques employed to measure the rheological characteristics of a medium through recording particle trajectories. Moreover, passive particle tracking microrheology is an emerging technique used to non-invasively probe the mechanical properties of individual cells, where no external forces are applied, and the particle motions are intrinsic to the surrounding material. Such intrinsic motions result from thermal energy or molecular motors (Mak *et al.* 2014).

Particle tracking microrheology utilizes Brownian motion of embedded particles to probe the local mechanics of soft materials by measuring their viscoelastic responses to external cues. This technique is represented in Figure 1.8, where embedded tracer beads are microscopically tracked over time, and each particle's trajectory is found and used to describe the overall motion regulated by the cell. Three other cell rheology techniques include Magnetic Twisting Cytometry (active), Internal Laser Tracking Microrheology (passive) and External Laser Tracking Microrheology (passive) (Hoffman *et al.* 2006).

Often, such particles are fluorescent microspheres delivered/embedded into cells, by ballistically injecting them into the cytoplasm of cells as in the case of Figure 1.8. Such complicated and potentially damaging particle introduction measures could be eluded by instead tracking naturally present cytoplasmic particles, such as mitochondria. Hence, passive mitochondrial particle tracking (MPT) is a sub-technique that is used record spatial fluctuations of tracer particles (the mitochondria) that are displaced due to the thermal energy of the surrounding medium (Mak *et al.* 2014, Selvaggi *et al.* 2010, Tseng *et al.* 2002). Mean-squared displacement (MSD) profiles are mapped to describe the particle dynamics and subsequently transformed to fluidity (stiffness) profiles and viscoelastic parameters, such as the storage and loss moduli of the surrounding medium (Tseng *et al.* 2002). Endogenous mitochondria serve as tracer particles due to the relative ease of non-invasive fluorescent labelling process and as no specialized tracer particle delivery systems are required.

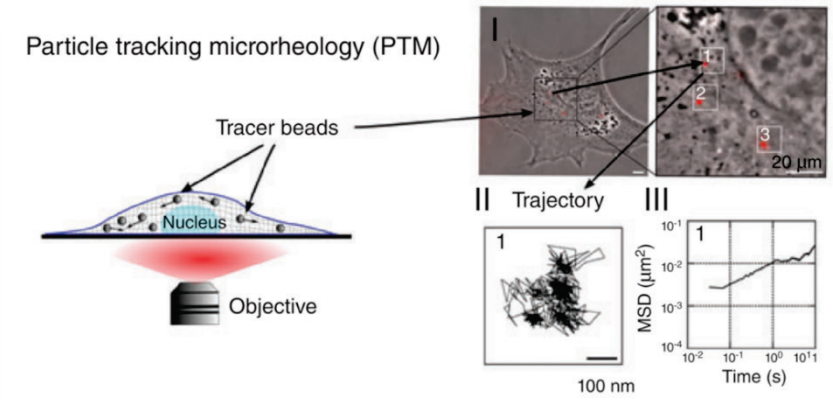

Figure 1.8. A Schematic diagram depicting 2D Particle Tracking Microrheology with tracer particles dispersed within the cell's cytoplasm following injection. Confocal microscopy with a high magnification objective is used to a single isolated fibroblast cell, with fluorescent tracer beads injected into the cytoplasm. The displacement trajectory of each bead tracked and described as a Mean-Square Displacement (MSD) profile over time. With permission from Moeendarbary and Harris (2014).

In the pursuit to construct tracer particle trajectories, microscopic time-lapse images of cells are recorded and undergo software-based frame-by-frame tracking analysis. A multiple particle tracking technique is favoured as the analysis of many particles offers the generation of a more accurate average MSD in a single MPT measurement. The dynamics of each particle is described by the time-dependent mean-square displacement, shown in Eq. 1 (Selvaggi *et al.* 2010):

$$\langle \Delta r^2(\tau)_{xy} \rangle = \langle [x(t+\tau) - x(t)]^2 + [y(t+\tau) - y(t)]^2 \rangle \quad (1)$$

where, $\Delta r^2(\tau)_{xy}$ refers to the 2D MSD of particle trajectories, the brackets $\langle \dots \rangle$, indicates the ensemble and time average. $x(t)$ and $y(t)$ refer to the spatial coordinates at time t, and τ refers to the lag time between the particle positions. In the case of viscoelastic materials, MSDs scale nonlinearly with time according to a power law, shown in Eqn. 2 below. The power law coefficient, α, known as the diffusivity coefficient, is a representative of the type of motion the particle undergoes.

$$\langle \Delta r^2(\tau) \rangle \sim t^{\alpha} \quad (2)$$

The schematic in Figure 1.9 shows the progression of the mechanical characterisation of cells using particle tracking, from tracked time-lapse images the trajectories of each particle and the correlating MSD profiles. From here, an average MSD profile can be deduced for a specific experimental condition, rendering an α value which would indicate the motion regime and subsequently, cellular stiffness.

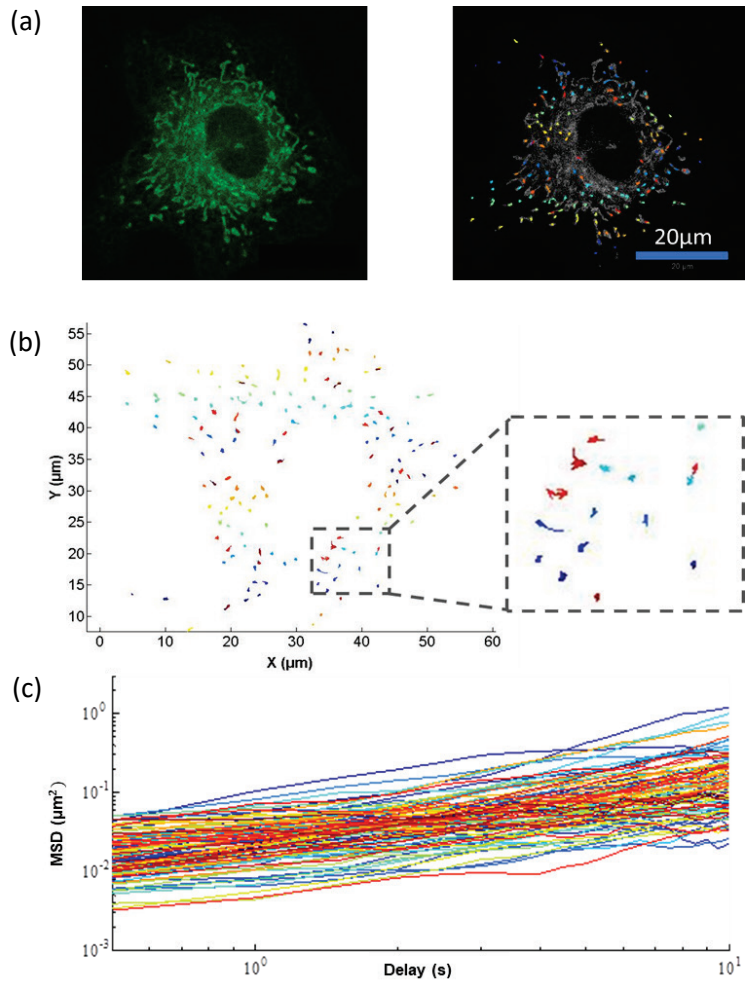

Figure 1.9. Representation of the mitochondrial post-processing process of an RGP cell. (a) Time-lapse images are tracked, (b) particle trajectories are transformed into (c) MSD profiles.

1.6. Problems Statements

Several challenges and problems were identified from a mechanobiological perspective when reviewing the current disease state fundamentals of cardiovascular disease, especially regarding myocardial infarction and cardiac fibrosis. On a cellular level, the role of the extracellular environment has shown to be cardinally important in the regulation and progression of these diseases and has emerged as a key focus of this study.

- Cardiovascular disease (CVD) is becoming a predominant burden in developing nations such as South Africa, with myocardial infarction (MI) being the largest reason behind the increased mortality rate.
- Current medical interventions only address the impairments and myocardial remodelling that develop after MI, in a pharmaceutical (biochemical) sense.
- Mechanical stimuli are known to be regulators of physiological processes; however, little is known about their role in pathologies such as cardiovascular and fibrotic disease such as MI.

- During MI, cardiac fibroblasts (CFs) transition in maladaptive, reactive phenotypes, i.e. cardiac myofibroblasts (MFs), and form a fibrotic scar at the tissue level leads to a loss in heart function and can cause cardiac death.
- A lack of a deeper understanding of cardiac fibroblasts is the reason for the lack of robust and accurate models of single cells mechanics in the context of myocardial infarction.
- It is unknown what distinguishes protective mechanobiological processes from maladaptive/reactive ones, and this hinders the development of targeted therapeutics for cardiac fibrosis and MI.
- More particularly, understanding the intrinsic mechanical properties of CFs and MFs, and how these are affected by mechanical cues from their extracellular environment is very limited if not absent.
- Lifestyle changes along with ageing are the most significant risk factors for progressing chronic CVD such as atherosclerosis, which precedes MI.

1.7. Aim and Objectives

In this study, we propose to investigate whether and how the mechanical properties and behaviour of cardiac cells are affected by the extracellular environment.

We hypothesize that cardiac fibroblasts and myofibroblasts, respectively, exhibit different mechanical properties within extracellular environments of different stiffness, and

The proposed work ***aims*** to assess the effect of the stiffness of 3D extracellular environments on the mechanical properties of human cardiac fibroblasts and myofibroblasts.

Objectives:

1. To identify biomaterial systems that mimic 3D extracellular environments,
2. To undertake mechanical characterisation of these biomaterial systems, and
3. To characterise the mechanical properties of cardiac fibroblasts and myofibroblasts in 3D environments of different stiffness.

2. Mechanical Characterisation of Biomaterials Systems used as 3D Extracellular Environments

2.1. Introduction

As a result of the growing appreciation for the role that the ECM plays in cellular behaviour and process regulation, hydrogels have increasingly been developed to investigate how environmental cues affect these cellular processes, especially in terms of morphogenesis, ageing and disease (Caliari and Burdick 2016). Hydrogels are structurally like natural extracellular matrices due to their crosslinked networks consisting of hydrophilic polymer chains. Polyethylene glycol (PEG) hydrogels are frequently selected due to their flexibility to be accurately manufactured with a stiffness that mimics that of any soft biological tissue, even if these are considerably higher (Zhang *et al.* 2014). This is a key property that makes PEG-based hydrogels desirable for *in vitro* studies such as ours.

Additionally, PEG-based hydrogels remain to date one of the most inert synthetic biomaterials, i.e. they do not provoke a long-term inflammatory response due to their resistance to protein absorption (Raeber *et al.* 2005). Therefore, they also possess the potential to interact specifically and molecularly with cells and guide their differentiation and behaviour. It is for these reasons that we study PEG gels as possible biomaterial injectates to provide a mechanical niche that promotes beneficial rather than adverse remodelling during MI. Likewise, PEG-based hydrogels are very promising in today's biomedical materials research and have been used in research on tissue regeneration and drug delivery. In terms of cell culture applications, PEG has been demonstrated to be useful in studies of stem cell differentiation, angiogenesis, and mechanobiology (Caliari and Burdick 2016).

To create 3D networks of PEG-based hydrogels, we selected an end-functionalised multiarmed PEG vinyl sulphone (PEG-VS) macromer of a 20 kDa molecular weight. 20 kDa-8-arm PEG-VS (Vinyl Sulphone) was synthesized according to previously published protocols (Lutolf M and Hubbell 2003) in the polymer laboratory of the Chris Barnard Division Cardiothoracic Research Group at the University of Cape Town. In addition to this, 20 kDa-8-arm PEG-VS was also purchased from JenkemTechnologies USA. Both of these PEG macromers produced hydrogels of a non-degradable nature.

The PEG macromer serves as a building block that reacts with protease-sensitive peptide crosslinkers to form elastically active chains. This architecture of a hydrogel network strongly influences its macroscopic properties. Thus, the network should, in theory, be controlled once the reaction is complete, by defining all precursor chains to have ideally become crosslinked as active network chains of 20 kDa, connected by the junctions of the 8-arm macromers.

In reality, some of the network's integrity will be compromised by molecular imperfections such as elastically defective loose dangling ends, intermolecular entanglements or network inhomogeneities (Lutolf M and Hubbell 2003). To create hydrogels that can be tailor-made as accurately as possible in their macroscopic properties, one must follow a hydrogel formation/synthesis protocol closely. Synthetic hydrogels lack the inherent bio-adhesive property for cells to bind to their matrix, which can be added through the addition of cell adhesion proteins such as ligands or peptides. Hence, steps must be followed to ensure constant crosslink and peptide adhesion densities. Below we discuss the methods followed to produce consistent PEG hydrogels, estimate time of gelation, and for the assessment of the adhesion peptide density.

Determining the mechanical properties of our hydrogels was a fundamental component of this study. Mechanical stiffness of hydrogel matrices had to be precisely established, as this was one of the main controlled conditions during experimentation. For various precursor concentration compositions, a series of macro- and microscale mechanical testing were performed. The effect of the addition of RGD peptides on the inherent mechanical properties of hydrogel matrices was studied. So too the addition of tracer particles microscopy applications, e.g. in TFM. Rheology, uniaxial tensile testing and micro-indentation were used to study the properties of PEG gels.

The 8-arm PEG-VS (20 kDa) macromer crosslinked with DTT was produced at different PEG concentrations as described before, suitable for each mechanical test. The key aim was to investigate to what extent the concentration of PEG had an effect on the elastic modulus of the hydrogel, i.e. the material stiffness. Since rheology experiments have typically been used to characterise hydrogels, this was assumed to be a reliable methodology for 8-PEG-VS. Although indentation characterisation studies have been applied on PEG hydrogel (Wise *et al.* 2016), additional tensile and indentation tests can provide a more comprehensive and comparative mechanical characterisation of this hydrogel. However, these methods require tailoring and validation. Micro-indentation testing and Uni-axial tensile testing were conducted within the Experimental Continuum Mechanics laboratory at the ETH Zurich, during a research visit done by the author.

2.2. Materials and Methods

2.2.1. Formation of hydrogels

PEG hydrogels were prepared by Michael-type addition of thiol-containing molecules onto the 8-arm PEG-VS. PEG hydrogels were crosslinked with dithiothreitol reagent (DTT, Sigma Aldrich, St Louis, USA). The PEG-VS macromer was dissolved in buffer medium, namely isotonic Phosphate-Buffered Saline (PBS, Sigma Aldrich, Appendix A: Preparation of Phosphate Buffered Saline) at the desired concentration of mass PEG dissolved per volume PBS. Solid substances were weighed with a laboratory-grade, 5-decimal microbalance (Mettler Toledo). It is important to note that discrepancies in the reproducibility for gels with the same properties may arise from minor weighing errors. In order to minimise such errors, stock solutions of PEG were prepared at larger volumes and used throughout a series of experiments. PEG stock solutions of 20% concentration (m/v) were typically prepared, and partial amounts of solution were taken from the stock to form gels.

Two sets of hydrogels were prepared such that there were distinct differences in their mechanical properties. In this instance, the concentration of PEG in the final gel mixture was altered. For this study, we typically prepared gels at 4% and 10% concentration (m/v) to represent a low and high mechanical stiffness, respectively.

To produce PEG hydrogel, the amount of PEG needed to reach the desired concentration in the final gel mixture (4% or 10%), was pipetted from the stock solution into a single-use, safe lock micro-centrifuge tube (Eppendorf). The crosslinker, DTT, was added from its stock solution of 12.32 mg/mL at half the volume to that of PEG solution. For cases where RGD adhesive ligand was added, it was added at one moiety of RGD per 100 arms of PEG (for a 3D matrix). Lastly, buffer solution (PBS) was added to reach the final gel mixture volume. If RGD was required for later cell adhesion, it was essential to have the same RGD peptide density over gels with different stiffnesses (as determined and specified in Section 2.2.3).

Appendix A: PEG Hydrogel Preparation, shows the derivation for creating 4% and 10% 100 µL PEG hydrogels, with Tables 2-4 indicating the exact amount of each constituent. These ratios were used throughout the study, with the required final gel mixture volume used as the independent parameter for each formulation. The mixture was then aspirated into the desired physical configuration for each experiment or application, where it was left to incubate at 37°C for 30 minutes, allowing binding between the PEG molecules. Following incubation, the formed hydrogel was left at atmospheric conditions for a further 30 minutes. Once gelation has occurred, gels were fully submerged into PBS and left to absorb fluid (swell) overnight, for at least 24 hours to achieve complete saturation with water.

2.2.2. Gelation time

The kinetics of the formation of hydrogel were determined and compared between the two mechanically differing gels. This comparison was made by measuring the gel transition time, through using the inverse tube method described by Jeong *et al.* (1999). In short, 100 µL 4% (m/v) PEG gel mixture was prepared at room temperature with PBS (pH 7.4), in a micro-centrifuge tube. The sample was then vortexed for 20 s, stopped and repeatedly monitored until it was found that the hydrogel mixture no longer flowed as a result of the force of gravity. The time of the inversion process from the instant the gel mixture is formed was recorded (n = 3). The assay was repeated for the 10% (m/v) PEG gel.

We found that the gelation times of the two hydrogels differ significantly, with the 10% PEG hydrogel gelling in the shortest amount of time of 2.16 ± 0.3 minutes. The 4% PEG hydrogel was found to have a gelation time of 5.53 ± 0.5 minutes . These times proved valuable in the upcoming experiments as they indicated the soonest time that it would take for the hydrogels to form. This gave us a notion of time within which we had to fix the gel mixture(s) into their final experimental configuration. During the usual protocol, however, samples were treated less dynamically (via aspiration & centrifuging) and involved curing via incubation at 37 °C. As a result of this factor, the times mentioned above served as a lower limit, and gelation would typically take longer on average.

2.2.3. Assessment of adhesion peptide density

When incorporating RGD cell adhesion peptides in a hydrogel, it is an essential practice to ensure that the adhesion peptide density is constant amongst hydrogels of low and high precursor (PEG) concentrations. Although the initial concentrations of RGD during formation may be equivalent, differences in swelling between the two gels would result in changes in the final RGD concentrations (Singh *et al.* 2014). The degree of swelling of both hydrogels was determined, and this was used to ensure consistency in RGD density. In the case of a 3D hydrogel matrix, the RGD adhesion peptide is covalently bonded to the PEG monomer, and a greater swelling will decrease the density of RGD that would be detectable for embedded cells to adhere. The effect of swelling was therefore investigated after 60 minutes of incubation in a humid environment, compared to that of an aqueous environment for at least 24 hours.

Equilibrium swelling experiments are used to determine the structural characteristics of hydrogels and to establish the repeatability of hydrogel formation protocols. The hydrogel property of swelling is the amount of water or buffer it has absorbed and is commonly used as an indicator of relative crosslinking density (Caliari and Burdick 2016). Swelling assays are performed to indicate batch-to-batch variations and in hydrogel formations. For this study, a swelling assay was conducted to determine the respective adhesion peptide density of the two PEG gels and to determine an adjusted ratio of PEG to RGD that

would ensure a constant adhesion density across all hydrogel matrices. The degree of swelling of a hydrogel is expressed as a volumetric swelling ratio (Q_v) according to Caliari and Burdick (2016):

$$Q_v = 1 + \frac{\rho_p}{\rho_s}\left(\frac{M_w}{M_d} - 1\right) \quad (3)$$

where M_d is the dry mass, M_w is the wet mass after swelling, ρ_p is the density of the hydrogel polymer (PEG), and ρ_s the density of the solvent (PBS). The mass swelling ratio (Q_M) after equilibrium (M_w/M_d) was therefore determined by weighing at different intervals.

For one swelling assay, master mixtures of 100 µL of both 4% and 10% PEG gel solution were made up from 20% PEG stock solution as previously described. Two 60 mm polystyrene Petri dishes were covered in Parafilm on their inner surface. Three 25 µL gels were pipetted from a master mix solution onto the Parafilm covered surface of a petri dish. The two dishes containing the 4% and 10% gels respectively, were incubated for 1 hour to ensure gelation.

Cured gels were made to reach their swelled state (equilibrium) by submersion in buffer fluid for 24 hours. For this step, each of the 3X 4% gels and 3X 10% gels were transferred into two separate microcentrifuge tubes with PBS. After that, they were dabbed with a paper towel to remove excess solvent and weighed with a weighing balance to obtain the wet mass (M_w), i.e. the weight of the swollen gel. The hydrogel is dried and weighed once again to determine the final mass of the dry gel (M_d). The mass of each gel was also measured and recorded following gelation. This value is known as the cured weight (M_r) and may be used to obtain the mass swelling ratio of the relaxed gel after curing/gelation. This swelling assay represents 1 of n = 3 technical repeats for each hydrogel.

2.2.4. Rheology

Rheology is used to study the deformation and flow of viscoelastic materials and has most widely been used to characterise multiarmed PEG-VS hydrogels (Bracher *et al.* 2013, Kyburz and Anseth 2013, Raeber *et al.* 2005, Zhang *et al.* 2014). Viscoelastic polymers such a PEG-based hydrogel generally behave more elastically in response to the rapidly applied force (in accordance to Hooke's law, where deformation is proportional to the applied force), and more viscously in response to slowly applied force (in accordance to Newton's law, where the rate of deformation is proportional to the applied force). In brief, viscoelastic polymers have the capacity to behave both like an elastic material and a Newtonian fluid.

A controlled-stress rheometer uses the working principle that involves applying torsion to a sample, measuring the resulting rotational velocity, and deriving the dynamic viscoelastic properties of hydrogels. Figure 2.1 illustrates the most common working configuration, known as the parallel plate (or plate-on-plate) system, where a sample is held in the thin gap (d) between a stationary bottom plate and an upper plate (of radius R) that is attached to a torsional arm. During testing, the rheometer is set to oscillatory mode, the torsional force (T) monitored at the oscillatory frequency, and the rotational velocity (ω) is recorded. The shear stress (τ) and shear strain (γ) are calculated according to Murata (2012) as:

$$\tau = F_\tau T \quad (4)$$

$$\gamma = F_\gamma \omega \quad (5)$$

where F_γ (R/d) is the shear strain factor and F_τ ($2/\pi R^3$) is the shear stress factor. From the complex dynamic shear modulus, $|G^*|$ (τ/γ), the storage modulus (G') and loss modulus (G'') are defined by:

$$G' = G^* cos\delta \quad (6)$$

$$G'' = G^* sin\delta \quad (7)$$

G' represents the elastic component of the sample and G'' the viscous component. Since we are interested in PEG hydrogel's elastic behaviour as a solid-like material (matrix), G' will serve best as an indicator of mechanical stiffness.

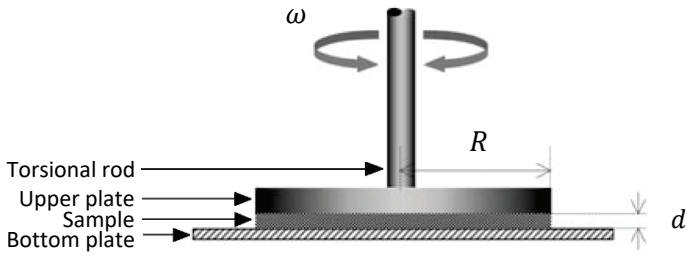

Figure 2.1. Schematic diagram of a controlled-stress rheometer and its parallel plate configuration for the measurement of dynamic viscoelastic properties (Murata 2012).

Sample Preparation

To produce PEG hydrogels that would serve as specimens for a parallel plate rheological study, they must be of suitable shape and nature. Circular, flat disc-shaped hydrogel samples were made to fit in between the parallel plate configuration shown schematically in Figure 2.1. We compared a low concentration PEG sample of 4% with a high concentration PEG sample of 10% PEG. Both these PEG-based hydrogels were expected to have a low enough fragility to be handled without failing. Thus, making it possible to form them separately before transferring them to the rheometer.

Initially, the stiffnesses of 100 µL gels (4% and 10%, n = 3) were measured without RGD peptides. For these measurements, 300 µL master mixes were prepared for both 4% and the 10% gels, and three 100 µL samples of each were pipetted onto three separate sterile siliconized (Sigmacote; Sigma Aldrich) glass microscope slides (Marienfeld). The siliconizing reagent was added to each slide by 2 to 3 drops to ensure separation of gels from glass following gelation. The glass slides are approximately 76 x 26 mm and 1 mm thick. Square coverslips of approximately 0.55 mm thickness were placed at either end of the microscope slides, that would allow that the hydrogels would be forged to their thickness.

Finally, a second siliconized glass slide was placed over and aligned with each initial slide. This configuration of the formation setup is depicted in Figure 2.2. Following gelation (30 minutes incubation at 37C, 30 minutes atmospheric conditions), the top microscope slides were removed, and the gels were carefully placed in PBS to swell overnight to be ready for rheometry in 24 hours, i.e. the following day (Figure 2.3 b).

The addition of RGD peptides may influence the hydrogel stiffness. Therefore, the effect of this change was also investigated by preparing 4% and 10% hydrogels as described above, and by also

incorporating RGD adhesion peptides within the gels. All ratios for producing hydrogels of these two concentrations, with and without RGD, are specified in Appendix A: PEG Hydrogel Preparation.

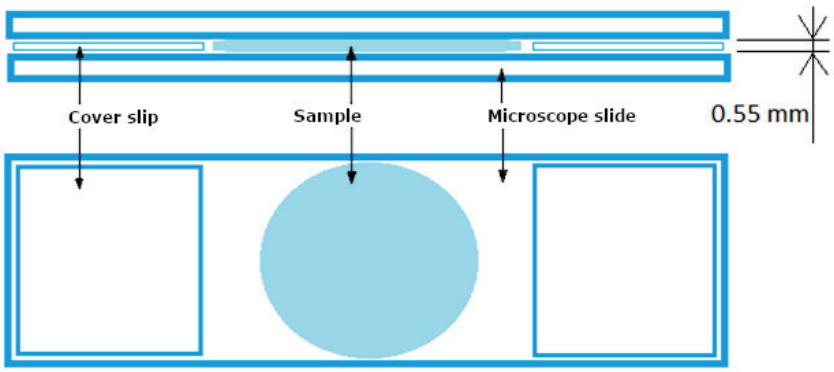

Figure 2.2. Schematic diagram of the sample preparation configuration. The side view (top) indicates the gel sample form between two glass microscope slides, separated by 0.55mm coverslips, and the top view (below) indicating the circular shape that the sample embodies.

Test Conditions

Storage and loss moduli (G' and G'') on swollen gel samples were obtained by performing **small-strain oscillatory shear** tests on a Kinexus Pro rheometer (Malvern Instruments, United Kingdom; Figure 2.3 a), within a plate-on-plate geometry at a temperature of 25°C and humidified atmosphere. These shear parameters are measured for each gel using a dynamic frequency sweep sequence from 10Hz to 0.1 Hz in a constant-strain (0.05) mode. We tested four conditions, namely 4% and 10% concentrated PEG gels with and without the addition of RGD adhesion peptide and repeated the experiment three times (n = 3).

(a) 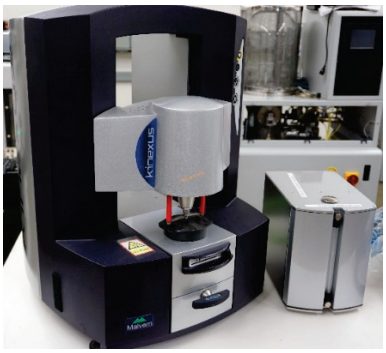 (b) 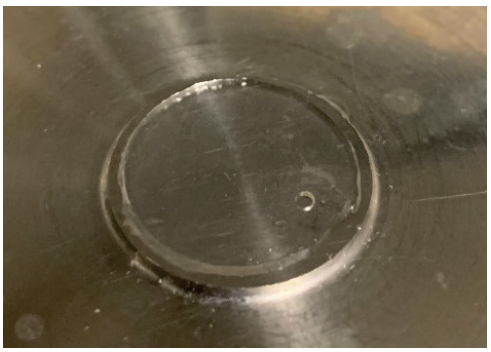

Figure 2.3. Photograph of (a) a Kinexus Pro Rheometer and (b) a PEG hydrogel sample produced for rheometry, lying on the bottom plate component of the rheometer's plate-on-plate geometry.

2.2.5. Micro-indentation testing

Small-strain micro-indentation was utilised to characterise the mechanical response of our experimental substrates accurately. The apparatus for indentation testing is the FemtoTools FT-MTA03 Micromechanical Testing System (FemtoTools AG, ZH, Switzerland) was used, equipped with a cubic zirconia Indenter sphere (R = 100 µm) glued to the end of the system's force probing rod. The

force probe, with a ± 2000 µN force range, were set to make N = 6 indentations of u = 5 µm deep in an array of 300 µm x 300 µm. It was suspected that the broad displacement range combined with low-force sensing capabilities would make this particular FemtoTools system and its spherical tip configuration (photographed in Figure 2.4 a) potentially ideal means for the mechanical testing of soft and viscoelastic PEG-based hydrogels. No protocol, however, exists for our material.

This tool allows us to estimate the linearised mechanical response using a Hertzian approximation, and with minimal sample preparation. It is therefore efficient for testing the relatively expensive PEG, as it only expends low gel volumes. The PEG hydrogels were prepared at 5.5% (low), 7% (moderate), and 10% (high) concentrations (m/v). We produced cylindrical samples with a width of W (or diameter), and height of H (or depth) as shown in Figure 2.4 b. The schematic diagram depicts the test configuration with parameters and conditions for simulation modelling.

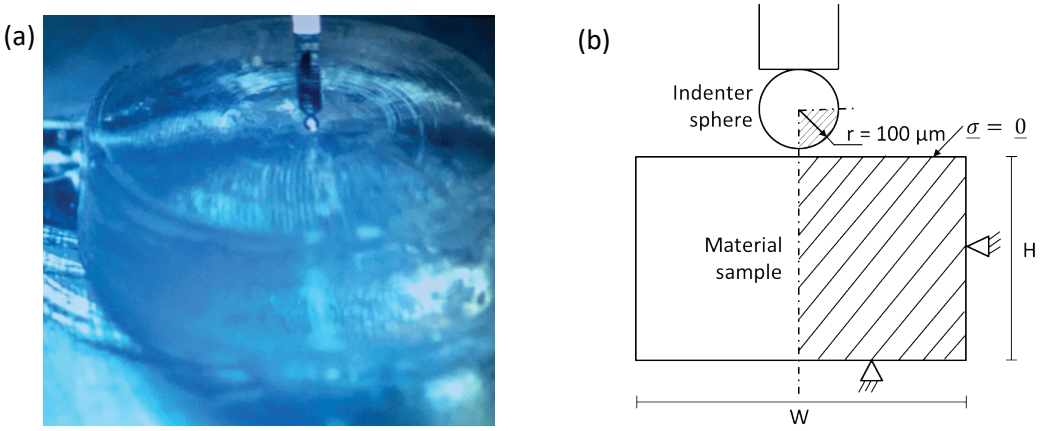

Figure 2.4. The micro-indenter configuration of the FemtoTools FT-MTA03 Micromechanical Testing System's force probe tip (with cubic zirconia sphere), (a) photographed as it indents a cylindrical PEG gel sample and (b) schematically depicted with dimensions and boundary conditions. The setup can be modelled using an axisymmetric model (dashed line represents symmetry axis), fixed at its bottom and side boundaries of the specimen. These fixations model maximum boundary effects, for e.g. if the sample is confined in a well, with no relative movement between the gel and the well surface. Zero stress is assigned to the top surface.

Simulation for Optimal Sample Geometry

To optimize the smallest sample volume needed for any boundary effects to be circumvented and to obtain a sample that behaves like a semi-infinite continuum, the micro indentation was simulated in a Finite Element Analysis (FEA) model. Subsequently, the axisymmetric model was built in Abaqus/CAE (SIMULIA, USA) using the shaded geometry in Figure 2.4 b above, with the indenter sphere sketched as a wire element (constrained as a rigid body) and the substrate (material sample) as a planar shell. The Abaqus/Standard (implicit) solver was used for this analysis. A generalised neo-Hookean hyper-elastic and isotropic material behaviour and type was selected to model the substrate (E = C1/6 + D1; where C1 = 6 and D1 = 0). The substrate was then meshed with quadratic elements and locally seeded as to become finer in the region of interaction and gradually coarser further from it (outer mesh visualised in Figure 2.5).

The Surface-to-surface contact (standard) was defined, opposed to a general contact, with the indenter as the master surface and the top of the substrate material as the slave surface. The interaction property was further defined as normal tangential and frictionless behaviour. Once the mesh had been optimised, the FEA model was run, which rendered the stress distribution field shown

in Figure 2.5. Note that these dimensions represent the semi-infinite (SI) case (W = 10 mm, H = 10 mm), with the interaction region, cropped and enlarged (on the right).

With the FEA model built, we aimed to determine the optimal specimen geometry by establishing the minimum dimensions that will still experience no significant boundary effects. Using the output (.odb) file from Abaqus, we ran a Python script that gives us output data files of the indentation displacement (U) and the resulting reaction force (RF). This force/displacement curve represents a 'global response' of the system, which is a relevant quantity for the indentation test. These data files were again handled in Python to plot the force/displacement reaction curve of the SI case (dotted curve in Figure 2.6). From the SI case, we first incrementally decrease width (W) until we found a significant difference in the at the final displacement point of its curve. Once found, we repeated the same process for height (H). The incremental changes to decrease either width or height, as well as fittingly adapting the mesh for each change, was edited within the Abaqus/CAE script file. By running the simulation with the edited script for each dimension parameter change, we produced a new associated output (.odb) file each time, that was processed and plotted against the previous simulation(s).

Hence, we found the dimension for both W and H, where the reaction force curve would exceed an influence error threshold of 1% compared to the controlled semi-infinite (SI) case of that dimension.

$$\frac{Force - Force_{SI}}{Force_{SI}} < 0.01 \tag{8}$$

For example, the effect of decreasing W is shown in Figure 2.6, with the difference between W = 10 mm (SI case) and W = 1 mm at u = 5 µm indicated by the red dotted lines. This dimension exceeds our error threshold, according to Eq. 8. Following a similar repetition for the height dimension, the final selected dimensions based on the errors were W = 6 mm and H = 2 mm. Samples produced at such an optimal geometry could generate the maximum number of repeat experiments per material volume expended.

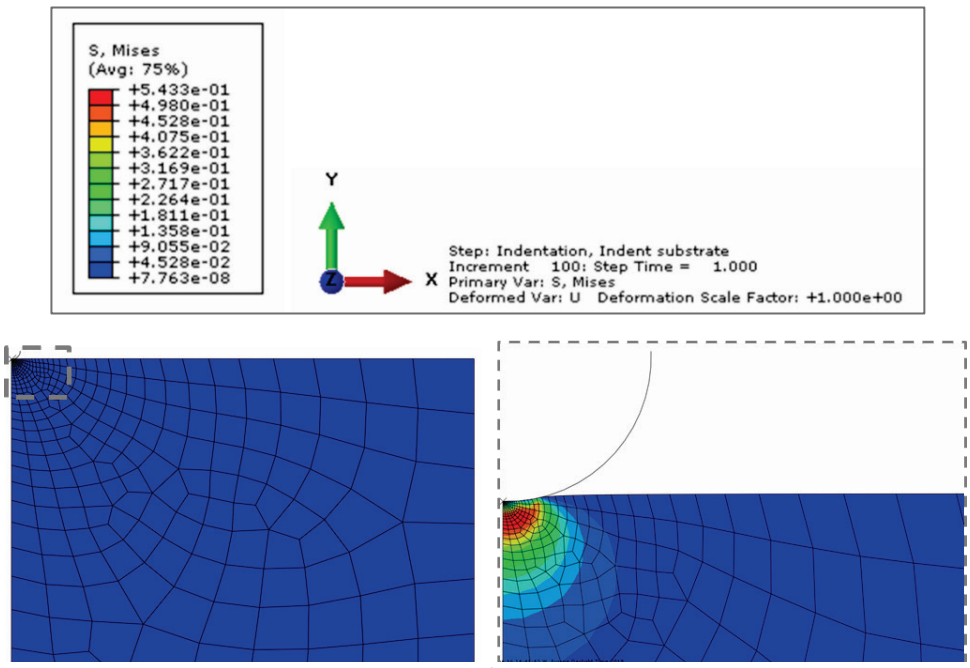

Figure 2.5. Micro-indentation FEA Model in Abaqus/CAE, simulating the semi-infinite case of the geometry parameters, cropped and enlarged around the interaction region. The model is setup up to investigate the effects of boundary conditions on global response of the system to the indentation displacement.

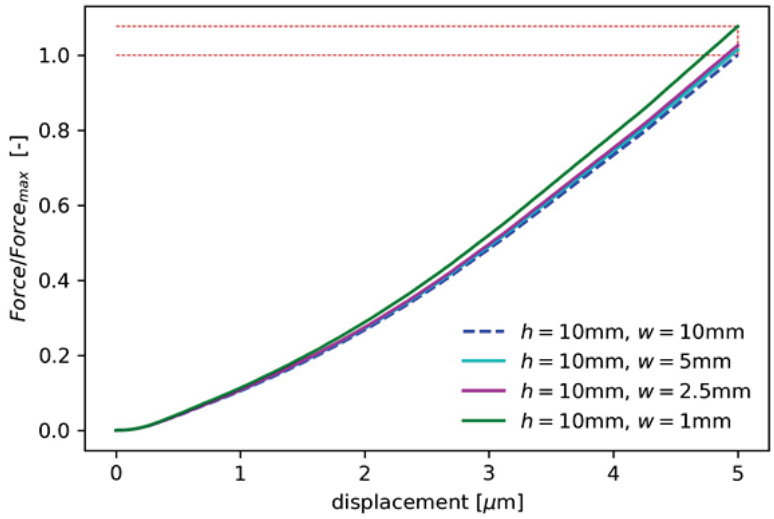

Figure 2.6. Reaction Force vs Displacement graph for the FEA micro-indentation simulation investigating the change in the width (W) parameter of the substrate geometry. The blue dotted line indicates a large enough geometry to experience zero boundary effects from the indentation, i.e. the semi-infinite (SI) case, with each other line indicating a change resulting from a decrease in width (w). The red dotted horizontal lines show the error difference between the SI case and w = 1 mm, which is an example of a very large boundary effect (>> 1%).

Test Conditions and Analysis

A mould was machined out of Teflon (polytetrafluoroethylene – PTFE) due to its hydrophobic properties and very smooth surface topography, with ten cavities of the determined dimension parameters. Initially, samples were polymerised in the mould cavities, removed and submerged in PBS buffer overnight to swell. Gelation of 4% (m/v) 8-PEG-VS-DTT hydrogels in this configuration was troublesome and as such we opted for a slightly increased concentration for our low concentration / soft substrate of 5.5% PEG.

Upon the first round of indentation characterisation, the results were found to be scattered. When viewed under a tabletop laser microscope, the surface topology was found to be undesirable in certain instances. In addition, as we removed samples from submersion to be tested, we recognised that the drying of samples during testing might cause their surface structures to become compromised. Such loss of smooth surface topology, or 'wrinkling', may have occurred due to immense water absorption (swelling) of the polymer chains followed by the loss thereof. We suspected that this might have attributed to the irregularity in the results. According to Lutolf M and Hubbell (2003), the swelling ratio of PEG-based hydrogels decreases with an increase in precursor concentration, an effect which is intensified with higher macromer molecular weights as with our 20 kDa PEG. Consequently, we found a higher scatter in the results of our softer substrate (5.5 % m/v), confirming our suspicion for the reason behind the spread in the initial results.

To overcome these discrepancies, samples were held within the mould during testing and buffer liquid was held over them to keep their matrices immersed (Figure 2.7 b) and to test them in their "swollen state". This condition would also replicate the case during experimentation (microscopy). Therefore, we deepened the mould cavities a further 1.5 mm to a final 3.5 mm (see final mould parameters in Figure 2.7 a). The final gel volumes prepared per sample were thus 56.6 mm^2 (≈60 mm^2). Following the modifications, the second test (Figure 2.7 c) produced processed data for each repetition with near-zero scatter in the resultant force curves. The accuracy was seen by how neatly the Force-

Displacement slopes of 6 repeat indentations performed on 10% (m/v) PEG gel were aligned from Figure 2.8 a to b, indicating that PEG-hydrogel is highly feasible material for micro indentation testing and that we established a sound protocol for testing it. Furthermore, we investigated the potential effects of the addition of fluorescent microbeads (FluoSpheres, Carboxylate-Modified Microspheres, 0.04 µm; Thermo Fisher Scientific, Waltham, USA). These can be used to do tracking analysis, e.g. in TFM. They were added to both moderate and high concentrated substrates, at a ratio of 1% of their final gel volumes, to be compared to controlled cases of each without the addition of microbeads.

The output data from Femtotool gave the displacement (µm) of the indentation probe over the time period, as well as it's position coordinates. The x-position stays constant for each of the six repeated indentations, whereas the change in the z-position correlates with the displacement for each probing. A Force (µN) column was also given, showing the reaction force measured by the probe at all time indexes of the experiment. A python script plots force vs displacement for each repetition such as in Figure 2.8 a. The software also selected the point(s) of each probing at which the elastocapillary force from the initial probe-gel contact plays no role, cuts off the data below it, and aligns all the remaining plots as in Figure 2.8 b, for the elastic region of the slope to be analysed.

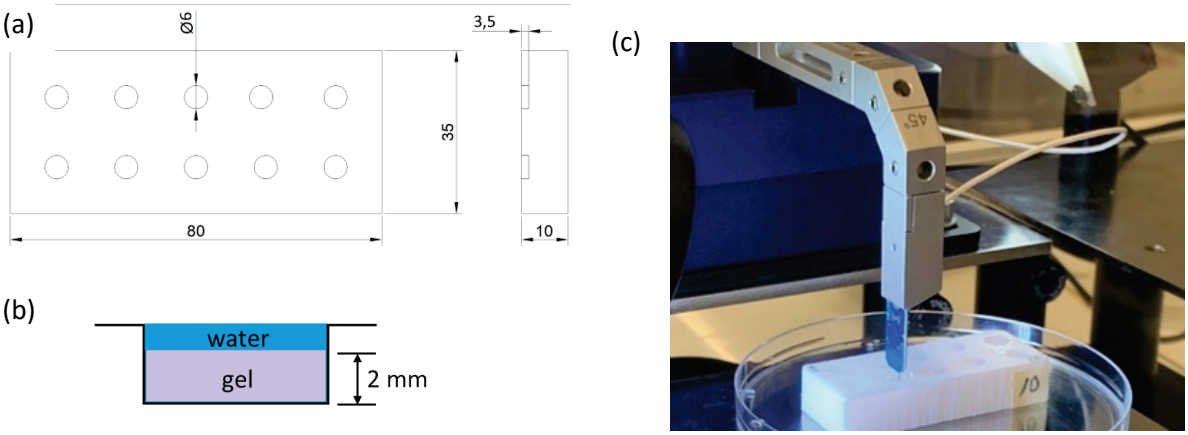

Figure 2.7. Engineered Teflon mould for micro-indentation mechanical characterisation of PEG hydrogel. (a) Dimensions sketch of the mould (units in mm), (b) immersion depiction during testing, and (c) a photograph of the samples being tested using the FemtoTools FT-MTA03 Micromechanical Testing System.

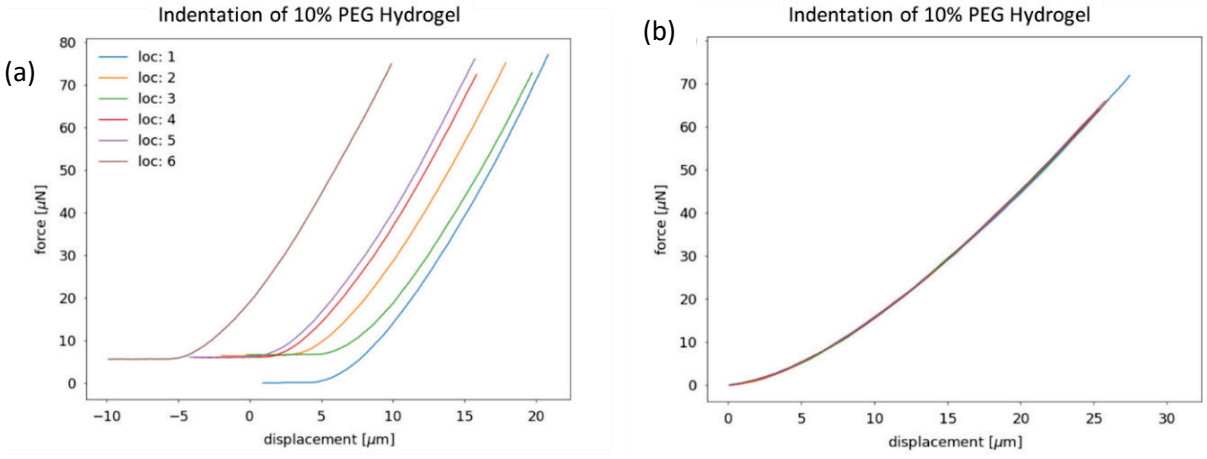

Figure 2.8. Force-displacement graph for micro-indentation test run of 10% (m/v) PEG hydrogel (a) plotted separately and (b) aligned.

2.2.6. Uniaxial tensile testing

Tensile loading in the context of PEG-based hydrogels was worth investigating, as there was no literature found on this form of macroscale mechanical testing for PEG gel. Compression tests have, however, been done on other forms of synthetic hydrogels. Uni-axial (UA) tension testing is the most widely employed method to determine the critical material properties of engineering materials, commonly performed monotonically to failure at a specific strain rate. Although a full 3D characterisation of hyper-elastic materials requires multiaxial data, a simple UA test still yields valuable data on the mechanical behaviour, such as estimations of the Young's Modulus to compare indentation data, and a measure for uniaxial failure strain. The purpose for the UA testing exceeded the requirements for the cell study, and additionally served to investigate the comparative nature of the mechanical characterisation techniques used in this study.

Sample Preparation

With no prior knowledge on PEG gel's response under UA tension, we selected relatively high concentrations of PEG gels of 14% and 18% (m/v), to ensure that enough deformation would occur before failure. A rudimentary / 'low-tech' solution to ensure the material failure will not occur at clamping sites and to get a truly coherent tensile force throughout the material, was to fix the sample by gluing them to the metal clamp surfaces with cyanoacrylate glue. Thereby, there was no need to tighten the clamps that may damage the material and initiate failure.

UA specimens were moulded using the standard PEG gel formation protocol in a Teflon mould to geometries that reach a length of 70 mm, with a width of 10 mm and a thickness of 1 mm. For testing, the ends were fixed to clamps as shown in the photograph below (Figure 2.9 a; 14% concentrated PEG hydrogel UA test sample) leaving a gage region in between the clamps (L = 40 mm, W = 10 mm, t = 1 mm; N = 2). A spacer is used to clamp the specimen at the exact right length. Due to swelling, geometries may have enlarged from the mould; therefore, the width is measured with a Vernier calliper. The loose ends were cut off and placed back in a buffer the solution for later accurate determination of each sample's specific thickness.

Once clamped, white powder was spread on the top surface of the gauge region (to create contrast), followed by black carbon powder that would serve as landmark particles. Time-series images of the gauge region were taken during testing, and these particles aided the post-processing software to analyse the local deformation behaviour for each test. These particles were applied with a paintbrush, as demostrated in Figure 2.9 b. One can see an example of a resultant image file in Figure 2.10 b.

(a) (b)

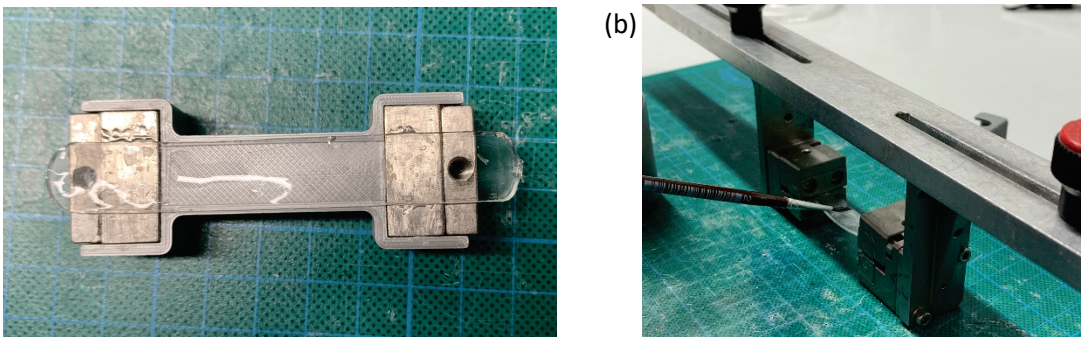

Figure 2.9. A photograph of (a) a 14% (m/v) PEG hydrogel UA test sample fixed to the bottom set of clamps before UA Tensile Testing (with 3D printed placeholder) and (b) it clamped and being marked with carbon powder for imaging processing (landmarking).

Test Conditions

Gels were removed from buffer solution after 24 hours of swelling, prepared as described above and tested within 20 minutes. For each concentration condition, a sample was stretched at a strain rate of 2% per minute, to ensure very gradual deformation and enough strain to be recorded before failure. Once again, this was selected due to the uncertainty of how the PEG gel would perform. The pre-tensile configuration is shown in Figure 2.10 a. As such, samples were incrementally stretched during which time the controller recorded data and camera setup acquired images of the gage region (Figure 2.10 b), until failure (Figure 2.10 c). The data of n = 2 specimens per condition was tested as this test is materially expensive.

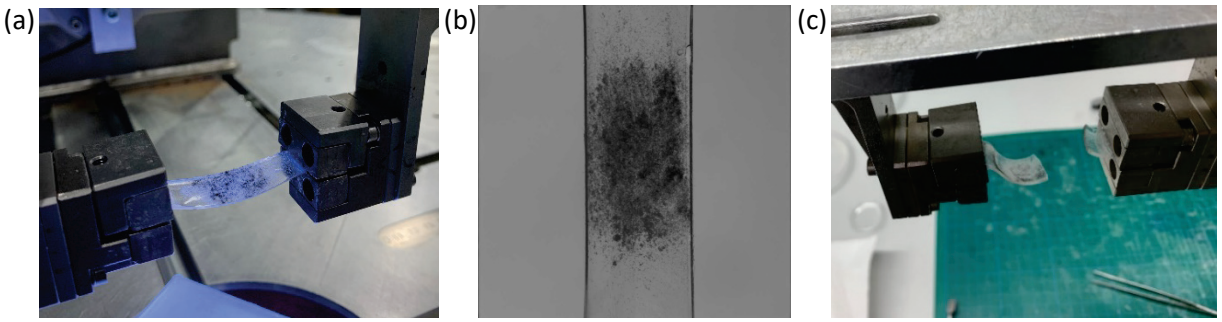

Figure 2.10. Photograph frames depicting three stages of Uniaxial Tensile Testing of PEG hydrogel from (a) the initial position, (b) to it being strained and (c) eventually failing.

Following testing, the exact thickness of each UA specimen had to be established. Due to swelling, a UA sample is likely to have increased in thickness (t > 1 mm). The dismembered end(s) of each sample from the clamping setup described before were used under a tabletop laser microscope, to find the actual sample thickness (t > 1 mm) with close accuracy. The determined thickness, together with length and width values, was added to an input geometry data file for the post-processing analysis software to use.

2.3. Results

The results from the extensive study to characterise PEG hydrogels as synthetic biomaterial to be used in *in vitro* microscopy experiments are given in this section.

2.3.1. Assessment of adhesion peptide density

The effect of swelling is depicted in Figure 2.11, showing the derived volumes of 4% PEG gels to be 32.735 µL and 26.5 µL at the intervals following 24 hours of swelling time and when dried out, respectively. 10% PEG gels were found to have final equilibrium and dry volumes of 28.51 µL and 25.13 µL, respectively. These volume changes between each interval are further represented as a percentage of increased volume (degree of swelling), Q_v - 1 (from Eq. 3), in Figure 2.12. A substantial increase of 23.53 % ($p = 0.001$) was found in the swelling of 4% PEG hydrogels when comparing their volumes after swelling (24 hours) to those after drying. 10% PEG hydrogels also showed a considerable Q_v of 12.02 % ($p = 0.04$).

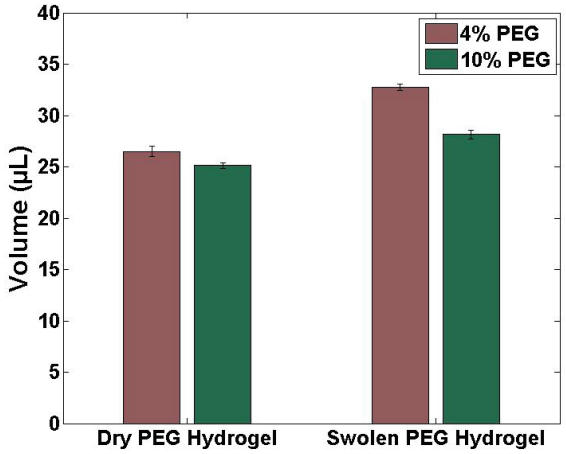

Figure 2.11. Swelling of 8-arm-PEG-VS hydrogels of 4% and 10% (m/v) concentrations depicted as gel volumes after 90 minutes of incubation (Gelled; LEFT) and 24 hours of submersion in PBS (Fully Swelled; RIGHT), n = 3.

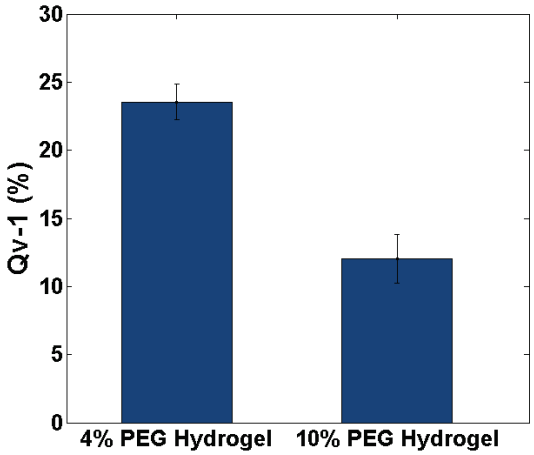

Figure 2.12. The Volumetric Swelling ratio (Qv) of 8-arm-PEG-VS hydrogels of 4% and 10% (m/v) concentration.

From the swelling assay results, the final volume of an entire 100 µL 4% gel swells to 130.94 µL, notably higher than the final swelling volume of the 10% gel of 112.62 µL. This difference was incorporated when determining the necessary RGD amounts for each. The overall density of RGD would be detectable by cells embedded in a 3D hydrogel matrix, as typically the case in 3D experiments. Using a volume calculation combining the PEG arm density and the relative swelling after polymerisation, an RGD concentration per cubic area (mol/cm^3) was be derived (Appendix A: Assessment of Adhesion Density).

A 1:100 ratio (1 RGD molecule per 100 arms of 8-arm PEG) as commonly assumed for 3D matrices, generated a density of 0.0142 nmol/cm^3 for the final volume of the 4% PEG hydrogel. To achieve this same RGD adhesion peptide density for the 10% PEG hydrogel, the ratio of RGD constituents to PEG is changed to 1 RGD per 289.75 PEG monomers in the final 3D gel matrix. Therefore, by using a 1:100 for 4% gels and 1:289.75 for 10% gels, we would ensure an equal adhesion peptide density between the two types of hydrogels.

2.3.2. Rheology

In the results from the small-scale oscillatory shear rheology, we obtain both storage and loss moduli (G' and G'') which indicate that the samples had the stiffness and viscosity of fully polymerised hydrogels. We are, however, interested in the elastic behaviour of our samples, and thus focus on G'. Since G' proved to be constant at all frequencies in the sweep and for all repeat tests, it could be taken as equal to the elastic modulus at equilibrium, which translates to the stiffness of the hydrogel (Pa).

PEG hydrogel networks prepared from the same macromer (20 kDa 8-PEG-VS) showed exceedingly different properties depending on the concentration of precursor solution (m/v). The gels range from a low concentration (4%) to a high concentration (10%), and the elastic modulus (stiffness) increased with the precursor concentration. Figure 2.13 shows that without RGD peptides incorporated, the elastic modulus (G') of 4% and 10% concentrated PEG gel is 500.23 ± 13 Pa and 2721 ± 39 Pa, respectively. Incorporating RGD ligands decreases stiffness for both 4% and 10% (m/v) PEG gels to 301.5 ± 15 Pa and 2439 ± 278 Pa, respectively. The difference in stiffness between 4% and 10% (m/v)

gels for both these cases (without and with RGD) are substantial (p = 0.001). Furthermore, the introduction of RGD induced a significant decrease in the 4% gel (p = 0.01) as well as for the 10% gel (p = 0.04).

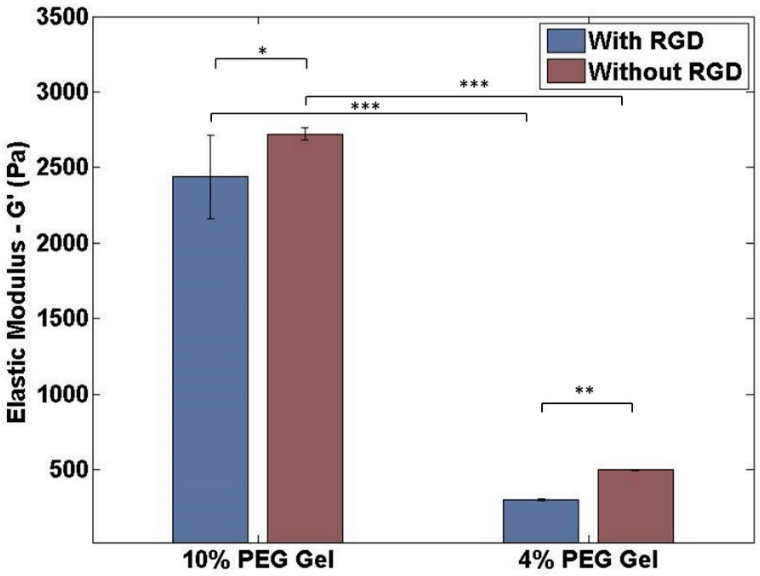

Figure 2.13. The result of mechanical characterisation by rheometry showing the stiffness of PEG-based hydrogels with and without the addition of RGD cell adhesion peptide, n=3.

2.3.3. Micro-indentation

It was found, through running the micro-indentation analysis software of the ECM group, that in higher concentrations (10%), PEG hydrogels are generally well characterised with this method. Incoherence occurred in lower concentrations. From this, we concluded that manufacturing errors become significant at the low concentration (5.5%) used due to the small amount of PEG monomer being handled manually. Furthermore, the signal to noise ratio decreases for softer materials, introducing an additional source of uncertainty. However, it was found that a low-to-moderate concentration of 7% PEG showed a Young's Modulus of 39.2 kPa, while a higher concentration of 10% showed 65.3 kPa.

The addition of nano fluorescent beads (Carboxylate-Modified Microspheres) to be used in potential TFM or similar material tracking studies, showed no definite effect on the elastic properties of our PEG-based hydrogel (Figure 2.14). This non-definitive effect could be expected for particles as small as 0.04 µm. Furthermore, they are merely mixed into the gels and are left suspended within their matrices. In other words, no bonding takes place, and no polymer chains are affected.

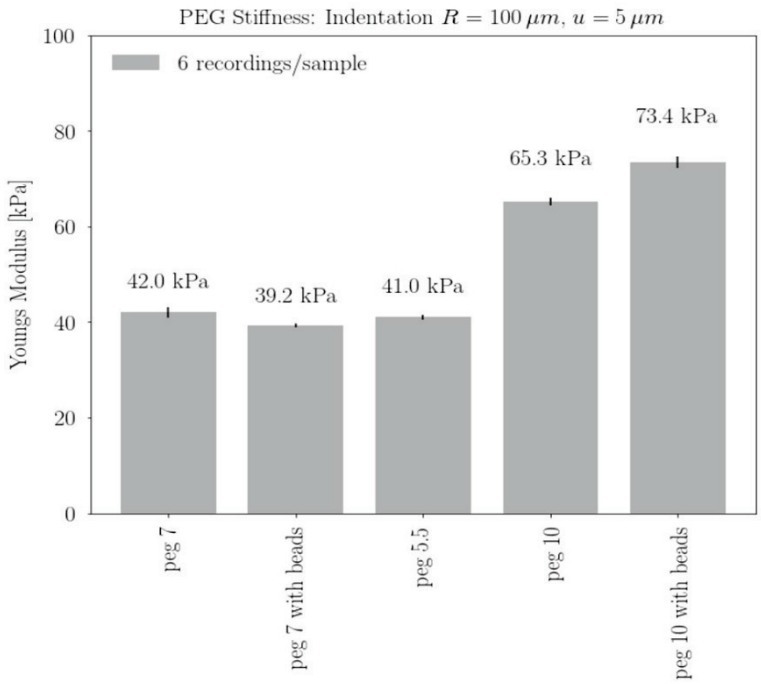

Figure 2.14. The result of mechanical characterisation, showing the Young's Modulus of PEG-based hydrogels of 5.5%, 7% (with & without fluorescent microbeads) and 10% (with & without fluorescent microbeads) precursor concentration by micro-indentation.

2.3.4. Uniaxial tensile testing

Once collected, the data was analyzed using the ECM group's UA tensile test analysis software in Jupyter Notebook. Firstly, force, displacement and time data is cropped and analyzed to process the global case of the test. Ensuing, the optical tracking region is identified using the landmark particles for the local test. The tracking is processed and filtered (to exclude non-homogenous motion).

Finally, transverse strain is computed and compared to the theoretical transverse strain, computed via incompressibility assumption to validate material incompressibility. Cauchy stress is only meaningfully computed from the measured quantities if incompressibility is given. The linear regions of both Kirchhoff stress *vs* strain and Cauchy stress *vs* strain is shown in the plots in Figure 2.15 (for 14% concentrated PEG hydrogel). For both cases, the global and local stress-strain profiles closely align, indicating no slippage of the specimen. From these results, it was found that 14% and 18% concentrated PEG hydrogel have elastic (Young's) moduli of 78.19 ± 8.42 kPa and 121.49 ± 11.9 kPa, respectively.

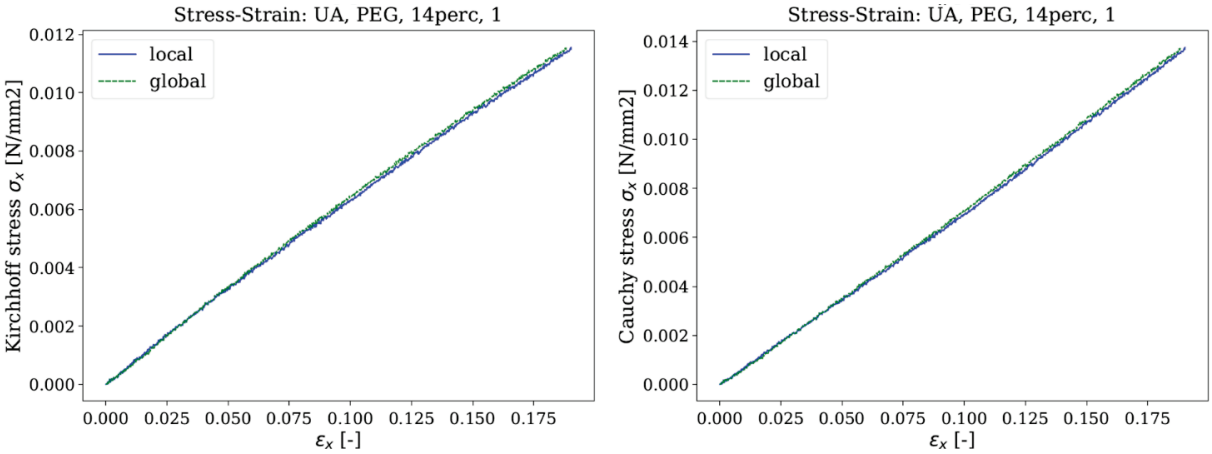

Figure 2.15. Resulting elastic behaviour of 14% (m/v) PEG hydrogel as found by Uniaxial tensile testing, with (a) Kirchhoff stress vs true strain and (b) Cauchy stress vs true strain.

2.4. Discussion

This study aims to understand the role of the extracellular environment has on the mechanics of cardiac fibroblasts and endothelial cells. Due to this study being *in vitro*, it was imperative to characterise the biomaterial substrate to be used to mimic 2D and 3D environments. PEG hydrogels offer ideal properties such as their ease to be manufactured at various stiffnesses, as well as being inert and non-degradable. Consequently, through a series of tests and experiments, we have successfully determined its structural and functional behaviour.

Through the swelling assay, we established the swelling properties of our 20 kDa PEG-VS-DTT hydrogel, at a low and a high precursor concentration. We quantified this through the volumetric swelling ratio and found that the gels with lower concentrations (such as 4% m/v) absorb a very significant amount of liquid, compared to gels with higher concentrations (such as 10% m/v) that absorbs less. This trend for synthetic hydrogels is often verified throughout literature and confirmed for PEG-based hydrogels by Lutolf M and Hubbell (2003) (although different crosslinker was used here). Using the knowledge of the swelling behaviour of our biomaterial, we could adjust our calculation to ensure a constant amount of RGD ligands per equilibrium hydrogel volume, for each case necessary. RGD was used in our rheology tests, and more importantly when culturing cells in 3D microenvironments for microrheology experiments. For these cases, constant RGD density was established for cells to detect a similar regularity of attachment sites.

The rheology study studied the difference in the mechanics of PEG-based hydrogels of low concentration and high concentration, and how each would affect their respective stiffness. PEG hydrogels were subjected to a dynamic oscillatory shear to gain insight into their elastic behaviour. The stiffness was represented as G', the elastic component (storage modulus) of the shear modulus, monitored over frequencies from 10 Hz to 0.1 Hz. The shear modulus, also known as the modulus of rigidity, is the product of shear stress (Eq. 4) over shear strain (Eq. 5), meaning the deforming force acts parallel to the sample surface. Through the use of this stiffness indicator, it was found that the higher concentration gel of 10% PEG was significantly stiffer than that of the lower concentration gel of 4% PEG (2721 ± 39 Pa and 500.23 ± 13 Pa), as a result of the correlating difference in macromer concentration. This range in G' values found for PEG gels is substantiated by rheology studies done by Kim J *et al.* (2016), Lutolf M and Hubbell (2003) and Zustiak *et al.* (2010).

This considerable difference in stiffness between PEG gels of low and high precursor concentration was also found for gels with and without the addition of RGD adhesion peptides within their matrices. However, when comparing gels with the same PEG concentration, RGD induced a significant change in the stiffnesses of the 10% ($p = 0.04$) and the 4% ($p = 0.01$), decreasing the overall stiffness of the PEG hydrogel for both cases. This finding indicates impeding some PEG arms from crosslinking with an RGD ligand, does influence the stiffness of the hydrogel matrix even at the relatively low RGD levels per VS arm used here. The effect caused by RGD may suggest that additional swelling assay(s) may have to be conducted to establish whether RGD incorporation influences the volumetric swelling ratio for a hydrogel, which would mean that the hydrogel formulation (to ensure constant RGD densities) should ideally be readjusted according to this potential change in swelling.

We found that PEG-VS hydrogel crosslinked with DTT, to be a highly feasible material to characterise using micro-indentation testing. This discovery was uncovered by simulating an optimal procedure to determine mechanical stiffness in terms of material usage, consuming the minimal amount of PEG for this micro-scale test. Here, we tested for the modulus of elasticity (E) as the stiffness parameter, which is a product of the normal stress applied by the indenter sphere over the normal strain of the material. With custom-made samples and a specialised procedure, we established a substantial difference in the stiffness of a 'moderately' (7%) concentrated PEG gel to that of a high (10%) concentrated PEG gel. This finding confirmed our conclusion from the rheology study, which was that PEG gel stiffness is directly proportional to the precursor concentration used to form the material. The values of these two mechanical characterisation tests, rheology and micro-indentation, may have differed (in one order of magnitude) due to the two different mechanisms of deformation employed (G' vs E), combined with the different size scale (macro- vs microscale) that they were performed at, respectively. However, the ratio of PEG concentration-to-stiffness for both tests was found to be within proximity, which was essential for our conclusion.

In order to provide a comparison between the properties measured small-strain micro-indentation (E) and oscillatory shear rheology (G), we can assume hydrogel incompressibility so that $E = 3G$ (from $G=E/[2*(1+v)]$; where $v < 0.5$). Rattan *et al.* (2018) found this correlation to be true when comparing the two tests on Resilin-like polypeptide hydrogels. However, the larger difference that we found may be further be attributed to the level of strains. Since most hydrogels are generally nonlinear materials, their elastic moduli would be a function of strain levels, i.e. E (or G) are much higher when it is measured at low-strain regime. Rattan *et al.* (2018) used a micro-indentation depth of their probe radius, 750 µm, whereas we tested at a much smaller strain level of merely 5 µm. Therefore, it is not surprising that the value obtained from our method, which is closer to nano-indentation, is 8 times greater than that from the rheological methods (instead of a factor of 3). This is worth studying in our future research.

Once more, for the case of the UA tensile test, the normal elastic modulus (E) is determined, with the deforming force acting at right angles to the surface of the material. In this case, we tested materials with much higher PEG concentrations due to the uncertainty of our biomaterial's elastic behaviour. The result found fits well with the previous test, micro-indentation, that also produces the same stiffness parameter. From 14% to 18% PEG concentration, the hydrogel's elastic modulus progress drastically, suggesting a relatively low exponential relationship between precursor concentration and stiffness occurring from 14% (m/v) and higher, which is not an uncommon trend in previous literature studies on PEG-based hydrogels (Lutolf M and Hubbell 2003).

Knowing these properties, *in vitro* 3D extracellular environments could be created at desired conditions. To attain these mimetic environments, cells were embedded into stiffness-tuned 3D PEG hydrogel matrices, with RGD ligands to adhere to, thus imitating their native myocardial environment.

3. Mechanical Characterisation of Cardiac Fibroblasts and Myofibroblasts in 3D Environments

3.1 Introduction

The preparation required to implant living cells into a biomaterial matrix is stepwise and meticulous. It involves using knowledge of cell life cycle and culturing, together with that of biomaterial formation processes. In this study, the cell culture process was done firstly by isolating the subject cells *in vitro*, and distributing them in an environment with the nutrients, temperature, pH level, gases and humidity that they need to grow and proliferate.

Once the cells reached the level of confluency required, the 3D environment preparation could commence, starting with combining the constituents for the hydrogel mixture. Several cells are extracted and injected and uniformly aspirated into a liquid gel mixture, after which hydrogel formation takes place. This mixing allows cells to be freely suspended and to adhere to the matrix structure during gelation. This 3D cellular environment had to be created in a configuration that would allow for microscopy-experimentation.

In this experimental study, we utilised particle tracking microrheology to examine the interaction between 3D matrix mechanics and intracellular displacement fluctuations; the latter that effectively represents cellular mechanics. More specifically, we quantitatively investigated the role of the ECM on the intracellular stiffness (cytoplasmic fluctuations) of CF and MF cells within its native myocardial environment. Measurements are made without perturbing cells by using mitochondria that are endogenous and abundant throughout the cells, as tracer particles (Kim JE *et al.* 2018).

3.2 Materials and Methods

3.2.1. Cell culture

Cell culture was performed in the Cardiovascular Research Unit, at the University of Cape Town, in a Biosafety Level 2 Laminar Flow Hood and under strict sterile conditions. Murine cardiac fibroblasts cells were harvested from adult rats by digestion according to Golden *et al.* (2012), and the isolated cells were frozen down in a liquid nitrogen container in 1.5 mL long-term storage cryonic vials (Thermo Fisher) at 500,000 cells per vial. As illustrated in Figure 3.1 a, to begin with cell culture, a frozen vial of cells was removed from the container and warmed until just thawed. Immediately thereafter, it was plated in a T75 cell culturing flask for growth with Dulbecco's Modified Eagle Medium (DMEM; high glucose) (Thermo Fisher), supplemented with 10% fetal bovine serum (FBS) (Thermo Fisher) and 1% penicillin-streptomycin (Pen-strep). The Pen-strep solution is made of 100 U/mL penicillin (Thermo Fisher) and 100 µg/mL streptomycin (Thermo Fisher). For cell maintenance before passaging or experimentation, cells were grown in a humidified incubator to near confluence in 25 cm^2 tissue flasks at 37 °C and 5% CO^2. Cell growth and proliferation were monitored daily, and the media was routinely replaced every 3-4 days, as illustrated in Figure 3.1 b.

Once 80% confluence was reached, cells were rinsed twice with Phosphate Buffered Saline (PBS), and then trypsin-EDTA (Ethylenediaminetetraacetic acid) (Biochrom GmbH, Germany) was added for cell detachment. Upon complete detachment, the cell-trypsin mixture was transferred to a 50 mL Falcon tube (BD Biosciences, San Jose, CA, USA) and centrifuged (Megafuge 1.0R, Heraeus Hanau, Germany)

at 1,500 revolutions per minute for 5 minutes (Figure 3.1 c and d). The supernatant was carefully removed to retain the collected 'pellet' of cells at the bottom of the tube, 1 mL of medium added, and cells were resuspended by gently aspirating the medium. To count cells, a hemocytometer chamber (Superior, Germany) was used. 20 µL of the cell suspension was added to a microcentrifuge tube, together with 20 µL of trypan blue (0.4% m/v, Sigma Aldrich) dye. 10 µL of the evenly mixed solution was pipetted between the coverslip and the hemocytometer, and grid 1 and 5 were counted and averaged. Cell concentration (cells/ mL) was calculated by:

$$\text{Concentration} = \text{average number of cells} \times 2 \times 10 \times 10^4 \left[\frac{cells}{ml}\right].$$

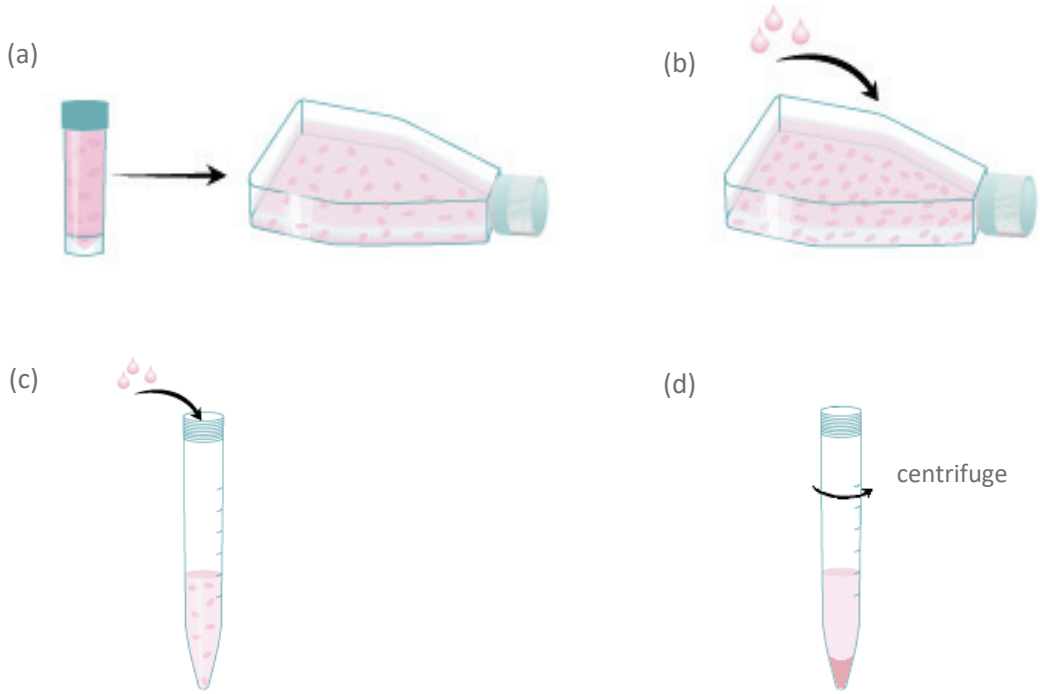

Figure 3.1. An illustration of the process of culturing Rat Cardiac Fibroblast cells. Cells were thawed in a cryonic vial (a), plated in a T75 flask to proliferate in incubation with the periodical change of growth medium (b). Trypsinised cells were added to a centrifuge tube (c) and spun down to be collected in a pellet at the bottom of the tube (d) (R&Dsystems 2020).

Assuming the approximate concentration of cells per millilitre of media, one can determine which volume to extract to get a required number of cells. For our experiment, we decided to use 30,000 cells per microscopy sample. Upon counting the cells from one particular flask, for example, we concluded that there were 3,720,000 cells/mL. To isolate enough cells for three samples (90,000), we aliquoted 24 µL from the cell-medium mixture into the sample. The excess cells were then either:

- plated again into a new flask(s) to form a new passage that could be used for follow-up or repeat experiments,
- plated to grow a larger number of cells, or
- frozen down in at least 500,000 cells per vial for future experiments.

During a week of experimentation, various flasks of cells were cultured in parallel as described above. However, these healthy and heterogenous CF cells were only half of the subject cells used in this experiment, as myofibroblast (MF) cells were also required. To obtain these, we followed a process to differentiate phenotypically activated MF cells from a passage of regular CF cells.

3.2.2. Differentiating cardiac myofibroblasts from cardiac fibroblasts

Before culturing for experimentation, the murine CF cells were treated to induce the inflammatory signals that will activate a response comparable to that of ischaemic injury and followed by maladaptive fibrosis. Such a response must be developed further than just the initial steps of stress-induced activation to retain structural integrity (proto-myofibroblast), to the stage of uncontrolled, pathological remodelling, i.e. the myofibroblast. This cardiac MF phenotype is characterised by a highly increased concentration of α-smooth muscle actin (α-SMA) stress fibres in its cytoplasmic region to account for the surplus of mechanical stress present. The overabundance of α-SMA is promoted by the release of transforming growth factor-beta 1 (TGF-β1), eventually leading to the formation of fibrotic scar tissue after MI.

Since it was not feasible to induce the intracellular mechanical stress required to differentiate cardiac MFs, we stimulated CFs with TGF-β1 (Peprotech) growth factor for 72 hours *in vitro* to induce the differentiation, imitating the environment that exists during cardiac remodelling (Pappritz *et al.* 2018). To validate whether this stimulation procedure indeed generates MFs, we conducted a *differentiation assay* using immunofluorescence microscopy. This involved following the stimulation of CF cells with TGF-β1, fluorescently staining for α-SMA, and comparing the presence of α-SMA protein of the differentiated cardiac MF cells to that of controlled CF cells. A higher α-SMA expression in the CF cells treated with growth factor compared than those that are not treated is indicative of developed cardiac MF cells (Pappritz *et al.* 2018).

The murine CFs were seeded out in 24-well culture plates (30,000 cells/well) for immunofluorescence. Once 80% confluence was reached, the cells were serum-starved overnight in DMEM containing 0.5% FBS, and 1% Pen-strep. Afterwards, cells were washed once with PBS, and a row was incubated with 5 ng/mL TGF-β1 supplemented media (10% FBS, 1% Pen-strep) in n = 6 wells, for up to 72 hours. In another row of n = 6 wells, the unstimulated control cells were also incubated during this period with the supplemented DMEM. The differentiation assay was repeated once more in the remaining two rows (n = 2) of the 24-well culture dish. For the immunofluorescence staining, we initially treated cells with Cy3-conjugated streptavidin antibody (red) for α-SMA, and with 4',6-diamidine-2'-phenylindole (DAPI) for nuclear visualisation, as per Pappritz *et al.* (2018). However, following the first round of microscopy, an overall lack of signal was found for these stains. It was then decided to alternatively use Cy3-conjugated Anti-Mouse IgG fluorescent antibody (red) for α-SMA staining, and Hoechst 33342 (blue) for nuclear staining (both from Jackson Immunoresearch, USA).

The process for immunofluorescence staining was performed using the newly selected dyes at room temperature, as follows:

After 72 hours of incubation with TGF-β1-supplemented DMEM, the media was removed, and cells were washed three times with PBS. The cells were then fixed with 4% paraformaldehyde for 10 minutes and rinsed thrice more with PBS. After that, 0.5 % Triton X-100 (Sigma Aldrich) biochemical detergent in PBS was added to permeate the cell membrane for access to cellular proteins and organelles. The perforations in the membranes allow for the primary antibody α-SMA (1:200; Dako, Hamburg, Germany) to attach to actin fibres within the cells. This solution was left for 30 minutes and then washed thrice. It was at this point that the Anti-mouse IgG fluorescent antibody (1:500) was added as the secondary antibody for 15 minutes to bind to the primary antibody, then washed. Finally, Hoechst (1:250) was added as a nuclear label, which is very similar to DAPI.

Figure 3.2 below shows the fluorescent microscope images taken at a 10x objective, allowing for a large group of cells to be visualised, and creating an overall impression of their cellular structures. We used a microscope (Carl Zeiss, Germany) with a laser in the Cy-3 spectrum (approx. 550 nm excitation

& 600 nm emission) to allow the red-fluorescent dye to be seen, as well as in the blue-fluorescent DAPI spectrum (approx. 358 nm excitation & 461 nm emission). By overlapping these two filters, one can see the blue-stained nuclei of each cell as well as its red-stained α-SMA protein structure. Being fibroblasts, they are generally large, elongated and spindle-shaped cells with actin processes extending outward from their bodies towards points of focal adhesions.

The frames on the left Figure 3.2 a and c represent the control experiment, with images taken of regular murine CF cells; whereas the images on the right Figure 3.2 b and d, represent the differentiation experiment, with the cells stimulated with TGF-β1. For more distinct comparison, the top row of images, Figure 3.2 a and b, are of a similar concentration of cells per frame. Similarly, the bottom row (Figure 3.2 c and d), has a uniform (higher) cellular concentration. The same imaging settings (e.g. time, aperture, and gain) were kept when capturing images throughout the wells for this assay to conclude an observational point of reference. The CF cells stimulated with TGF-β1 in the right column show a more extensive spread of red-stained α- SMA fibre structures than the untreated control CF cells in the left column. Therefore, based on the literature as well as the results from this differentiation assay, it can be derived that the cardiac fibroblast cells treated with growth factor supplemented media as described in the protocol above, have progressed into myofibroblast cells.

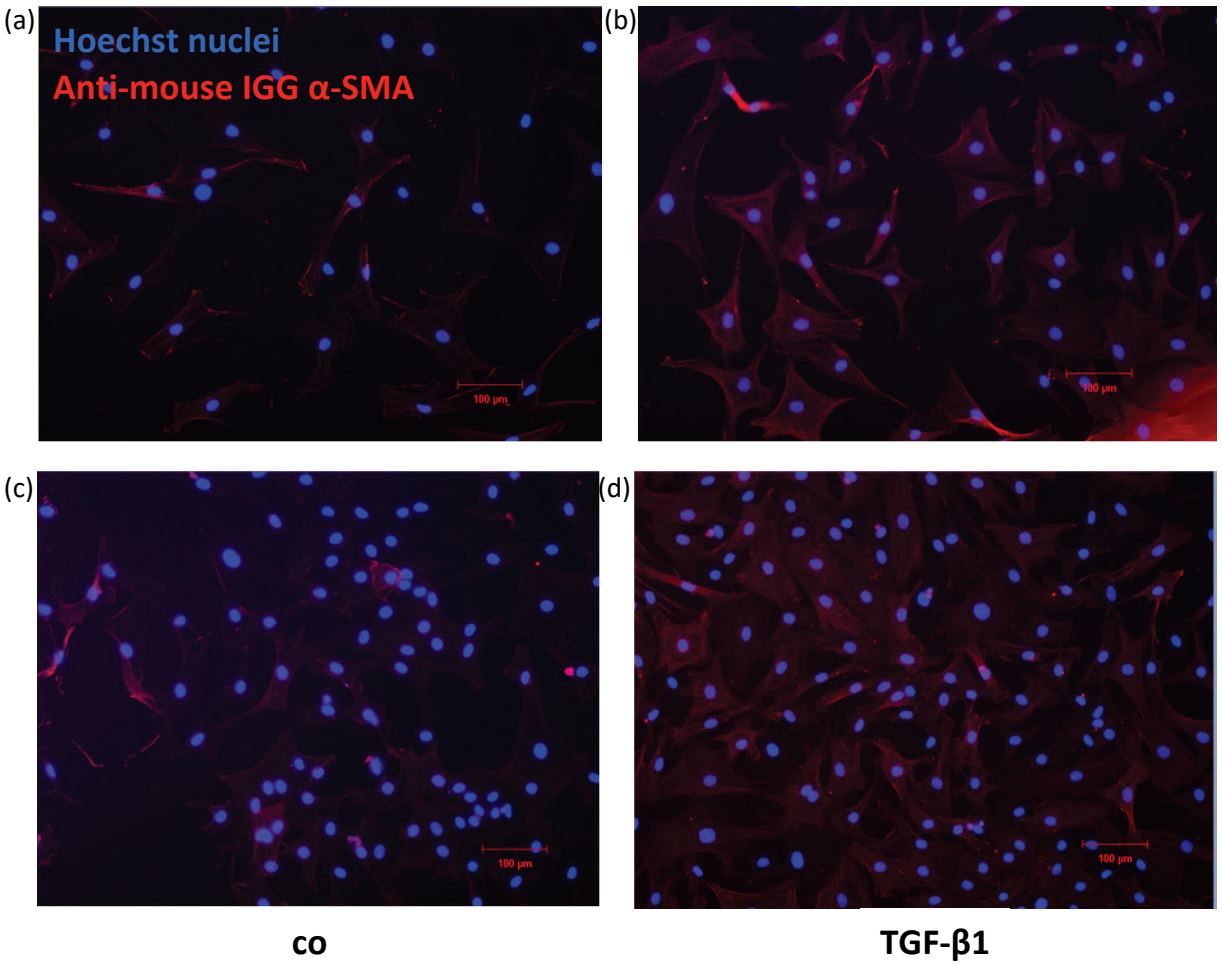

Figure 3.2. TGF-ß1-induced differentiation of cardiac fibroblasts. α-SMA marked by a Cy3-conjugated Anti-mouse IgG antibody (red) and Hoechst dye for nuclear staining (blue). Regular CF cells (control condition) (a) & (c) and differentiated myofibroblasts (b) & (d).

3.2.3. Preparing cells in 3D environments

To create 3D microrheology samples that are consistent and reproducible, one must perform the following steps precisely. We began by isolating the needed cells from their respective growing environments. To obtain CF cells, we isolated cells from an 80% confluent flask, by transferring them (using trypsin-EDTA) to a Falcon tube, centrifuging, and counting them as described before in Section 3.1.1 To accumulate MF cells for experimentation, stimulated cells were cultured within a T75 flask, and the TGF-β1-supplemented media was changed every 72 hours until 80% confluency was reached. After that, they were counted too, and we were left with two tubes of determined amounts CF and MF cells, both suspended in 1 mL of media.

To prepare a 3D microenvironment sample of a specific condition, we used a hydrogel volume of 50 µL. We were investigating the influence that four conditions would have on cellular stiffness, namely CF phenotype cells in a soft and a stiff environment, and MF phenotype cells in a soft and a stiff environment. Thus, for one experiment, 100 µL of both 4% and 10% PEG gels were required (2 × 50µL samples of each). Each condition of the experiment was prepared in a compartment of a 4-chamber glass bottom petri dish as rendered in Figure 3.3 a.

Due to the tiny volumes, we created a total gel mixture of 135 µL, allowing for an excess of 35 µL that may be squandered during formation and pipetting. This ensured a reliable final gel volume and concentration. The gel mixtures were prepared according to the constituent ratios tabulated in Appendix A: PEG Hydrogel Preparation: Table A.4 and Table A.5, including RGD adhesion peptide, to create an inhabitable environment for the cells.

The gel formation protocol was followed according to Section 2.2.1. However, before aliquoting the final gel mixture volumes for curing, media containing 2X 30,000 cells were removed from both CF and MF cell mixtures. 30,000 cells of each phenotype were added to fill up 50 µL of both 4% and 10% PEG gel mixtures in four separate microcentrifuge tubes, each representing an experimental condition. Each mixture was aspirated twice. In immediate succession, the cell-suspended gel mixtures were aliquoted individually as 50 µL drops (hemispherical blobs/globules) onto the glass surface(s) of the four chambers of the petri dish, in the order the depicted in Figure 3.3 b.

The blob samples were left to cure a for at least 30 minutes until they formed viscoelastic hydrogel samples. Finally, each sample was immersed in 500 µL of media, the petri dish was covered in parafilm, and it was stored in incubation conditions overnight. Below in Figure 3.4 is a graphical depiction of a microrheology sample (viewed from the side) with cells suspended at various positions throughout the 3D hydrogel matrix. This configuration will allow for an objective lens of a confocal microscope to focus from below. The sample preparation was repeated twice more, to perform a total of three repeat experiments (n = 3).

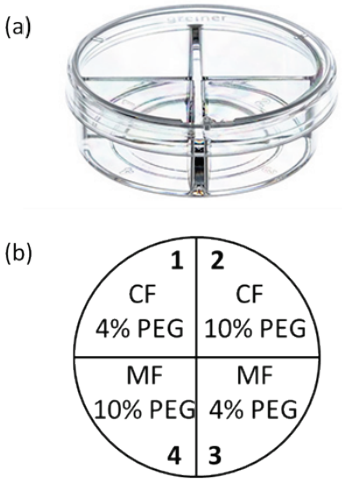

Figure 3.3. Four-chamber Glass bottom petri dish used for confocal microscopy. (a) is a rendered image and below (b) the sample allocation of each chamber.

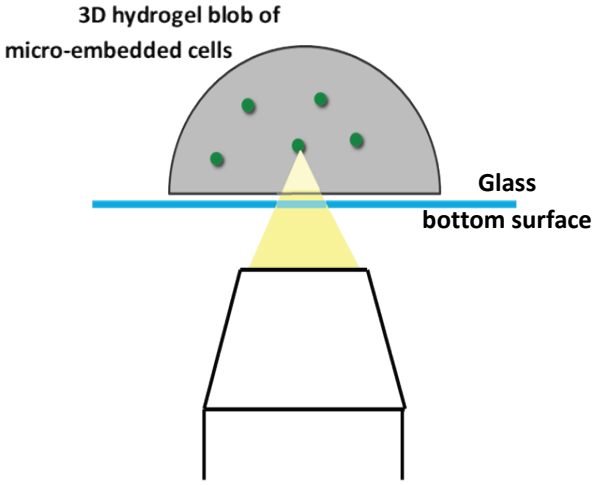

Figure 3.4. Schematic diagram of 3D environment prepared for each condition for microrheology, with a side-sectioned representation of the hydrogel globule in grey with containing CF or MF cells as green dots (not to scale).

3.2.4. Mitochondria tracer particle preparation

To track the mitochondria within the cells, we labelled them with Mitotracker Green fluorescent dye (Life Technologies) before microscopy. The optimal concentration of Mitotracker had to be established, as a too low concentration will not sufficiently label the mitochondria and produce little or no signal during microscopy, and a too high concentration will be toxic for the cells, killing them. The appropriate Mitotracker amount was determined by exposing cells to a range of concentrations.

We found that 300 mM of Mitotracker was significant to penetrate both 4% and 10% gels within 1 hour and label the cells. The process and formula used to achieve this concentration of Mitotracker are stated in Appendix A: Supplementary Data for Chapter 2: Mitotracker Dilution. Once established, experimental samples prepared for passive mitochondrial particle tracking (MPT) in a four-chamber petri dish were removed after 24 hours of incubation. The growth media was changed with 300 nM added Mitotracker Green solution and incubated for at least 1 hour (at 37°C and in 5% CO_2) for the mitochondria of cells to be labelled and traceable (see Figure 3.5 a). The procedure followed to attain this concentration of Mitotracker is detailed in Appendix A: Mitotracker Dilution. When using the Mitotracker Green solution, any exposure to light sources was avoided (as is common practise with a fluorescent substance), to prevent bleaching and loss of immunofluorescence.

The CF and MF cells seeded in both soft and stiff 3D PEG hydrogel matrices, after Mitotracker incubation, were now labelled and ready for particle tracking microrheology. One may keep the Mitotracker solution media or choose to replenish it with new media. A drop of oil was added onto the objective lens, and the appropriate stage was inserted. The Petri dish sample was placed within the stage of the confocal microscope and the chamber was adjusted to its environmental setting (incubation conditions, with CO_2 and 37°C), which takes roughly 5 minutes to settle.

Using the 10x objective at first in the brightfield channel, we set out to find cells in the 3D matrix region. The focus (z-plane) was moved from z = 0 at the bottom surface of the Petri dish's glass slip, through the glass to z = 175µm at the top (inside) surface. Here, some cells were seen that have landed on the surface, that have adhered and spread in typically elaborate 2D structures. We ensured, however, to move further upward and into the biomaterial matrix, where cells were suspended in 3D (at z > 500 µm). To get a single cell in the frame, we had to set the focus plane through a central section of a cell, where the signal is the strongest (see example in Figure 3.5, right). The aim was to track individual cells over a time period to examine the passive fluctuations of particles within the cell, solely based on the effect of the microenvironment. This process is depicted in Figure 3.5 b.

Cells were tracked for 100 seconds at 500 milliseconds per frame, i.e. 2 frames per second. Furthermore, it was aimed that at least 30 mitochondria particles are tracked per cells across the time period and that at least 9 cells are imaged per experimental condition. For example, 9 CF cells in 4% PEG matrix were tracked, and so too for the other three conditions. Cells that appeared to have their membranes impaired or that are in the process of dividing were ignored.

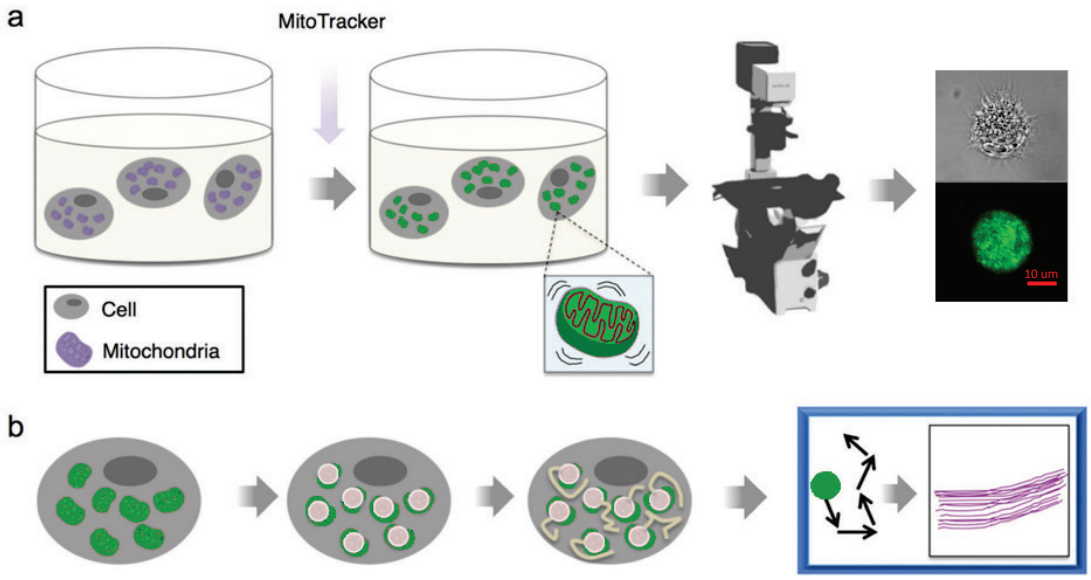

Figure 3.5. A schematic of the MPT microrheology procedure. (a) Cells embedded in a PEG hydrogel matrix various concentration, incubated for 24 hours and another hour following the addition of Mitotracker Green solution. Image acquisition performed using a confocal microscope at an objective to capture single isolated cells. (b) Imaging software used to track the displacement of tracer particles over time, from which the mean-square displacements are calculated (purple slopes on the right) (Kim JE et al. 2018).

3.2.5. Microscopy and image acquisition

A Zeiss LSM 880 confocal microscope (Carl Zeiss, Germany) was used with dual lasers to excite TPMT (transmission photomultiplier tube - brightfield) and MTGr (photomultiplier tube - fluorescent green) channels. Images were acquired with 63x1.4NA oil immersion objective and equipped with an electron-multiplying CCD monochrome camera. The sample in the environmental chamber was moved in the x-y plane with the joystick and focussed in the z-direction with the focus-control knob to establish the image plane.

For the imaging of a single cell, the image plane was used to locate a suspended in the 3D matrix. In order to avoid boundary effects, cells located adjacent to the glass bottom surface were disregarded. At first, cells were pinpointed in TPMT (brightfield) view, and when found we manually switched to the MTGr (green) channel to display the fluorescent green signal of the tracer particles. The imaging plane was then finely focused within the cell. Previously, the system was calibrated with a microsphere sample to identify system noise (Mak *et al.* 2014).

In the image acquisition software (ZEN Black, Carl Zeiss), the gain is adjusted to set the desired white light intensity, the laser power is kept below 2%, and the pinhole may be made smaller to show sharper detail or larger to allow more light through. Once finalised for image acquisition, these settings were saved and reloaded for each repeat experiment. From this point onward, the gain was the only setting occasionally being adjusted to optimise for the level of the signal being presented by each cell. Finally, the continuous series of 200 images were acquired over 100s per cell, split along the two channels (TPMT and MTGr).

3.2.6. Particle tracking analysis and post-processing

To reconstruct the spatial tracer particle trajectories, the recorded time-lapse images underwent software-based frame-by-frame tracking analysis, recording individual particle displacements. ImageJ opensource imaging software was used to track the displacement vs time of each tracer particle, and thus for classifying the particle trajectories.

Figure 3.6. A schematic representation of the stack over time-lapse images to be taken and the resulting trajectory of a mitochondria particle created through frame-by-frame tracking analysis.

For each cell, the time series of 200 images (500 ms per frame over 100 s) is exported from the image acquisition software as a stack of images (Tagged Image File Format – TIFF). The images were split three ways in the order Mitotracker (MTGr), Brightfield (TPMT), and the two channels superimposed/overlaid (see Figure 3.11). The TIFF file was imported into ImageJ as an Image Sequence (8-bit, Grayscale). At first, the scale was set in ImageJ by using the 10 µm scale bar from the imported image as a reference. The image was then cropped in the Mitotracker frame (fluorescent channel) and around the region of the cell, as seen in Figure 3.9 a. The image frame rate property was set to 0.5s (500 ms) per frame before running the tracking analysis.

The ImageJ plugin TrackMate (Fiji) by Tinevez *et al.* (2017) was installed, as it was developed for single-particle tracking and provided the tools necessary for MPT microscopy. It also has grown a large user base since before its publication and has successfully been used in many studies (Borzenkov *et al.* 2019, Tanenbaum *et al.* 2014). As we launched TrackMate, we ran its LoG (Laplacian of Gaussian) detector algorithm as a segmentation filter. The LoG filter automatically identifies spot-like features that appear bright against the dark background. We then specified the estimated area diameter ('blob diameter') in which these particles will displace, as 1.2 µm. The blob diameters can be seen sketched as small purple circles in Figure 3.8 b. One may preview this function, and then choose to change its

quality and manually limit the number of spots identified as an initial threshold, before calculating additional features and renderings (essentially fine-tuning the LoG filter). In the following step, the user can set filters to eliminate outlying spots detected in regions other than in the cell that may have occurred from random noise signalling.

From here, we configured a LAP (Linear Assignment Problem) tracker to merge the spots of the entire stack of images into trajectories. The concise ('simple') version of this particle-linking algorithm (Jaqaman *et al.* 2008) was used where only spatial distance is the input parameter and criteria to join two spots from successive frames. In other words, the requirement of linking two points in a trajectory relies on their relative distances. For this, we specified three configuration fields. We set the maximal allowed *linking distance*, which defines the maximum spatial search range for aspiring matching spots, as 0.5 µm. The second field is the maximal *gap-closing distance* which defines that two segments on a track may not be bridged if the distance between the last point of the first segment and the first point of the last segment exceeds this value. We set the gap-closing distance to 0.5 µm. Finally, and imperatively, is the maximal *frame interval* between two spots to be bridged. We allowed the algorithm to search up to the duration of 5 frames to detect spots for gap-closing between two segments.

Once the LAP tracker is run, the user is tasked with filtering the tracks identified, by specifying a minimum number of linked spots in a track. We aimed to have at least 80 or more spots per particle trajectory (with the maximum possible being 200, due to the number of images available). This filtering step's window of the TrackMate analysis is displayed in Figure 3.7. In this captured example, the trade-off specification of 80.52 spots per track was made, and 96 tracks were found. The tracks are seen within the blob diameter circles of Figure 3.8 b. As mentioned in section 3.2.4, we aimed to reach at least 30 particle trajectories per cell. However, fluorescent labelling in 3D PEG matrices were not as coherent throughout all the samples as with 2D. Thus, in reality, we tracked on average about 30 particles per cell, with the absolute minimum being 15 trajectories for a cell. The data gathered about the particles' trajectories were exported and saved as an XML (Extensible Mark-up Language) data file. An example of the general format of an output XML file used in this study provided in a data set on UCT's open data platform, Zivahub: https://zivahub.uct.ac.za/account/articles/12999653 (Haasbroek 2020).

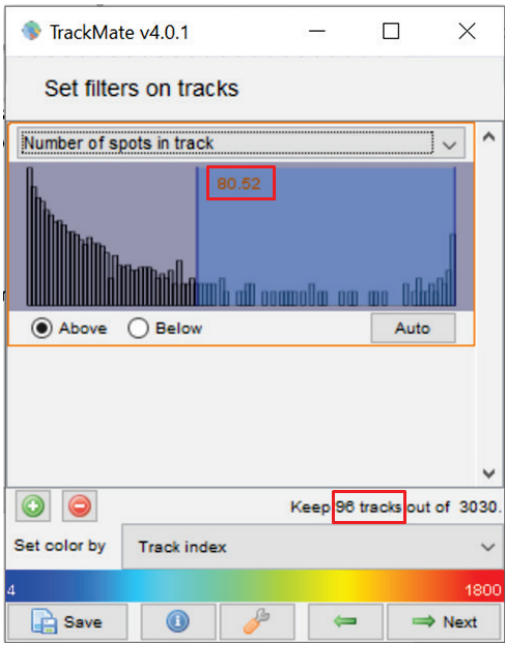

Figure 3.7. A Window from the ImageJ plugin TrackMate allowing the user to specify a lower limit to the number of spots per particle trajectory. In this cell example, 96 tracks were found to have 80.52 or more points in them.

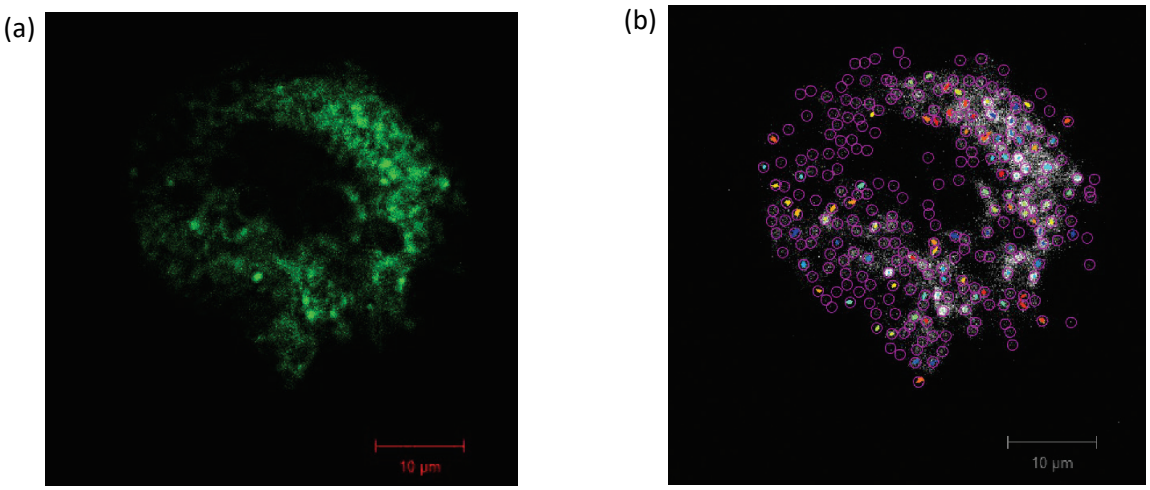

Figure 3.8. A cropped microscope image of the of a CF cell (a) in Mitotracker green channel signal before any processing and (b) following the TrackMate analysis identifying the displacement trajectories of its mitochondria particles.

The post-processing comprised of using the trajectory data of a cell's tracer particles to establish its mean-square displacement (MSD), giving an indication of the overall mode of the intracellular motion. The post-processing was done in MATLAB, and the code file is provided in the Zivahub data set (https://zivahub.uct.ac.za/account/articles/12999653). At first, we imported the cell data (XML) file to be analysed into MATLAB and handled the data file's format to extract the relevant x-y displacement data for each particle (line 1-25). The code was then merged with a pre-established script, namely '@msdanalyzer' (Tarantino *et al.* 2014) (lines 26-70), and used to as a tool to plot the displacements as tracks on an x-y plot (Figure 3.9), as well as process, calculate and linearly plot the MSD for the cell (Figure 3.10). In the MSD plot, one can see the MSD values *vs* time as the dark centre line. The upper and lower limits (grey shaded area) and standard error increases as time progress,

indicating the importance of analysing the early timescales. Thus, in further analysis, a logarithmic scale was used to express MSD graphs. From this stage, and for every analysed cell, the MSD values across the time period t = 100s gathered from this process was copied from the MATLAB output sheet to an Excel sheet for storing and sorting the data. From this sheet, data was imported back into MATLAB scripts for further plotting, analysis and breakdown of results.

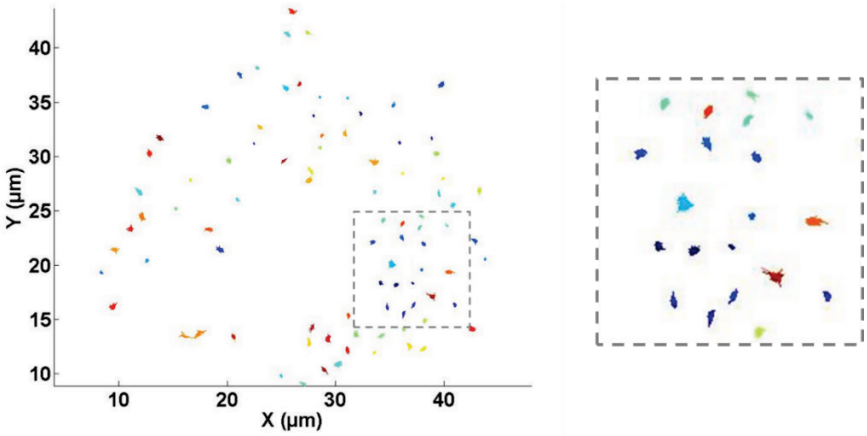

Figure 3.9. Mitochondria particle displacements (trajectories) of a CF cell plotted by MATLAB software. The movement is recorded over a 100s time period and due to the thermal energy of the surrounding medium.

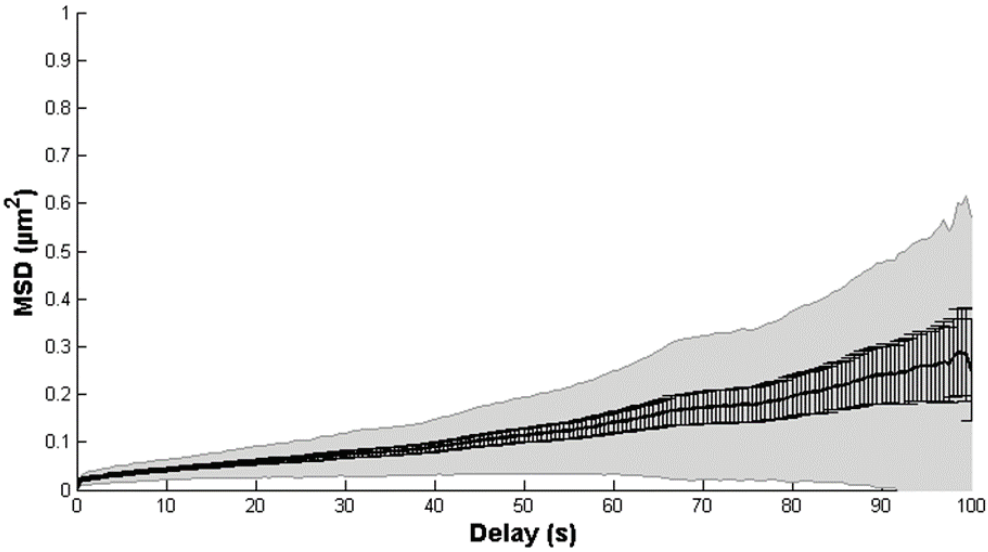

Figure 3.10. Mean-Square Displacement (MSD) plot (linear) produced following the particle tracking analysis and post-processing. The data values of the central line represent the MSD and the grey area the upper and lower limits, including standard error bars for each point.

3.3. Results

The intracellular mechanics of cardiac fibroblast cells in 3D, healthy or pathogenic, were hypothesised to depend on the properties of the 3D ECM. Moreover, the difference in cell phenotype from healthy CF to maladaptive MF may also affect intracellular forces. To investigate these relationships, we measured cell stiffness through mitochondrial particle tracking (MPT) microrheology. The labelled mitochondria serve as the tracer particles within the cells that are embedded in PEG hydrogels before

experimentation. Figure 3.11 shows each of the four conditions in our experiment, namely CF and MF cells embedded in 4%, and CF and MF cells embedded in 10% concentrated PEG-based matrices.

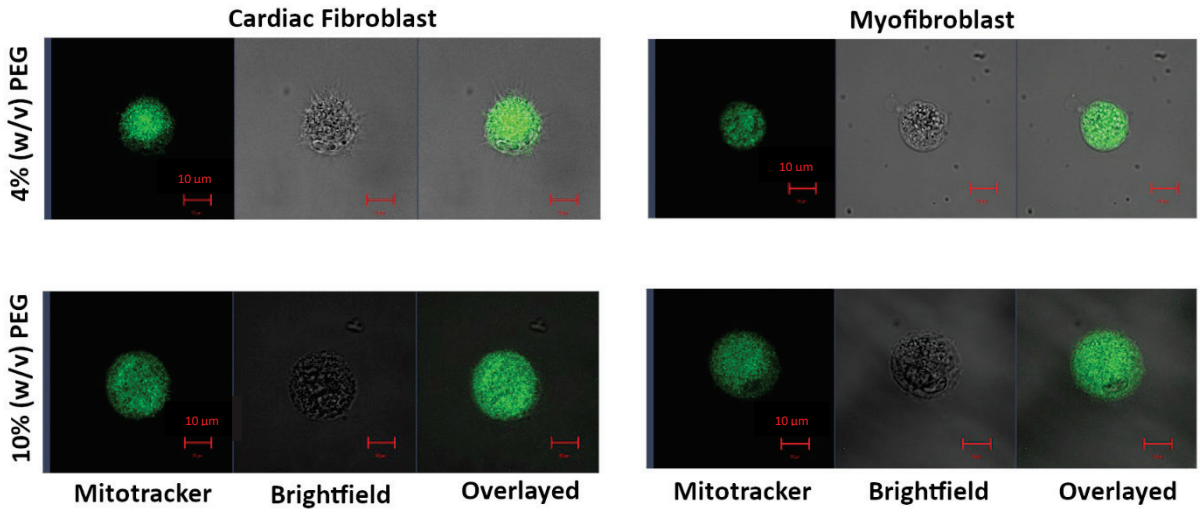

Figure 3.11. Isolated single CF and MF cells split(left-right) with green fluorescently labelled mitochondria, brightfield and merged images. The scale bar (red) is 10 µm.

The intracellular motion was observed, and the mitochondrial particle displacements were traced from 10 single isolated cells for each condition in three repeat experiments (n = 3), where a mean number of 30 mitochondrial particles were captured and tracked per cell. We used 15 as the minimum ("cut-off") number of trajectories per cell, as instances where less than 15 particles were tracked per cell, the mean-square displacement (MSD) profile for that cell became irregular and generally unreliable. Figure 3.12 shows the MSD profiles that were calculated from collections of mitochondrial trajectories for each cell and plotted as logarithmic MSD ensemble-averages for descriptive statistical evaluation. The analysis was performed for all four conditions.

The MSD is an indicator of a particles ability to traverse over a given time period. Particles with a larger MSD thus have a more remarkable ability to manoeuvre along more considerable distances within the cell during the time interval compared to particles with a lower MSD. As a result, the slope of the logarithmic MSD is indicative of its mechanical properties. Lower, flat MSDs indicate stiffer, solid-like materials whereas MSDs with higher inclined slopes indicate more fluid-like materials, characterised by increased intracellular motor-driven activity. To investigate this property and to classify the type of motion exhibited in the intracellular environment, we determined and analysed the (diffusive) exponent of the logarithmic MSD slope, α, which encapsulates the power law time interval dependence. This value gave us a quantitative indication of the role that the ECM has on the thermal fluctuations of CF and MF cells.

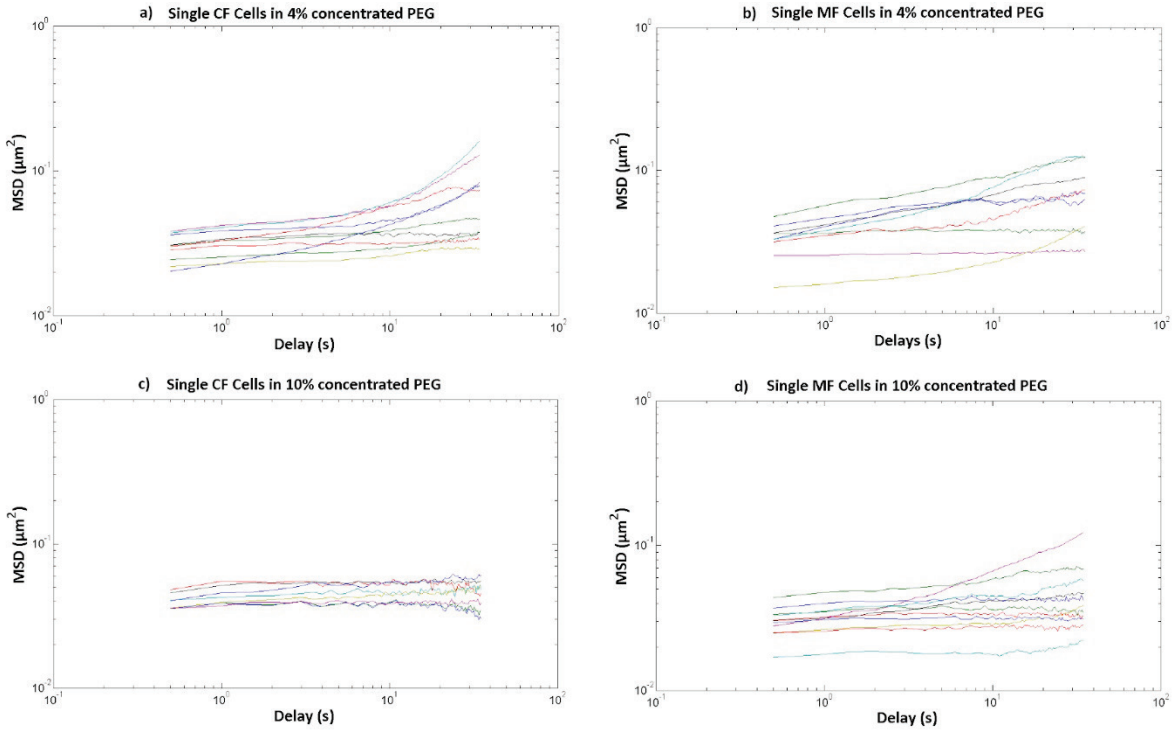

Figure 3.12. Intracellular fluctuations of CFs and MFs in 4% (m/v) and 10% (m/v) PEG hydrogels expressed as MSD over time delay (log scale). MSD profiles of 10 (a) CF and (b) MF cells in 4% PEG, and of 10 (c) CF and (d) MF cells in 10% PEG.

The MSD-dependent power law coefficient α provides a measurement of the degree of fluidity, where a larger value for α refers to a more fluid-like motion. (Hence, the term 'fluidity' will be used for α synonymously with power law coefficient or diffusivity coefficient.) An $\alpha \approx 0$ corresponds to fully constrained, sub-diffusive motion such as the thermal fluctuation in an elastic material, while $\alpha \approx 1$ corresponds to fluid, diffusive motion such as the thermal fluctuation of a Newtonian fluid (Kim JE *et al.* 2018). The motion of mitochondrial particles within cells experiences significant intracellular traffic which results in constrained particle fluctuation ($0 < \alpha < 1$). However, these particles can exhibit diffusive ($\alpha = 1$) or even super-diffusive ($\alpha > 1$), typical of cells undergoing active processes, e.g. migration, that would require enhanced molecular motor activity that would increase α into these regimes. It is the initial delay time of $\tau = 1 – 5$ s in which molecular motor activity still has negligible effects on the corresponding MSD values and slope. The power law is therefore investigated at these early delay times of intracellular particle tracking microrheology.

We aimed to determine whether cell stiffness of cardiac fibroblasts depended on their stage of fibrosis (normal/maladaptive), and the matrix stiffness (soft/stiff). This meant that we were faced with two independent variables, also referred to as factors, that were categorical and nominal of nature. The first factor, the "cell phenotype" was divided into two groups: "CF" and "MF". Secondly, "gel concentration" consists of "4% PEG" and "10% PEG" groups. To study the combined effects of these factors on the dependent variable of MSD (and subsequently, α), a two-way analysis of variance (two-way ANOVA) was performed in SPSS (IBM). Statistical significance is computed for $p < 0.05$ unless otherwise stated.

With the statistical analysis, we first investigated the interaction effect of the factors. The presence of an interaction effect indicates that the effect of one factor inversely depends on the other factor. For

example, the cell phenotype affects the behaviour of cells in 4% gels differently than in 10% gels. However, as shown in the two-way ANOVA tests results in Appendix B: Descriptive Statistics: Table B.3, we found that the interaction was non-significant, which meant that each independent variable, cell phenotype or gel concentration, had the same effect regardless of its counterpart. This non-significant interaction between cell phenotype and gel concentration was demonstrated for the immediate (τ = 0.5 s), intermediate (τ = 3 s), and large (τ = 5 s) delay times. Subsequently, we evaluated the main effects of gel concentration and cell phenotypes separately and independently (Appendix B: Particle Tracking Microrheology Data: Pairwise Comparisons: Table B.4 & Table B.5).

Our results found that the cell stiffness of CFs and MFs increased to a similar extent, with an increase in matrix stiffness from 4% to 10% PEG gel. This was preliminarily depicted by the difference in the slopes of the overall MSD profiles of CF in 4% compared to in 10% PEG (Figure 3.13 a), with a similar trend seen for MF cells in 4% compared to those embedded in 10% PEG (Figure 3.13 b). The slopes of the MSDs in 4% PEG had a higher inclination than those in 10% PEG, signifying a stiffer cytoplasm versus a more fluid-like one, respectively. In terms of magnitude, the MSD was larger also for both CF and MF cells in 4% PEG than in 10% PEG ($p \leq 0.033$, Table B.4) during all delay times (τ = 1-5s) with considerably large effect sizes ($\eta_p^2 > 0.147$).

The substantial effect of gel concentration was more specifically illustrated by the considerable difference in the diffusivity α of cells in soft (4%) and stiff (10%) matrices (Figure 3.13 c and d). As shown in Table B.2, α increases with progression in matrix stiffness from 4% to 10% PEG for both CF and MF cells, with fluidity α = 0.19-0.36 through all delay times for cells in soft matrices and α = 0.09-0.18 throughout all delay times for cells in stiff matrices ($p \leq 0.05$, Table B.4), observed for either normal CFs as well as for maladaptive MFs. This confirms that CFs behave according to the principles of mechanotransduction, using cytoskeleton-based rigidity-sensing mechanisms between themselves and their environment, and as a consequence, their inherent stiffness is regulated by their environment.

Upon closer examination, mitochondrial fluctuations reached relatively weak sub-diffusive motion within the 4% PEG matrices, with $\alpha > 0.2$ for larger delay times. The MSD profiles of cells in soft matrices initially have slanted slopes that indicate strongly sub-diffusive motion during immediate and intermediate delay times, progressing to steeper slopes that indicate weakly sub-diffusive motion during larger delay times. The mitochondrial particles within cells that are embedded in stiffer matrices are subjected to strong sub-diffusive motion in the region of $\alpha \approx 0.1$, across all delay times.

It was further deduced from Figure 3.13 that there is a larger, relatively increasing difference in α across short, medium and large delay times (τ = 0.5-5s) noted for CF cells. The difference in α for MF cells in soft and stiff matrices remains relatively constant across these delay times. This may allude to the fact that the addition of molecular motor activity is less prevalent in MF cells, whereas the apparent increase in α for CF cells across the three delay times may indicate an early incidence of motor-induced motions.

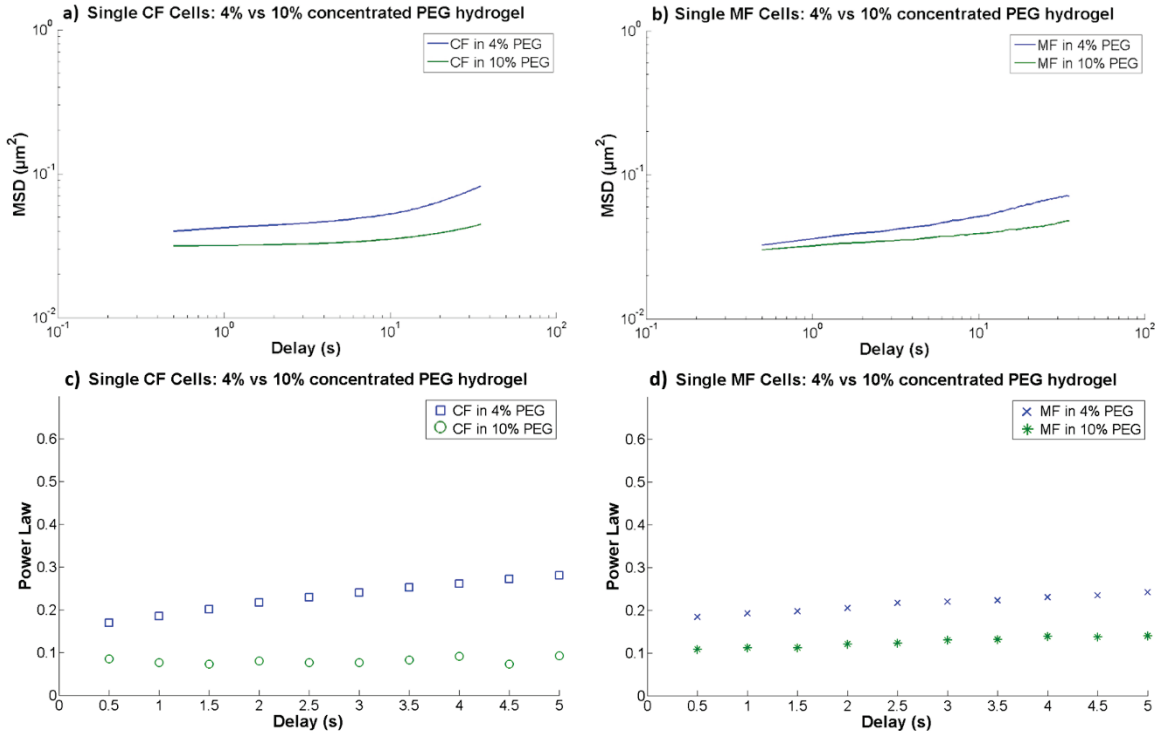

Figure 3.13. Microrheology characterisation of CF and MF single cells in 4% vs 10% (m/v) PEG hydrogel matrices. MSD profiles of CF (a) and MF (b) cells and α values of CF (c) and MF (d) cells, each in 4% PEG vs 10% PEG gel concentrations.

To investigate the effect of progression of the cell's phenotype on its intracellular activity, we similarly compared the MSD profiles and power laws (α) of CF versus MF cells, as seen in Figure 3.14. The progression of cells from CF to MF had very little to no effect on the MSD of cells in both 4% and 10% PEG hydrogel, as foreshadowed in the close proximities of the MSD profiles. Indeed, the difference in the main effect of CF vs MF cells on the MSD and α in either gel concentrations are shown to be statistically non-significant (Table B.5). Figure 3.14 a shows that the MSD had some comparable difference for the initial delay time of CF vs MF cells within 4% PEG matrix alone, with CF showing larger values than MF cells, to begin with (see also Figure 3.15 a). This difference in mean values at τ = 0.5 s is shown to be significant in simple effects analysis ($p = 0.044$, Table B.8). Furthermore, the simple effect of the cell phenotype on MSD and α had no significant difference at any other delay time (Table B.8 & Table B.9). This insignificance is reflected in the α values that follow the same trend across the delay times in the bottom row of Figure 3.14 (i.e. c and d).

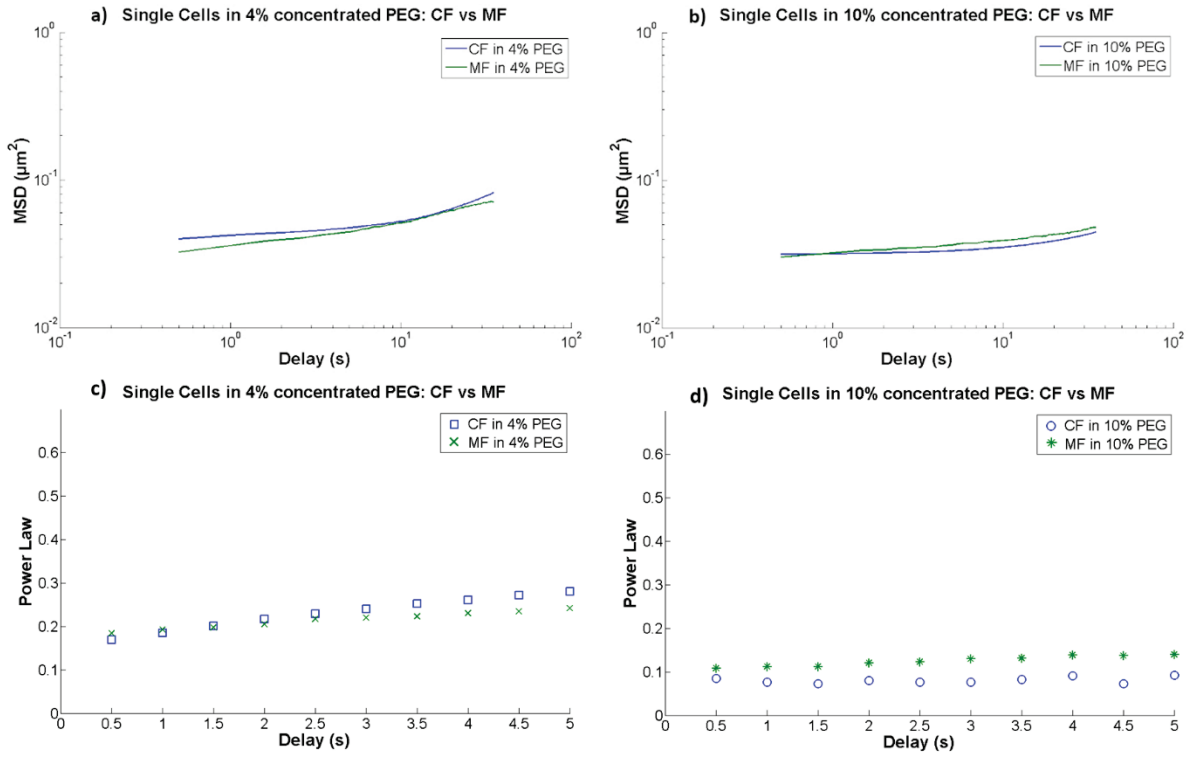

Figure 3.14. Microrheology characterisation of CF vs MF single cells in 4% and 10% (m/v) PEG hydrogel matrices. MSD profiles of CF and MF cells in 4% (a) and 10% (b) PEG hydrogel, and α values of CF and MF cells in 4% (c) and 10% (d) PEG hydrogel.

In summary, we have considered initial (τ = 0.5 s), intermediate (τ = 3 s) and large (τ = 5 s) delay time data for MSD and α. The results are presented in Figure 3.15 and compare all four conditions per delay time. MSD and α decrease substantially with the increase in gel concentration from 4% to 10% PEG (i.e. increase in 3D matrix stiffness) during initial, intermediate and large delay times for CF and MF cells. As a result, cells were stiffer in 4% than in 10% PEG. The progression between CF and MF cells only influenced the MSD value at the initial delay time in 4% PEG matrix. Furthermore, the cell phenotype had no considerable effect at any other delay time and in any other environment, on MSD and α. Thus, the progression of cell phenotype from CF to MF imposed no rise or reduction in cellular stiffness in softer or stiffer matrices.

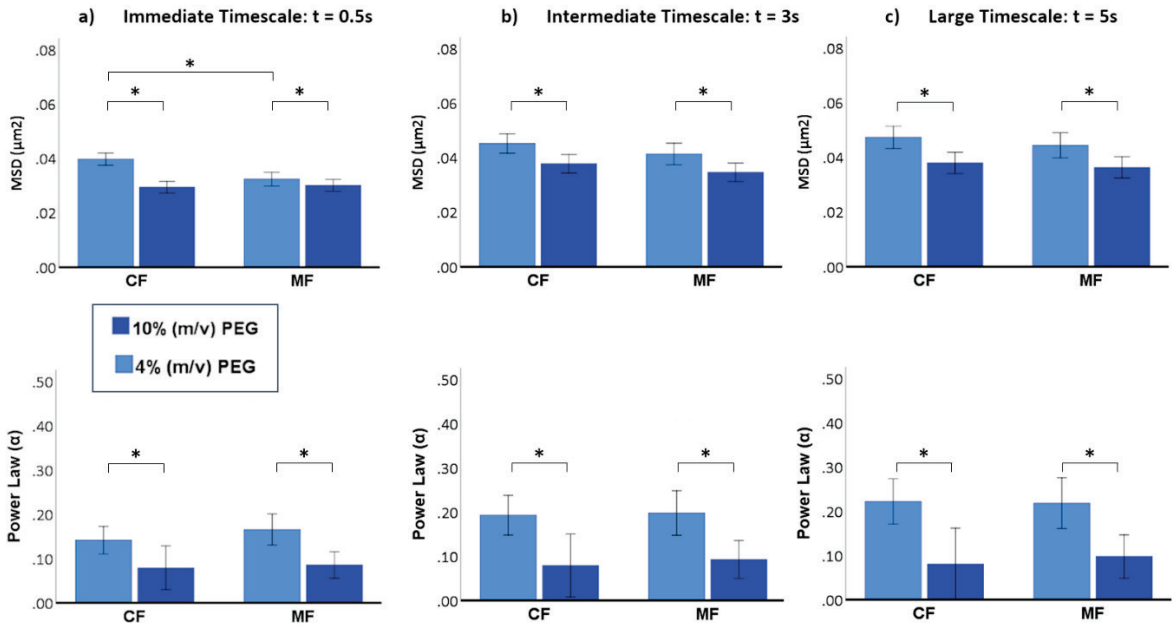

Figure 3.15. Multiple comparison of MSD and α of CF and MF cells in soft and stiff 3D PEG-based matrices (4% and 10% m/v PEG) concurring with (a) initial ($MSD|_{\tau = 0.5\,s}$ and $\alpha|_{\tau = 0.5\,s}$), (b) intermediate ($MSD|_{\tau = 3\,s}$ and $\alpha|_{\tau = 3\,s}$), and (c) large ($MSD|_{\tau = 5\,s}$ and $\alpha|_{\tau = 5\,s}$) delay times.

3.4 Discussion

This study aimed to provide an improved understanding of the role of the extracellular environment in cardiac fibroblasts and their activated phenotype, cardiac myofibroblasts. It was done by performing a mechanical quantification of these cell types through passive mitochondrial particle tracking microrheology experiments. The non-cellular-invasive experimental technique was successfully used to measure the spatial fluctuations of intracellular mitochondria particles over time, as a result of the thermal energy of the 3D ECM. The average displacement of the mitochondria was processed to give us an indication of the fluidity of the cells *in vitro*, as a result of the passive perturbations of their extracellular environment, which were mimicked by viscoelastic PEG hydrogels.

Mean-square displacement (MSD) profiles were obtained from mitochondria trajectories and analysed for each cell type (CF and MF) in two environmental conditions (4% and 10% m/v PEG gel). Lower and flat MSDs reveal more stiff and rigid cells, whereas gradually sloped MSD curves allude to greater fluidity and intracellular motor-driven movement. The logarithmic slope of the MSDs at various delay times was derived for each condition, giving us the diffusivity coefficient, or fluidity, α (Eq. 2). Using this parameter, we could quantitatively define the intracellular motion and effectively, the stiffness of the cells; where $\alpha \approx 0$ relates to constrained motion and $\alpha \approx 1$ relates to diffusive motion.

The constrained motion versus the diffusive motion could be compared to the thermal fluctuations in an elastic material versus a Newtonian fluid, respectively. We focussed on the α values of early delay times (τ = 0.5-5 s), to interpret values that closely reflect the viscoelastic properties of the cells, as delay times larger than this reflect additional internal stress fluctuations beyond the thermal fluctuations, due to increasing molecular motor activity as time progresses (Kim JE *et al.* 2018). In

other words, larger delay times cannot be relied upon to render an accurate depiction of intracellular mechanics and the stiffness of the cells. This principle of considering the early time intervals had to be applied to our study, as values up to t = 100 s were available.

From our MPT study, we concluded that changes in the PEG concentration, i.e. the stiffness (as found in Chapter 2) of our hydrogel matrix/microenvironment, respectively affects the stiffness of CF and MF cells to the same extent. An increase in PEG hydrogel concentration from 4% to 10% resulted in a decrease in the MSD at all three early delay times (Figure 3.15, top row). This result indicates that the stiffness of CF an MF cells increases with an increase in PEG concentration (and hydrogel stiffness); an outcome that was also found by Kim JE *et al.* (2018) when characterising cancer cells through MPT microrheology in 3D collagen matrices of various stiffnesses. We found that α decreases significantly as PEG concentration increases from 4% to 10% too, for both CF and MF across all delay times of interest (Figure 3.15, bottom row). This indicates that both cell phenotypes behave in a more fluid-like fashion in decreased concentrated PEG hydrogels and that intracellular CF and MF stiffnesses are increased and decreased by stiffer and softer *in vitro* microenvironments, respectively. Kim JE *et al.* (2018), however, did not reflect this trend; but instead found the power law exponent values of their cells to be directly proportional to increasing collagen concentration.

Furthermore, we found no sufficient evidence that either low or high PEG concentration had a profoundly distinctive effect on the stiffness of phenotypically different cells, CFs and MFs. This effect is depicted visually by very similar MSD profiles of CF and MF in 4% PEG as well as in 10% PEG, as well as quantitively by the non-significant difference in the power law exponent value, α, between the two cell states at any delay time. This finding is somewhat unexpected, as an increased ECM deposition, expression of α-SMA and contractile properties present in MFs (Nakayama *et al.* 2014) would presumably accompany a noticeable increase cellular stiffness compared to regular CFs. Instead, we observed a slightly higher fluidity in MF cells than in CF cells in the higher (10%) concentrated PEG gel, although not very considerably so. Before this discovery can be categorically accepted, we suggest to further scrutinise the transdifferentiation process stipulated by Pappritz *et al.* (2018) which we followed to develop MFs. In our differentiation assay, we could ensure with better certainty that it is α-SMA present and visualised; by removing the primary (middle) anti-body α-SMA from the preparation process, and only adding the Anti-Mouse IgG fluorescent antibody. If during fluorescent imaging, we observe darkness / no signal, we know that the fibres previously were α-SMA, validating our differentiation process.

Another approach to modulate the differentiation of fibroblasts into myofibroblasts is to use the mechanical cues of increased matrix stiffness. Increased stiffness is associated with increased trans-differentiation (Nakayama *et al.* 2014). During cell culture, valvular interstitial cells were found to become activated, α-SMA expressing MFs when adhered to photodegradable hydrogels with 32 kPa (high) elastic moduli, and remained inactivated when cultured on gels of 7 kPa (low) (Kloxin *et al.* 2010). During such a process, it is believed that the matric stiffness regulates MF differentiation by modulating actin polymerisation, causing the nuclear translocation of megakaryoblastic leukaemia factor-1 (MLK-1), a co-factor that regulates fibrotic genes (Huang *et al.* 2012). Thus, culturing gels on substrates on substrates of higher stiffness, together with the stimulation of TGF-β1, may ensure more reliant MF differentiation.

We have also not observed any substantial interaction effect when performing a two-way ANOVA test between our two independent variables (factors), cell phenotype and gel concentration, implying that the effect of one factor does not depend on that of the other. While this result could be primarily due to the indifference in the stiffness properties found between CFs and MFs, we also argue that this may be due to the morphology allowed for the cells in our created hydrogel microenvironment. Although

used in many recent studies, 3D cell culture in hydrogels as synthetic ECM are nano-porous structures that fully encapsulate cells often posing a physical barrier that limits cell processes like cell shape change, movement and expansion (Chaudhuri 2017).

In covalently bonded hydrogels like our 8-PEG-VS-DTT gel, it is generally understood that cells stay rounded and proliferation is repressed. This was mostly true for cells in our study, although there were several cases where cells have started to probe and spread with focal adhesion arms. Due to this, recent emphasis has been placed on the viscoelasticity of ECMs, rather than purely the elastic property of the hydrogel and its covalent crosslinking, that may also be cytotoxic in 3D cell culture. For example, it has been found by Mckinnon *et al.* (2014) that myofibroblast cells (C2C12) were able to attain a more spread morphology in PEG hydrogels that have a faster stress relaxation ($\tau_{1/2}$ ~ 10s). Likewise, fibroblast cells (3T3) embedded in RGD-linked alginate hydrogels with an increased rate of stress relaxation, were found to show a greater degree of spreading and proliferation (Chaudhuri 2017). By more closely varying the stress relaxation, creep or viscoelastic properties of our PEG hydrogel ECM, we could perhaps induce more native cell morphologies and more accurately study the behavioural differences between cardiac CFs and MFs in soft and stiff matrices, as well as the potential interaction between these two factors.

4. Conclusion and Recommendations

In the myocardium, as in many other tissues, cells interact with the surrounding three-dimensional extracellular matrix that plays a major role in regulating cellular behaviour processes, such as the response to ischaemic injury, resulting from chronic artery disease (atherosclerosis). MI is an event that stems from atherosclerosis and is defined by cell death due to sustained myocardial ischaemia. Acute MI results in adverse remodelling of the myocardium, eventually leading to contractile dysfunction and chronic heart failure. CFs are the most abundant cells in the heart and are responsible for the deposition of cardiac ECM. As a response to injury and for the process of wound healing, CFs are activated to become (proto-)MFs, with increased expression of SMA and contractile properties for beneficial remodelling and reconstruction.

The excessive ECM deposited by proto-MFs is usually removed by apoptosis following the tissue repair. However, the persistent presence of MFs over time leads to reactive fibrotic states, such as the acute and excessive secretion of collagen following MI to which there is no current treatment. Thus, it is crucial to gain a fundamental understanding about (i) the mechanism of differentiation from CF to MF cells and how closely these cell types are interrelated and (ii) the role of the ECM mechanics in regulating both cell states, to prevent, attenuate or reverse cardiac fibrosis. It was also identified that there is a lack of knowledge on the functionality of the cardiac fibroblast.

We proposed to investigate whether and how the mechanical properties and behaviour of cardiac cells are affected by the extracellular environment and hypothesised that a change in stiffness of the remodelling extracellular environment associated with fibrosis leads to a change of the mechanical properties and contractile forces of cardiac fibroblasts and myofibroblasts.

Hence, this dissertation aimed to investigate the effects of extracellular stiffness on mechanical properties of cardiac fibroblasts and myofibroblasts using engineered in vitro microenvironments with tuneable physical properties.

We reached this aim by fulfilling our key objectives (i) to identify biomaterial systems that mimic 3D extracellular environments, (ii) to undertake mechanical characterisation of these biomaterial systems, and (iii) to characterise the mechanical properties of cardiac fibroblasts and myofibroblasts in 3D environments of different stiffness.

Polyethylene Glycol (PEG) hydrogel is a desired biomaterial for many applications due to its non-toxicity, non-immunogenicity, and bio-inert characteristics. It was selected for our study as an extracellular matrix (ECM) mimicking hydrogel, as it offers highly tuneable qualities and can be manufactured to specific mechanical properties. Through different techniques of mechanical characterisation, it was established that the volumetric swelling ratio and more importantly, the elastic modulus of 20 kDa 8-arm PEG-VS hydrogel crosslinked with DTT reagent, is directly proportional to the concentration (m/v) of PEG precursor used to form the material. The addition of RGD (arginylglycylaspartic acid) as cell adhesion peptides, resulted in a decrease in the storage component of the shear modulus (G') of the hydrogel, as the peptides take up PEG arms which are potential crosslinks. This slight compromise to the structural integrity is relevant when tuning in vitro 3D extracellular environments to desired conditions.

Cardiac fibroblast (CF) cells were harvested from a rat and cultured to proliferate, and cardiac myofibroblast (MF) cells were obtained by stimulating these CFs with TGF-β1. Finally, these two states of cells were cultured and encapsulated in 3D PEG hydrogel matrices *in vitro*, and we investigated the

isolated effect of low (4% m/v) and high (10% m/v) concentrated PEG hydrogel matrices on the stiffness of CFs and differentiated MFs through passive MPT microrheology (4 conditions, 10 cells/condition, n = 3 repeats). As confirmed by the mechanical characterisation, the low and high PEG concentrations translate respectively to a low and high stiffness of the hydrogel matrix. We found overwhelming evidence that the ECM stiffness plays a definitive role in the inherent cellular stiffness of both CF and MF cells. An increase in the mechanical stiffness of the synthetic ECM caused a significant increase in cell stiffness. This trend was quantified by weak power law (diffusive) exponent value, α, the slope of the logarithmic MSD profile of the microrheology samples, and an indicator of cytoplasmic material fluidity. No considerable difference of cell fluidity was found between cell phenotypes (CF & MF) in soft matrices. In stiff matrices, MFs seemed to become somewhat stiffer across the delay times, although with no significant effect.

It was found that PEG-based hydrogels can be well characterised mechanically by micro-indentation and uniaxial tensile testing. By designing a material-specific optimal procedure, micro-indentation testing PEG-based hydrogels are new and can be repeated in future studies as it is the least expensive in terms of material usage. With the increasing popularity of PEG gels for various biomedical engineering applications, more diverse mechanical characterisation techniques may become necessary, and the techniques optimised and employed in this study may prove beneficial.

Our study also demonstrated that CFs behave according to the principles of mechanotransduction, using cytoskeleton-based rigidity-sensing mechanisms between themselves and their environment, and as a consequence, their inherent stiffness is regulated by their environment. This information is complimentary in the quest to develop potential therapies that will limit the degradation of the myocardial ECM following MI.

We recommend reassessing the CF to MF differentiation process, starting with the assay, to ensure distinguishably activated MFs. A positive finding would verify that there is no considerable difference between CF and MF cells in their behaviour resulting from a change in ECM mechanics. However, an additional mechanical intervention can be made to supplement the growth factor-induced trans-differentiation process, by culturing cells on stiffer 2D substrates together with the biochemical stimulation. A foolproof method of differentiation combined with a thoroughly scrutinised way to prove it (differentiation assay), will validate this aspect of the study.

Recent studies have made increasing use of natural and synthetic hydrogels to imitate and understand the role of the viscoelastic, time-dependent aspects of ECM mechanics and how it regulates cells. Although it has been established in hydrogel-based 3D culture studies that varying stiffness alone has an impact on cellular properties and biological processes, natural ECMs are not just elastic but also viscous. Specialised properties such as varying stress relaxation, creep, and viscoelasticity have potential impacts that are largely unclear (Chaudhuri 2017). Biomaterial design for in vitro studies has historically been utilised without taking into account the importance of viscoelasticity, which is expected to be a major technical specification moving forward (Chaudhuri *et al.* 2020). Myofibroblasts, for example, has been shown to spread into a more innate morphology in PEG hydrogels of with a higher rate of stress relaxation. We recommend looking into new approaches to characterise native ECM tissue *in vivo* as well as revisiting the developing processes to fine-tuning these time-dependent mechanics in hydrogels are seasoned for future investigation. This will allow us to create more accurate biomaterials that will further this discovery, by extensively advancing our knowledge of cell-matrix interaction and bring us closer to disease prevention e.g. anti-fibrotic therapies.

This study refocused attention towards the importance of cardiac fibroblasts, and their relevance in addressing cardiac fibrosis stemming from the global, ubiquitous problem of myocardial infarction. It

also sheds new light on the cell mechanics of CF and MF cells and the role that their microenvironment plays on their behaviour and encourages further investigations to bring forth therapies that induce beneficial remodelling of the ECM and prevent, attenuate or reverse cardiac fibrosis.

5. References

Anseth KS, Bowman CN, Brannon-Peppas L. *Mechanical properties of hydrogels and their experimental determination*. Biomaterials 1996, **17**(17): 1647-57.

Bax JJ, Baumgartner H, Ceconi C, Dean V, Fagard R, Funck-Brentano C, Hasdai D, Hoes A, Kirchhof P, Knuuti J. *Third universal definition of myocardial infarction*. Journal of the American College of Cardiology 2012, **60**(16): 1581-98.

Bellis SL. *Advantages of RGD peptides for directing cell association with biomaterials*. Biomaterials 2011, **32**(18): 4205-10.

Borzenkov M, D'alfonso L, Polissi A, Sperandeo P, Collini M, Dacarro G, Taglietti A, Chirico G, Pallavicini P. *Novel photo-thermally active polyvinyl alcohol-prussian blue nanoparticles hydrogel films capable of eradicating bacteria and mitigating biofilms*. Nanotechnology 2019, **30**(29): 295702.

Bracher M, Bezuidenhout D, Lutolf MP, Franz T, Sun M, Zilla P, Davies NH. *Cell specific ingrowth hydrogels*. Biomaterials 2013, **34**(28): 6797-803.

Byfield FJ, Reen RK, Shentu T-P, Levitan I, Gooch KJ. *Endothelial actin and cell stiffness is modulated by substrate stiffness in 2D and 3D*. J Biomech 2009, **42**(8): 1114-9.

Byron A, Humphries JD, Humphries MJ. *Defining the extracellular matrix using proteomics*. International Journal of Experimental Pathology 2013, **94**(2): 75-92.

Caliari SR, Burdick JA. *A practical guide to hydrogels for cell culture*. Nature methods 2016, **13**(5): 405-14.

Califano JP, Reinhart-King CA. *A balance of substrate mechanics and matrix chemistry regulates endothelial cell network assembly*. Cellular and molecular bioengineering 2008, **1**(2-3): 122.

Califano JP, Reinhart-King CA. *Substrate stiffness and cell area predict cellular traction stresses in single cells and cells in contact*. Cellular and molecular bioengineering 2010, **3**(1): 68-75.

Chang CW, Dalgliesh AJ, López JE, Griffiths LG. *Cardiac extracellular matrix proteomics: Challenges, techniques, and clinical implications*. PROTEOMICS – Clinical Applications 2016, **10**(1): 39-50.

Chaudhuri O. *Viscoelastic hydrogels for 3D cell culture*. Biomaterials science 2017, **5**(8): 1480-90.

Chaudhuri O, Cooper-White J, Janmey PA, Mooney DJ, Shenoy VB. *Effects of extracellular matrix viscoelasticity on cellular behaviour*. Nature 2020, **584**(7822): 535-46.

Chen C. *Mechanotransduction - a field pulling together?* Journal of cell science 2008, **121**(Pt 20): 3285-92.

Chen C, Li R, Ross RS, Manso AM. *Integrins and integrin-related proteins in cardiac fibrosis*. Journal of Molecular and Cellular Cardiology 2016, **93**: 162-74.

Deleon-Pennell KY, Meschiari CA, Jung M, Lindsey ML. *Chapter two - matrix metalloproteinases in myocardial infarction and heart failure*. in Khalil RA (Ed. Progress in molecular biology and translational science, Academic Press, 2017, **147**: 75-100.

Dobner S, Bezuidenhout D, Govender P, Zilla P, Davies N. *A synthetic non-degradable polyethylene glycol hydrogel retards adverse post-infarct left ventricular remodeling*. Journal of Cardiac Failure 2009, **15**(7): 629-36.

Drury JL, Mooney DJ. *Hydrogels for tissue engineering: Scaffold design variables and applications*. Biomaterials 2003, **24**(24): 4337-51.

Dugina V, Fontao L, Chaponnier C, Vasiliev J, Gabbiani G. *Focal adhesion features during myofibroblastic differentiation are controlled by intracellular and extracellular factors*. Journal of cell science 2001, **114**(18): 3285-96.

Engler AJ, Carag-Krieger C, Johnson CP, Raab M, Tang HY, Speicher DW, Sanger JW, Sanger JM, Discher DE. *Embryonic cardiomyocytes beat best on a matrix with heart-like elasticity: Scar-like rigidity inhibits beating*. Journal of cell science 2008, **121**(Pt 22): 3794-802.

Engler AJ, Richert L, Wong JY, Picart C, Discher DE. *Surface probe measurements of the elasticity of sectioned tissue, thin gels and polyelectrolyte multilayer films: Correlations between substrate stiffness and cell adhesion*. Surface science 2004, **570**(1-2): 142-54.

Frostegård J. *Immunity, atherosclerosis and cardiovascular disease*. BMC medicine 2013, **11**: 117-.

Gillette BM, Jensen JA, Tang B, Yang GJ, Bazargan-Lari A, Zhong M, Sia SK. *In situ collagen assembly for integrating microfabricated three-dimensional cell-seeded matrices*. Nature materials 2008, **7**(8): 636-40.

Goffin JM, Pittet P, Csucs G, Lussi JW, Meister J-J, Hinz B. *Focal adhesion size controls tension-dependent recruitment of α-smooth muscle actin to stress fibers*. The Journal of Cell Biology 2006, **172**(2): 259-68.

Golden HB, Gollapudi D, Gerilechaogetu F, Li J, Cristales RJ, Peng X, Dostal DE. *Isolation of cardiac myocytes and fibroblasts from neonatal rat pups* Cardiovascular development, Springer, 2012: 205-14.

Gyongyosi M, Winkler J, Ramos I, Do QT, Firat H, Mcdonald K, Gonzalez A, Thum T, Diez J, Jaisser F, Pizard A, Zannad F. *Myocardial fibrosis: Biomedical research from bench to bedside*. European Jounal of Heart Failure 2017, **19**(2): 177-91.

Haasbroek PD. *Supplementary data for msc dissertation "role of extracellular environment in mechanical properties of cardiac fibroblasts and myofibroblasts".* University of Cape Town, 2020, https://doi.org/10.25375/uct.12999653.

Hoffman BD, Massiera G, Van Citters KM, Crocker JC. *The consensus mechanics of cultured mammalian cells*. Proceedings of the National Academy of Sciences of the United States of America 2006, **103**: 10259-64.

Huang X, Yang N, Fiore VF, Barker TH, Sun Y, Morris SW, Ding Q, Thannickal VJ, Zhou Y. *Matrix stiffness-induced myofibroblast differentiation is mediated by intrinsic mechanotransduction*. American Journal of Respiratory Cell and Molecular Biology 2012, **47**(3): 340-8.

Huynh J, Nishimura N, Rana K, Peloquin JM, Califano JP, Montague CR, King MR, Schaffer CB, Reinhart-King CA. *Age-related intimal stiffening enhances endothelial permeability and leukocyte transmigration*. Sci Transl Med 2011, **3**(112): 112ra22.

Janmey PA, Miller RT. *Mechanisms of mechanical signaling in development and disease*. J Cell Sci 2011, **124**(1): 9-18.

Jaqaman K, Loerke D, Mettlen M, Kuwata H, Grinstein S, Schmid SL, Danuser G. *Robust single-particle tracking in live-cell time-lapse sequences*. Nature methods 2008, **5**(8): 695-702.

Jeong B, Bae YH, Kim SW. *Thermoreversible gelation of PEG− PLGA− PEG triblock copolymer aqueous solutions*. Macromolecules 1999, **32**(21): 7064-9.

Kadner K, Dobner S, Franz T, Bezuidenhout D, Sirry MS, Zilla P, Davies NH. *The beneficial effects of deferred delivery on the efficiency of hydrogel therapy post myocardial infarction*. Biomaterials 2012, **33**(7): 2060-6.

Kim J, Kong YP, Niedzielski SM, Singh RK, Putnam AJ, Shikanov A. *Characterization of the crosslinking kinetics of multi-arm poly(ethylene glycol) hydrogels formed via michael-type addition*. Soft Matter 2016, **12**(7): 2076-85.

Kim JE, Reynolds DS, Zaman MH, Mak M. *Characterization of the mechanical properties of cancer cells in 3D matrices in response to collagen concentration and cytoskeletal inhibitors*. Integrative Biology 2018, **10**(4): 232-41.

Kloxin AM, Benton JA, Anseth KS. *In situ elasticity modulation with dynamic substrates to direct cell phenotype*. Biomaterials 2010, **31**(1): 1-8.

Kohn JC, Zhou DW, Bordeleau F, Zhou AL, Mason BN, Mitchell MJ, King MR, Reinhart-King CA. *Cooperative effects of matrix stiffness and fluid shear stress on endothelial cell behavior*. Biophysical journal 2015, **108**(3): 471-8.

Krishnan R, Klumpers DD, Park CY, Rajendran K, Trepat X, Van Bezu J, Van Hinsbergh VW, Carman CV, Brain JD, Fredberg JJ, Butler JP, Van Nieuw Amerongen GP. *Substrate stiffening promotes endothelial monolayer disruption through enhanced physical forces*. American Journal of Cell Physiology 2011, **300**(1): C146-54.

Kyburz KA, Anseth KS. *Three-dimensional hmsc motility within peptide-functionalized PEG-based hydrogels of varying adhesivity and crosslinking density*. Acta biomaterialia 2013, **9**(5): 6381-92.

Lajiness JD, Conway SJ. *Origin, development, and differentiation of cardiac fibroblasts*. Journal of Molecular and Cellular Cardiology 2014, **70**(0): 2-8.

López B, Querejeta R, González A, Larman M, Díez J. *Collagen cross-linking but not collagen amount associates with elevated filling pressures in hypertensive patients with stage c heart failure*. Hypertension 2012, **60**(3): 677-83.

Lutolf M, Hubbell J. *Synthesis and physicochemical characterization of end-linked poly (ethylene glycol)-co-peptide hydrogels formed by michael-type addition*. Biomacromolecules 2003, **4**(3): 713-22.

Lutolf MP, Hubbell JA. *Synthetic biomaterials as instructive extracellular microenvironments for morphogenesis in tissue engineering*. Nature Biotechnology 2005, **23**(1): 47-55.

Mackenna D, Summerour SR, Villarreal FJ. *Role of mechanical factors in modulating cardiac fibroblast function and extracellular matrix synthesis*. Cardiovascular Research 2000, **46**(2): 257-63.

Mak M, Kamm RD, Zaman MH. *Impact of dimensionality and network disruption on microrheology of cancer cells in 3D environments*. PLOS Computational Biology 2014, **10**(11): e1003959.

Mckinnon DD, Domaille DW, Cha JN, Anseth KS. *Biophysically defined and cytocompatible covalently adaptable networks as viscoelastic 3D cell culture systems*. Advanced Materials 2014, **26**(6): 865-72.

Moeendarbary E, Harris AR. *Cell mechanics: Principles, practices, and prospects*. WIREs Systems Biology and Medicine 2014, **6**(5): 371-88.

Murata H. *Rheology-theory and application to biomaterials*. 2012.

Nakayama KH, Hou L, Huang NF. *Role of extracellular matrix signaling cues in modulating cell fate commitment for cardiovascular tissue engineering*. Advanced healthcare materials 2014, **3**(5): 628-41.

Nguyen QT, Hwang Y, Chen AC, Varghese S, Sah RL. *Cartilage-like mechanical properties of poly (ethylene glycol)-diacrylate hydrogels*. Biomaterials 2012, **33**(28): 6682-90.

Pappritz K, Savvatis K, Koschel A, Miteva K, Tschöpe C, Van Linthout S. *Cardiac (myo)fibroblasts modulate the migration of monocyte subsets*. Scientific Reports 2018, **8**(1): 5575.

Parlato M, Reichert S, Barney N, Murphy WL. *Poly(ethylene glycol) hydrogels with adaptable mechanical and degradation properties for use in biomedical applications*. Macromolecular bioscience 2014, **14**(5): 687-98.

Peppas NA, Hoffman AS. *Chapter i.2.5 - hydrogels*. in Ratner BD, Hoffman AS, Schoen FJ, Lemons JE (Eds.) Biomaterials science (third edition), Academic Press, 2013, https://doi.org/10.1016/B978-0-08-087780-8.00020-6: 166-79.

R&Dsystems. *Rat mesenchymal stem cells (1 x 10e6 cells/vial)*. Retrieved 5 March, 2020, from https://www.rndsystems.com/products/rat-mesenchymal-stem-cells-1-x-10e6-cells-vial-_psc003#assay-procedure.

Raeber GP, Lutolf MP, Hubbell JA. *Molecularly engineered PEG hydrogels: A novel model system for proteolytically mediated cell migration*. Biophysical journal 2005, **89**(2): 1374-88.

Rattan S, Li L, Lau HK, Crosby AJ, Kiick KL. *Micromechanical characterization of soft, biopolymeric hydrogels: Stiffness, resilience, and failure*. Soft Matter 2018, **14**(18): 3478-89.

Rienks M, Papageorgiou A-P, Frangogiannis NG, Heymans S. *Myocardial extracellular matrix: An ever-changing and diverse entity*. Circulation research 2014, **114**(5): 872-88.

Rodriguez ML, Mcgarry PJ, Sniadecki NJ. *Review on cell mechanics: Experimental and modeling approaches*. Applied Mechanics Reviews 2013, **65**(6).

Rohr S. *Arrhythmogenic implications of fibroblast-myocyte interactions*. Circulation: Arrhythmia and Electrophysiology 2012, **5**(2): 442-52.

Selvaggi L, Salemme M, Vaccaro C, Pesce G, Rusciano G, Sasso A, Campanella C, Carotenuto R. *Multiple-particle-tracking to investigate viscoelastic properties in living cells*. Methods 2010, **51**(1): 20-6.

Shen MY, Michaelson J, Huang H. *Rheological responses of cardiac fibroblasts to mechanical stretch*. Biochemical and Biophysical Research Communications 2013, **430**(3): 1028-33.

Singh SP, Schwartz MP, Lee JY, Fairbanks BD, Anseth KS. *A peptide functionalized poly (ethylene glycol)(PEG) hydrogel for investigating the influence of biochemical and biophysical matrix properties on tumor cell migration*. Biomaterials science 2014, **2**(7): 1024-34.

Statistics South Africa. *Mortality and causes of death in South Africa, 2016: Findings from death notification*. Pretoria, Statistics South Africa, 2018.

Suresh S, Spatz J, Mills J, Micoulet A, Dao M, Lim C, Beil M, Seufferlein T. *Connections between single-cell biomechanics and human disease states: Gastrointestinal cancer and malaria*. Acta biomaterialia 2005, **1**(1): 15-30.

Tanenbaum ME, Gilbert LA, Qi LS, Weissman JS, Vale RD. *A protein-tagging system for signal amplification in gene expression and fluorescence imaging*. Cell 2014, **159**(3): 635-46.

Tarantino N, Tinevez J-Y, Crowell EF, Boisson B, Henriques R, Mhlanga M, Agou F, Israël A, Laplantine E. *Tnf and il-1 exhibit distinct ubiquitin requirements for inducing nemo–ikk supramolecular structures*. Journal of Cell Biology 2014, **204**(2): 231-45.

Thygesen K, Alpert JS, Jaffe AS, Chaitman BR, Bax JJ, Morrow DA, White HD. *Fourth universal definition of myocardial infarction (2018)*. Journal of the American College of Cardiology 2018, **72**(18): 2231-64.

Tinevez J-Y, Perry N, Schindelin J, Hoopes GM, Reynolds GD, Laplantine E, Bednarek SY, Shorte SL, Eliceiri KW. *Trackmate: An open and extensible platform for single-particle tracking*. Methods 2017, **115**: 80-90.

Tomasek JJ, Gabbiani G, Hinz B, Chaponnier C, Brown RA. *Myofibroblasts and mechano-regulation of connective tissue remodelling*. Nature Reviews Molecular Cell Biology 2002, **3**(5): 349-63.

Trichet L, Le Digabel J, Hawkins RJ, Vedula SRK, Gupta M, Ribrault C, Hersen P, Voituriez R, Ladoux B. *Evidence of a large-scale mechanosensing mechanism for cellular adaptation to substrate stiffness*. Proceedings of the National Academy of Sciences 2012, **109**(18): 6933-8.

Tschope C, Lam CS. *Diastolic heart failure: What we still don't know. Looking for new concepts, diagnostic approaches, and the role of comorbidities*. Herz 2012, **37**(8): 875-9.

Ustyugov A, Chicheva M, Lysikova E, Vikhareva E, Sipyagina N, Malkova A, Straumal E, Bovina E, Senatov F, Salimon A. *Development of 3D cell culture on ultra-high molecular weight polyethylene (uhmwpe) as the basis of cellular matrix*. Biomedical Chemistry: Research and Methods 2018, **1**(3): e00048-e.

Van Putten S, Shafieyan Y, Hinz B. *Mechanical control of cardiac myofibroblasts*. Journal of Molecular and Cellular Cardiology 2016, **93**: 133-42.

Walpita D, Hay E. *Studying actin-dependent processes in tissue culture*. Nature Reviews Molecular Cell Biology 2002, **3**(2): 137-41.

Wang N, Tolić-Nørrelykke IM, Chen J, Mijailovich SM, Butler JP, Fredberg JJ, Stamenović D. *Cell prestress. I. Stiffness and prestress are closely associated in adherent contractile cells*. American Journal of Physiology-Cell Physiology 2002, **282**(3): C606-C16.

Weber KT, Sun Y, Bhattacharya SK, Ahokas RA, Gerling IC. *Myofibroblast-mediated mechanisms of pathological remodelling of the heart*. Nature Reviews Cardiology 2013, **10**(1): 15-26.

Wells RG. *Tissue mechanics and fibrosis*. Biochimica et Biophysica Acta (BBA)-Molecular Basis of Disease 2013, **1832**(7): 884-90.

White HD, Chew DP. *Acute myocardial infarction*. The Lancet 2008, **372**(9638): 570-84.

Wise P, Davies NH, Sirry MS, Kortsmit J, Dubuis L, Chai C-K, Baaijens FPT, Franz T. *Excessive volume of hydrogel injectates may compromise the efficacy for the treatment of acute myocardial infarction*. International Journal for Numerical Methods in Biomedical Engineering 2016, **32**(12): e02772.

Yesildag C, Ouyang Z, Zhang Z, Lensen MC. *Micro-patterning of PEG-based hydrogels with gold nanoparticles using a reactive micro-contact-printing approach*. Frontiers in Chemistry 2019, **6**(667).

Yeung T, Georges PC, Flanagan LA, Marg B, Ortiz M, Funaki M, Zahir N, Ming W, Weaver V, Janmey PA. *Effects of substrate stiffness on cell morphology, cytoskeletal structure, and adhesion*. Cell motility and the cytoskeleton 2005, **60**(1): 24-34.

Zalipsky S, Harris JM. *Introduction to chemistry and biological applications of poly(ethylene glycol)* Poly(ethylene glycol), American Chemical Society, 1997, **680**: 1-13.

Zaragoza C, Marquez S, Saura M. *Endothelial mechanosensors of shear stress as regulators of atherogenesis*. Curr Opin Lipidol 2012, **23**(5): 446-52.

Zhang Z, Loebus A, De Vicente G, Ren F, Arafeh M, Ouyang Z, Lensen MC. *Synthesis of poly(ethylene glycol)-based hydrogels via amine-michael type addition with tunable stiffness and postgelation chemical functionality*. Chemistry of Materials 2014, **26**(12): 3624-30.

Zustiak SP, Durbal R, Leach JB. *Influence of cell-adhesive peptide ligands on poly(ethylene glycol) hydrogel physical, mechanical and transport properties*. Acta biomaterialia 2010, **6**(9): 3404-14.

Appendix A: Supplementary Data for Chapter 2

This section provides supplementary data for chapter 2 “Mechanical Characterisation of Biomaterials Systems used as 3D Extracellular Environments”.

Preparation of Phosphate Buffered Saline

2.9 g of $Na_2HP0_4.\ 12H_2O(8mM)$, 0.2 g of $KH_2O_4(1.4\ mM)$, 0.2 $g\ of\ KCl(2.7mM)$ and 8 g of $NaCl(137\ mM)$ were weighed out and dissolved in 900 mL of NanoPure water, stirred at 240 with a stirrer bar. The pH was adjusted to 7.4; the solution was correctly labelled and autoclaved.

Preparation of Dulbecco’s Modified Eagle’s Medium

To prepare 1L of DMEM medium, 900 mL of NanoPure water is measured, and the powered DMEM is added and stirred using a stirrer rod into it until fully dissolved. The packaging containing the powder is rinsed with a small amount of water to gather all the traces of medium followed by 3.7 g of sodium bicarbonate ($NaHCO_3$). Once all is dissolved, the media has to be adjusted to fall within 0.1-0.3 of pH 7.4, by adding 1N HCl or 1N $NaOH$. If the pH level is sufficient, more water is added to fill the entire 1L volume, and the medium is filter sterilized using a membrane of 0.2 µm porosity or less.

Preparation Iso-osmotic PBS for Hydrogels

Solution A: 5.17 g of Sodium dihydrogen phosphate dihydrate ($NaH2HPO4H2O$) was dissolved in 250 ml of nanopore water

Solution B: 26.85 g of Sodium phosphate dibasic dodecahydrate ($Na2HPO4.\ 12H2O$) was dissolved in 500 ml of nanopore water

Combined: 65 ml of solution A + 435 ml of solution = 500 ml, and then added 4.38 g of $NaCl$. The solution had a pH of exactly 7.5

PEG Hydrogel Preparation

Table A.1. Constituents for the Formation of PEG Hydrogel showing Molecular Weight, number of arms, and concentration of the stock solution.

	Molecular Weight [kDa]	arms	Conc [mg/mL]
8-PEG-VS	20,000	8	200
DTT	154	2	12,32
RGD	1025	1	6

PEG component

200 mg/mL = 20 mg/µL → 20% PEG stock solution

10 mg / 100 µL → 10% PEG
4 mg / 100 µL → 4% PEG

Moles in 100 µL of 4% PEG:

$$n_{PEG} = \frac{m}{M} = \frac{4 \times 10^{-3}}{20{,}000} = 2 \times 10^{-7}\ mol$$

Moles in 100 µL of 10% PEG:

$$n_{PEG} = \frac{m}{M} = \frac{10 \times 10^{-3}}{20{,}000} = 5 \times 10^{-7}\ mol$$

DTT component

Weight of DTT corresponding to 4 mg PEG:

$$m_{DTT} = \frac{m_{PEG}}{M_{PEG}} \times \frac{no.arms}{no\ of\ SH\ per\ chain} \times M_{DTT} = \frac{4 \times 10^{-3}}{20{,}000} \times \frac{8}{2} \times 154 = 0.1232\ mg$$

Weight of DTT corresponding to 10 mg PEG:

$$\frac{10 \times 10^{-3}}{20{,}000} \times \frac{8}{2} \times 154 = 0.308\ mg$$

Table A.2. 100 µL 4% PEG hydrogel mixing ratio without RGD from 20% PEG stock solution.

Solution Volume	mass [mg]	volume [mL]	volume [µL]
8-PEG-VS	4	0,02	20
DTT	0,1232	0,01	10
PBS buffer		0,07	70
Gel Volume [mL]		0,1	**100**

Table A.3. 100 µL 10% PEG hydrogel mixing ratio without RGD from 20% PEG stock solution.

Solution Volume	mass [mg]	volume [mL]	volume [µL]
8-PEG-VS	10	0,05	50
DTT	0,308	0,025	25
PBS buffer		0,02	20
Gel Volume [mL]		0,1	**100**

RGD component

1 RGD per 100 arms → $\frac{1}{8} \times 100 = 12.5$

Weight of RGD corresponding to 4 mg PEG:

$$m_{RGD} = n.M = \frac{2 \times 10^{-7}}{12.5} \times 1025 = 0.0164\ mg = 16.4\ \mu g$$

Weight of RGD corresponding to 10 mg PEG:

$$\frac{5 \times 10^{-7}}{12.5} \times 1025 = 0.041\ mg = 41\ \mu g$$

Table A.4. 100 µL 4% PEG hydrogel mixing ratio with RGD from 20% PEG stock solution.

Solution Volume	mass [mg]	volume [mL]	volume [µL]
8-PEG-VS	4	0,02	20
DTT	0,1232	0,01	10
RGD	0,0164	0,00273333	2.73
PBS buffer		0,06726667	67.73
Gel Volume [mL]		0,1	**100**

Table A.5. 100 µL 10% PEG hydrogel mixing ratio with RGD from 20% PEG stock solution.

Solution Volume	mass [mg]	volume [mL]	volume [µL]
8-PEG-VS	10	0,05	50
DTT	0,308	0,025	25
RGD	0,041	0,00683333	6.83
PBS buffer		0,01816667	18.17
Gel Volume [mL]		0,1	**100**

Assessment of Adhesion Density

RGD density in 112.6 µL (final volume) of 4% PEG:

$m_{RGD} = 0.0164\ mg$ (from above)

$$n_{RGD} = \frac{m}{M} = \frac{0.0164 \times 10^{-3}}{1025} = 1.6 \times 10^{-8}\ mol$$

$$\rho_{RGD} = \frac{1.6 \times 10^{-8}\ mol}{112.6\ \mu L} = \frac{1.6 \times 10^{-8}\ mol}{0.1126\ cm^3} = 1.42 \times 10^{-7}\ \frac{mol}{cm^3} = 0.0142\ \frac{nmol}{cm^3}$$

1:100-equivalent ratio of RGD in 130.94 µL (final volume) to 10% PEG:

$$m_{RGD\ (10\%\ PEG)} = \frac{Q_{v\ (10\%\ PEG)}}{Q_{v\ (4\%\ PEG)}} \times m_{RGD\ (4\%\ PEG)}$$

$$= \frac{112.62}{130.94} \times 0.0164 \times 10^{-3} = 0.01415\ mg$$

$$\frac{10 \times 10^{-3}}{20 \times 10^{-3}} \times \frac{x}{8} \times 1025 = 0.01415 \times 10^{-3}$$

$$x = 289.75\ PEG\ (:1\ RGD)$$

Mitotracker Dilution

Mitotracker Green is packaged as 20 vials of 50ug each. We need to dilute in DMSO to create a stock solution of 1 mM of Mitotracker.

To make up 1 mM:

Molecular weight (MW) = 671.88 g/mol (from label on package)

$$\left(\frac{1\ mol}{671.88\ g}\right) \times \left(\frac{50\ \mu g}{x\ L}\right) = 1\ mM = 1\ \times 10^{-3}\ mol/L$$

$$x = 74.42\ \mu L\ in\ DMSO$$

To dilute stock solution of 1mM to the desired concentration for experimental conditions, we dilute Mitotracker in media.

Use the constant mass equation:

$$C_1V_1 = C_2V_2$$

For example, for 200 nM Mitotracker solution diluted in 5 ml media:

$$(1\ mM) * (V_1) = (200\ nM) * (5\ mL)$$

$$V_1 = 1\ \mu L$$

As such,

- For 200 nM – dilute 1 µL in 5 mL media,
- For 300 nM – dilute 1.75 µL in 5 mL media, and
- For 500 nM – dilute 2.5 µL in 5 mL media.

Appendix B: Particle Tracking Microrheology Data

Particle Tracking Analysis and Post-processing

An example XML MPT data file and the MATLAB code for MSD analysis are provided as supplementary data for download on ZivaHub under https://zivahub.uct.ac.za/account/articles/12999653.

(Please note that this private link of the yet unpublished data record is for the examiners of the dissertation. The private link will be replaced with the public link once the examination is completed and the data record published.)

Descriptive Statistics

Table B.1 summarises the MSD values of Cardiac fibroblasts (CF) and Myofibroblasts (MF) during different delay times.

Table B.1. MSD (mean and standard deviation) of mitochondrial fluctuations from 10 isolated single CF and MF cells in 4% and 10% (m/v) concentrated PEG hydrogels during various delay times. (MSD is measured in [μm^2]).

Delay (s)	Mean ($\bar{m}$)				Standard Deviation (SD)			
	4% PEG		10% PEG		4% PEG		10% PEG	
	CF	MF	CF	MF	CF	MF	CF	MF
0,5	0,03980	0,03248	0,03400	0,03015	0,00600	0,00911	0,00570	0,00666
1	0,04221	0,03589	0,03420	0,03206	0,00654	0,01148	0,00802	0,00739
2	0,04395	0,03954	0,03460	0,03376	0,00683	0,01343	0,00924	0,00752
3	0,04528	0,04141	0,03500	0,03470	0,00721	0,01490	0,01184	0,00813
4	0,04635	0,04312	0,03540	0,03534	0,00775	0,01599	0,01422	0,00888
5	0,04735	0,04441	0,03580	0,03637	0,00825	0,01705	0,01354	0,00957
6	0,04858	0,04639	0,03620	0,03735	0,00903	0,01831	0,01344	0,01042
7	0,04959	0,04815	0,03660	0,03748	0,00973	0,01935	0,01280	0,01110
8	0,05022	0,04883	0,03690	0,03829	0,01005	0,02043	0,01513	0,01157
9	0,05136	0,05030	0,03730	0,03865	0,01107	0,02148	0,01399	0,01253
10	0,05234	0,05103	0,03770	0,03907	0,01174	0,02178	0,01520	0,01340
20	0,06397	0,06230	0,04160	0,04284	0,02227	0,03001	0,01904	0,01921
30	0,07575	0,06937	0,04550	0,04639	0,03538	0,03370	0,02406	0,02409
40	0,08734	0,06901	0,03693	0,04716	0,05250	0,03181	0,01303	0,03005
50	0,09629	0,06477	0,02792	0,04414	0,07020	0,02814	0,00836	0,03239

Table B.2 summarizes α (mean and standard deviation) of CF and MF cells for various delay times.

Table B.2. Logarithmic MSD-dependent power law alpha (α) from 10 isolated single CF and cells in 4% and 10% (m/v) concentrated PEG hydrogels during various delay times

Delay (s)	Mean ($\bar{m}$)				Standard Deviation (SD)			
	4% PEG		10% PEG		4% PEG		10% PEG	
	CF	MF	CF	MF	CF	MF	CF	MF
1	0,18544	0,19238	0,09240	0,11188	0,11537	0,10894	0,09045	0,10811
2	0,21631	0,20515	0,11071	0,12090	0,13629	0,12412	0,09478	0,12447
3	0,23985	0,22019	0,12430	0,12973	0,15404	0,13799	0,09602	0,13060
4	0,26085	0,23072	0,13555	0,13848	0,16890	0,14681	0,09808	0,13601
5	0,27982	0,24201	0,14532	0,13966	0,18241	0,15224	0,10569	0,14276
10	0,35468	0,26493	0,18445	0,15975	0,24229	0,17079	0,14955	0,15781

Two-way ANOVA

Table B.3 summarizes the results of the two-way ANOVA for both the MSD and α data, with the focus being on the interaction effect of the factors.

Table B.3. Results of two-way ANOVA demonstrating non-significance of interaction between cell phenotype and gel concentration in MSD and α for various delay times.

Delay (s)	MSD			α		
	F (1, 29)	p	η_p^2	F (1,29)	p	η_p^2
0.5	2.389	0.133	0.076	0.054	0.818	0.002
1	1.104	0.302	0.037	0.019	0.891	0.001
2	0.526	0.474	0.018	0.001	0.973	0.000
3	0.292	0.593	0.010	0.007	0.934	0.000
4	0.286	0.597	0.001	0.028	0.868	0.001
5	0.267	0.609	0.001	0.029	0.866	0.001
10	0.114	0.738	0.004	0.002	0.962	0.000
20	0.075	0.787	0.003			
30	0.212	0.649	0.007			
40	.827	0.371	0.028			
50	1.428	0.242	0.047			

Pairwise Comparisons

Table B.4 summarises the pairwise comparisons of both MSD and α, between gel concentrations, i.e. between 4% and 10% (v/w) PEG hydrogel. These indicate the main effects of gel concentration on MSD and α and thereby lumps together the cell phenotypes.

Table B.4. Comparison of the main effect of Gel Concentration (4% PEG vs 10% PEG) on MSD and α of cells during various delay times.

Delay (s)	MSD			α		
	***F* (1, 29)**	***p***	η_p^2	***F* (1, 29)**	***p***	η_p^2
0.5	5.721	0.023	0.165	3.662	0.066	0.112
1	4.986	0.033	0.147	4.088	0.050	0.124
2	5.536	0.026	0.160	3.986	0.045	0.121
3	5.153	0.031	0.151	4.184	0.050	0.126
4	5.705	0.024	0.164	4.225	0.049	0.127
5	5.356	0.028	0.156	4.605	0.040	0.137
10	5.438	0.027	0.158	3.923	0.047	0.119
20	5.935	0.021	0.170			
30	5.902	0.022	0.169			
40	5.602	0.025	0.162			
50	5.441	0.027	0.158			

Table B.5 summarises the pairwise comparisons of both MSD and α, between cell phenotypes, i.e. between CF and MF cells. These indicate the main effects of the cell phenotype on MSD and α and thereby lumps together the gel concentrations.

Table B.5. Comparison of the main effects of Cell Phenotype (CF vs MF) on MSD and α of cells during various delay times.

Delay (s)	MSD			α		
	***F* (1, 29)**	***p***	η_p^2	***F* (1, 29)**	***p***	η_p^2
0.5	1.255	0.277	0.041	0.168	0.685	0.006
1	0.817	0.374	0.027	0.182	0.673	0.006
2	0.269	0.608	0.009	0.040	0.842	0.001
3	0.210	0.650	0.007	0.031	0.862	0.001
4	0.056	0.815	0.002	0.022	0.882	0.001
5	0.020	0.890	0.001	0.012	0.915	0.000
10	0.014	0.905	0.000	0.063	0.803	0.002
20	0.008	0.929	0.000			
30	0.003	0.958	0.000			
40	0.099	0.756	0.003			
50	0.259	0.591	0.010			

Table B.6 and Table B.7 state the analysis of the simple effects of gel concentration (4% vs 10% PEG) in terms of MSD and α, respectively. This is in order to examine each factor closely as a condition of the other. It was, however, less applicable for our study single we did not find a significant interaction.

Table B.6. Comparison of the simple effects on the MSD of cells in 4% vs 10% PEG hydrogel during various delay times.

Delay (s)	CF			MF		
	***F* (1, 29)**	***p***	η_p^2	***F* (1,29)**	***p***	η_p^2
0.5	6.267	0.018	0.178	0.469	0.499	0.016
1	4.359	0.046	0.131	0.915	0.347	0.031
2	3.830	0.060	0.117	1.736	0.198	0.056
3	3.193	0.084	0.099	1.960	0.172	0.063
4	3.455	0.073	0.106	2.251	0.144	0.072
5	3.241	0.082	0.101	2.116	0.156	0.068
10	0.030	0.864	0.001	0.087	0.770	0.003

Table B.7. Comparison of the simple effects on α of cells in 4% vs 10% PEG hydrogel during various delay times

Delay (s)	CF			MF		
	***F* (1, 29)**	***p***	η_p^2	***F* (1,29)**	***p***	η_p^2
0.5	1.143	0.294	0.038	3.016	0.093	0.094
1	1.563	0.221	0.051	2.827	0.103	0.089
2	1.667	0.207	0.054	2.523	0.123	0.080
3	1.832	0.186	0.059	2.253	0.123	0.080
4	1.998	0.168	0.064	2.335	0.137	0.075
5	2.169	0.152	0.070	2.556	0.121	0.081
10	1.510	0.229	0.049	2.697	0.111	0.085

Table B.8 and Table B.9 state the simple effects analysis of gel concentration (CF vs MF) in terms of MSD and α, respectively.

Table B.8. Comparison of the simple effects on MSD of CF vs MF cells during various delay times.

Delay (s)	4% PEG			10% PEG		
	***F* (1, 29)**	***p***	η_p^2	***F* (1,29)**	***p***	η_p^2
0.5	4.425	0.044	0.132	0.080	0.779	0.003
1	2.403	0.132	0.077	0.009	0.925	0.000
2	0.973	0.332	0.032	0.018	0.895	0.001
3	0.627	0.435	0.021	0.003	0.958	0.000
4	0.374	0.546	0.013	0.037	0.848	0.001
5	0.272	0.606	0.009	0.059	0.810	0.002
10	0.030	0.864	0.001	0.087	0.770	0.003

Table B.9. Comparison of the simple effects on α of CF vs MF cells during various delay times.

Delay (s)	4% PEG			10% PEG		
	***F* (1, 29)**	***p***	η_p^2	***F* (1,29)**	***p***	η_p^2
0.5	0.259	0.614	0.009	0.013	0.909	0.000
1	0.146	0.705	0.005	0.057	0.813	0.002
2	0.017	0.896	0.001	0.023	0.881	0.001
3	0.005	0.942	0.000	0.028	0.869	0.001
4	0.000	0.989	0.000	0.042	0.839	0.001
5	0.003	0.960	0.000	0.032	0.859	0.001
10	0.056	0.814	0.002	0.017	0.897	0.001